REPORT DOCUMENTATION PAGE

Form Approved OMB NO. 0704-0188

1. REPORT DATE (DD-MM-YYYY)	2. REPORT TYPE	3. DATES COVERED (From - To)
18-09-2015	Final Report	15-Jun-2011 - 14-Jun-2015

4. TITLE AND SUBTITLE	5a. CONTRACT NUMBER
Final Report: A Study of GaAsSb Nanowires by Molecular Beam Epitaxy for Near IR Applications	W911NF-11-1-0223
	5b. GRANT NUMBER
	5c. PROGRAM ELEMENT NUMBER
	206022

6. AUTHORS	5d. PROJECT NUMBER
Shanthi Iyer and C.Lewis Reynolds	
	5e. TASK NUMBER
	5f. WORK UNIT NUMBER

7. PERFORMING ORGANIZATION NAMES AND ADDRESSES	8. PERFORMING ORGANIZATION REPORT NUMBER
North Carolina A&T State University 1601 East Market Street Greensboro, NC 27411 -0001	

9. SPONSORING/MONITORING AGENCY NAME(S) AND ADDRESS (ES)	10. SPONSOR/MONITOR'S ACRONYM(S)
U.S. Army Research Office P.O. Box 12211 Research Triangle Park, NC 27709-2211	ARO
	11. SPONSOR/MONITOR'S REPORT NUMBER(S)
	59052-EL-REP.12

12. DISTRIBUTION AVAILIBILITY STATEMENT

Approved for Public Release; Distribution Unlimited

13. SUPPLEMENTARY NOTES

The views, opinions and/or findings contained in this report are those of the author(s) and should not contrued as an official Department of the Army position, policy or decision, unless so designated by other documentation.

14. ABSTRACT

Ga assisted growth of axial and core-shell configured GaAs/GaAsSb/GaAs heterostructured nanowires containing different Sb compositions by molecular beam epitaxy are reported. Substrate preparation prior to the growth was found to be critical for achieving all vertical NWs with high nanowire (NW) density in the 8x108/cm2 range. The morphological, structural and optical properties of these NWs were correlated using low temperature photoluminescence (PL), Raman spectroscopy, transmission and scanning electron microscopies and X-ray diffraction. Red shift up to 0.0 eV in the 4K photoluminescence (PL) spectra is obtained with increasing Sb

15. SUBJECT TERMS

Nanowires, GaAsSb, dilute nitride, core-shell nanowires,radial nanowires, axial nanowires, telecommunication wavelength, nanoheterostructure, micro photoluminescence, Be doping, scanning transmission electron microscopy, Raman, xray, transmission

16. SECURITY CLASSIFICATION OF:			17. LIMITATION OF ABSTRACT	15. NUMBER OF PAGES	19a. NAME OF RESPONSIBLE PERSON
a. REPORT	b. ABSTRACT	c. THIS PAGE	UU		Shanthi Iyer
UU	UU	UU			19b. TELEPHONE NUMBER
					336-285-3710

Report Title

Final Report: A Study of GaAsSb Nanowires by Molecular Beam Epitaxy for Near IR Applications

ABSTRACT

Ga assisted growth of axial and core-shell configured GaAs/GaAsSb/GaAs heterostructured nanowires containing different Sb compositions by molecular beam epitaxy are reported. Substrate preparation prior to the growth was found to be critical for achieving all vertical NWs with high nanowire (NW) density in the 8x108/cm2 range. The morphological, structural and optical properties of these NWs were correlated using low temperature photoluminescence (PL), Raman spectroscopy, transmission and scanning electron microscopies and X-ray diffraction. Red shift up to 0.9 eV in the 4K photoluminescence (PL) spectra is obtained with increasing Sb incorporation in core-shell configured nanowires. Though a maximum shift up to only 1.1 eV was achieved in the axial configuration, it was largely free of planar defects. First reports of bandgap tuning up to 1.3 µm in GaAs/GaAsSb/GaAs based core-shell nanowires by incorporation of dilute amount of N are also presented. The observation of room temperature PL emission on as-grown nanowires demonstrates the advantage that the dilute nitride system offers in the NW configuration. Be doping of the GaAs NW ensemble was examined to realize an axial p-i-n heterostructured NW photodetector. NW aspect ratio, growth rate, NW density and doping efficiency were found to be strongly influenced by group V/III ratio, Be effusion cell temperature and the core/shell configuration.

Enter List of papers submitted or published that acknowledge ARO support from the start of the project to the date of this printing. List the papers, including journal references, in the following categories:

(a) Papers published in peer-reviewed journals (N/A for none)

Received	Paper
09/14/2015 10.00	Pavan Kumar Kasanaboina, Estiak Ahmad, Jia Li, C. Lewis Reynolds, Jr., Yang Liu, Shanthi Iyer. Self-catalyzed growth of dilute nitride GaAs/GaAsSbN/GaAs core-shell nanowires by molecular beam epitaxy., Applied Physics Letters, (11 2015): 103111. doi:
09/16/2015 11.00	Pavan Kumar Kasanaboina, Sai Krishna Ojha, Shifat Us Sami, C Lewis Reynolds Jr., Yang Liu , Shanthi Iyer. Bandgap tuning of GaAs/GaAsSb core-shell nanowires grown by molecular beam epitaxy., Semiconductor Science and Technology (Proof copy scheduled to be published in September 2015 issue), (09 2015): 0. doi:
TOTAL:	**2**

Number of Papers published in peer-reviewed journals:

(b) Papers published in non-peer-reviewed journals (N/A for none)

Received	Paper
TOTAL:	

Number of Papers published in non peer-reviewed journals:

(c) Presentations

Pavan Kumar Kasanaboina, Sai Krishna Ojha, Shifat Us Sami, Lewis Reynolds, Yang Liu, Shanthi Iyer, "Growth Temperature Dependence of the GaAs/GaAsSb Core-Shell Nanowires Grown by Molecular Beam Epitaxy", Oral Presentation in 57th Electronic Materials Conference in Narrow Bandgap Materials and Devices Session L, Columbus, Ohio, June 24, 2015,

Pavan Kumar Kasanaboina, Sai Krishna Ojha, Shifat Us Sami, C. Lewis Reynolds Jr., Yang Liu and Shanthi Iyer, "Engineering of GaAs/GaAsSb Nanowires for Next Generation IR Photodetectors", poster presentation, 4th Annual Graduate Poster Competition COE 2015, NC,USA(April 24th , 2015).

Sai Krishna Ojha, Pavan Kumar Kasanaboina, Lewis Reynolds, Tom Rawdanowicz and Shanthi Iyer, "Be doping of core & core/shell GaAs nanowires through molecular beam epitaxy", poster presentation, 4th Annual Graduate Poster Competition COE 2015, NC,USA (April 24th , 2015)

Pavan Kumar Kasanaboina, Sai Krishna Ojha, Shifat U. Sami, Lewis Reynolds, Yang Liu and Shanthi Iyer, "Effect of Sb on Morphology and Optical Properties of GaAs/GaAsSb Nanowires Grown by Molecular Beam Epitaxy", Poster presentation, Fitzpatrick Institute for Photonics (FIP) Annual Symposium, Duke University, Durham, NC (March 9-10, 2015).

Sai Krishna Ojha, Pavan Kumar Kasanaboina, Lewis Reynolds, Tom Rawdanowicz and Shanthi Iyer, "Effect of Be doping on core & core/shell GaAs nanowires through molecular beam epitaxy", Fitzpatrick Institute for Photonics (FIP) Annual Symposium, Duke University, Durham, NC,USA(March 9-10th, 2015) poster presentation

Pavan Kumar Kasanaboina, Sai Krishna Ojha, Shifat Us Sami, Lewis Reynolds and Shanthi Iyer Structural and Optical Characteristics of GaAs/GaAsSb Core-Shell Structured Nanowires Grown By Molecular Beam Epitaxy, MRS/ASM/AVS Meeting Joint Symposium 2014, Raleigh,NC, Oral presentation, Nov 7,2014.

Sai Krishna Ojha, Pavan Kumar Kasanaboina, Lew Reynolds and Shanthi Iyer," Compositional variation of Sb in Ga assisted axial GaAs/GaAsSb/GaAs heterostructure nanowires on chemically etched Si substrate", MRS/ASM/AVS Joint Symposium 2014, poster presentation, Raleigh, NC.(Nov 7th,2014)

Md Shifat Us Sami, Jia Li, Sai Krishna Ojha, Pavan Kumar Kasanaboina and , Shanthi Iyer, "A Low Temperature Micro-photoluminescence Study of Self-assisted MBE Grown Core and Core-Shell Configured GaAsSb(N)/GaAs Nanowires for Nanoscale Photodetectors", MRS/ASM/AVS Joint Symposium at NCSU, Friday, November 7, 2014.

Md Shifat Us Sami, Jia Li, Sai Krishna Ojha, Pavan Kumar Kasanaboina and Shanthi Iyer, " Micro-photoluminescence Study of Self-assisted MBE Grown Core and Core-Shell GaAs/GaAsSb Nanowires", Nano Manufacturing 2014 – Conference at JSNN, Wednesday, September 24, 2014

Pavan Kumar Kasanaboina, Sai Krishna Ojha, Shifat Us Sami, Lewis Reynolds, Jia Li and Shanthi Iyer, "Compositional Modulation of GaAs/GaAsSb Radial Heterostructured Nanowires for Telecommunication Applications," Nano manufacturing-2014,Joint School of Nanoscience and Nanoengineering, Greensboro, NC, Poster presentation, Sep 24,2014

Sai Krishna Ojha, Pavan Kumar Kasanaboina, Lewis Reynolds, Tom Rawdanowicz and Shanthi Iyer, "Comparison of Ga assisted axial GaAs/GaAsSb/GaAs heterostructure nanowires with and without chemical etching on Si substrate ", poster presentation, Nano Manufacturing 2014 Conference, Greensboro, NC(Sep 24th,2014)

Sai Krishna Ojha, Pavan Kumar Kasanaboina, Lewis Reynolds, Tom Rawdanowicz and Shanthi Iyer, "A study of Be doping in Ga assisted GaAs Nanowires by Molecular Beam Epitaxy", NAMBE 2014, poster presentation, Flagstaff, Arizona (Sep 8, 2014)

Sai Krishna Ojha, Pavan Kumar Kasanaboina, Lewis Reynolds, Thomas Rawdanowicz and Shanthi Iyer, "Growth Optimization of GaAsSb

Inserts in Ga Assisted GaAs/GaAsSb Heterostructure Nanowires for IR Photodetector Applications", 56th Electronic Materials Conference (EMC) and Exhibition, Santa Barbara, CA, (June 24-27, 2014).

Pavan Kasanaboina, Sai Krishna Ojha, Lewis Reynolds, Thomas Rawdanowicz, R.M.White and Shanthi Iyer, "Building of Nano structures: A Selective Area Growth of GaAs Nanowires", College of Engineering Poster Competition, NCA&T State University, Greensboro, NC, Poster presentation,(April,25th 2014); Got a runner up award ($350) for the best poster.

Sai Krishna Ojha, Pavan Kumar Kasanaboina, Lewis Reynolds, Thomas Rawdanowicz and Shanthi Iyer, "Effect of Be doping and GaAsSb inserts in self-assisted GaAs nanowires(NWs) for IR device Applications", College of Engineering Poster Competition, NCA&T State University, Greensboro, NC, Poster presentation,(April,25th, 2014)

Pavan Kumar Kasanaboina, Sai Krishna Ojha,Lewis Reynolds, Thomas Rawdanowicz, R.M.White and Shanthi Iyer, " Design of p-GaAs Nanowires for p-i-n Heterostructured Nanowire Photodetector/Solar Cell", Nano manufacturing-2013,Joint School of Nanoscience and Nanoengineering, Greensboro,NC, Poster presentation, Sep 25,2013

Sai Krishna Ojha, Pavan Kumar Kasanaboina, Lewis Reynolds, Thomas Rawdanowicz and Shanthi Iyer, "Effect of GaAsSb Inserts in Ga Assisted GaAs/GaAsSb Heterostructured Nanowires and Be Doping in GaAs NWs", MRS Fall Meeting 2013, Oral presentation,(Dec 03 2013).

Sai Krishna Ojha, Pavan Kumar Kasanaboina, Lewis Reynolds, Thomas Rawdanowicz and Shanthi Iyer, "Study of Double Segmented GaAsSb Inserts in Ga Assisted GaAs/GaAsSb Heterostructure Nanowires for IR Photodetector Applications", MRS/ASM/AVS/AReMS Meeting 2013,Raleigh,NC, Oral presentation,(Nov 15,2013)

Pavan Kasanaboina, Sai Krishna Ojha, Lewis Reynolds, Thomas Rawdanowicz, R.M.White and Shanthi Iyer, "Design and Optimization of p-GaAs Nanowires for Photodetector/Solar Cell Applications", MRS/ASM/AVS/AReMS Meeting 2013,Raleigh,NC, Poster presentation, (Nov 15,2013)

Sai Krishna Ojha, Pavan Kumar Kasanaboina,Lewis Reynolds, Thomas Rawdanowicz and Shanthi Iyer, "Study of double segmented GaAsSb inserts in Ga Assisted GaAs/GaAsSb Heterostructure Nanowires for IR photodetector applications, "NanoManufacturing Conference 2013,Greensboro, NC 27401,Poster presentation,(Sept 25,2013)

Pavan Kasanaboina, Sai Krishna Ojha, Lewis Reynolds, Thomas Rawdanowicz, R.M.White and Shanthi Iyer, "Design of p-GaAs Nanowires for p-i-n Heterostructured Nanowire Photodetector/Solar Cell", Nano manufacturing-2013,Joint School of Nanoscience and nanoengineering, Greensboro, NC, Poster presentation,(Sep 25,2013)

Sai Krishna Ojha and Shanthi Iyer, "Ga Assisted GaAs/GaAsSb Heterostructure Nanowires for P-I-N Photodetectors", NCA&TSU College of Engineering Poster Presentation, April 25, 2013.

S. K.Ojha, S.Iyer, L. Reynolds and T. Rawdanowicz, "Molecular Beam Epitaxy Growth of GaAsSb Heterostructure Nanowires", MRS/ASM/AVS North Carolina Symposium, Raleigh, NC, Nov. 16th 2012.

Non Peer-Reviewed Conference Proceeding publications (other than abstracts):

<u>Received</u>   <u>Paper</u>

TOTAL:

Number of Non Peer-Reviewed Conference Proceeding publications (other than abstracts):

Peer-Reviewed Conference Proceeding publications (other than abstracts):

<u>Received</u>   <u>Paper</u>

06/12/2015   5.00   Pavan Kumar Kasanaboina, Sai Krishna Ojha, Shifat Us Sami, Lewis Reynolds Jr., Yang Liu and Shanthi
Iyer. Tailoring of GaAs/GaAsSb core-shell structured nanowires for IR photodetector applications,
SPIE Photonics-2015. 10-FEB-15, . : ,

TOTAL: **1**

Number of Peer-Reviewed Conference Proceeding publications (other than abstracts):

(d) Manuscripts

Received		Paper
06/12/2015	6.00	Pavan Kumar Kasanaboina, Estiak Ahmad, Jia Li, C. Lewis Reynolds Jr., Yang Liu and Shanthi Iyer. Self-Catalyzed Growth of Dilute Nitride GaAs/GaAsSbN/GaAs Core-Shell Nanowires by Molecular Beam Epitaxy, Nanotechnology (06 2015)
07/18/2014	3.00	Sai K Ojha, Pavan K Kasanaboina, C L Reynolds, T A Rawdanowicz, R M White, Shanthi Iyer. A study of Be doped GaAs nanowires grown by Ga assistedmolecular beam epitaxy, Journal of Physics: Condensed Matter (07 2014)
08/24/2015	9.00	Pavan Kumar Kasanaboina, Sai Krishna Ojha, Shifat Us Sami, C. Lewis Reynolds Jr., Yang Liu, Shanthi Iyer. Bandgap Tuning of GaAs/GaAsSb Core-Shell Nanowires Grown by Molecular Beam Epitaxy, Semiconductor Science and Technology (07 2015)
09/02/2014	4.00	Pavan Kumar Kasanaboina, C Lew Reynolds.Jr , Thomas A Rawdanowicz, Ryan M White, Shanthi Iyer, Sai Krishna Ojha. A study of Be doped GaAs nanowires grown by Ga assisted molecular beam epitaxy, Thin Solid Films (07 2014)
TOTAL:	**4**	

Number of Manuscripts:

Books

Received	Book
TOTAL:	

07/18/2014 2.00 Shanthi Iyer, L.Reynolds, T.Rawdanowicz, Sai Krishna Ojha, Pavan Kumar Kasanaboina, Adam Bowen. A Study of Ga Assisted Growth of GaAs/GaAsSb AxialNanowires by Molecular Beam Epitaxy, Boca Raton FL: CRC Press, (04 2014)

10/07/2013 1.00 Shanthi Iyer, Lew Reynolds, Thomas Rawdanowicz, Sai K. Ojha, Pavan K. Kasanaboina . GaAs/GaAsSb Heterostructure Nanowires for P-I-N Photodetectors , Boca Raton, Florida: Taylor and Francis Books, Inc., (12 2013)

TOTAL: **2**

Patents Submitted

Patents Awarded

Awards

Graduate Students

NAME	PERCENT_SUPPORTED	Discipline
Manish Sharma	0.00	
Estiak Ahmad	0.00	
Md Shifat Us Sami	0.00	
Pavan Kumar Kasanaboina	0.70	
Sai Krishna Ojha	1.00	
FTE Equivalent:	**1.70**	
Total Number:	**5**	

Names of Post Doctorates

NAME	PERCENT_SUPPORTED
Jia Li	0.50
FTE Equivalent:	**0.50**
Total Number:	**1**

Names of Faculty Supported

NAME	PERCENT_SUPPORTED	National Academy Member
Shanthi Iyer	0.30	
FTE Equivalent:	**0.30**	
Total Number:	**1**	

Names of Under Graduate students supported

NAME	PERCENT_SUPPORTED
FTE Equivalent:	
Total Number:	

Student Metrics
This section only applies to graduating undergraduates supported by this agreement in this reporting period

The number of undergraduates funded by this agreement who graduated during this period: 0.00

The number of undergraduates funded by this agreement who graduated during this period with a degree in science, mathematics, engineering, or technology fields:...... 0.00

The number of undergraduates funded by your agreement who graduated during this period and will continue to pursue a graduate or Ph.D. degree in science, mathematics, engineering, or technology fields:...... 0.00

Number of graduating undergraduates who achieved a 3.5 GPA to 4.0 (4.0 max scale):...... 0.00

Number of graduating undergraduates funded by a DoD funded Center of Excellence grant for Education, Research and Engineering:...... 0.00

The number of undergraduates funded by your agreement who graduated during this period and intend to work for the Department of Defense 0.00

The number of undergraduates funded by your agreement who graduated during this period and will receive scholarships or fellowships for further studies in science, mathematics, engineering or technology fields:...... 0.00

Names of Personnel receiving masters degrees

NAME
Md Shifat Us Sami
Total Number: 1

Names of personnel receiving PHDs

NAME
Sai Krishna Ojha
Total Number: 1

Names of other research staff

NAME	PERCENT_SUPPORTED
FTE Equivalent:	
Total Number:	

Sub Contractors (DD882)

1 a. NORTH CAROLINA STATE UNIVERSITY   1 b. 2901 Sullivan Drive

                  Raliegh   NC   276957514

Sub Contractor Numbers (c):

Patent Clause Number (d-1):

Patent Date (d-2):

Work Description (e): Acquire, analyze, and provide TEM images of nanowires (NW) and NW devices grown b

Sub Contract Award Date (f-1): 6/15/11 12:00AM

Sub Contract Est Completion Date(f-2): 6/14/15 12:00AM

1 a. NORTH CAROLINA STATE UNIVERSITY   1 b. 2901 Sullivan Drive

                  Raliegh   NC   276957514

Sub Contractor Numbers (c):

Patent Clause Number (d-1):

Patent Date (d-2):

Work Description (e): Acquire, analyze, and provide TEM images of nanowires (NW) and NW devices grown b

Sub Contract Award Date (f-1): 6/15/11 12:00AM

Sub Contract Est Completion Date(f-2): 6/14/15 12:00AM

Inventions (DD882)

5 **1.3 μm Emission from Dilute Nitride GaAs/GaAsSbN/GaAs Core-Shell Nanowires grown by Epitaxy**

Patent Filed in US? (5d-1) Y

Patent Filed in Foreign Countries? (5d-2) N

Was the assignment forwarded to the contracting officer? (5e) Y

Foreign Countries of application (5g-2):

  5a: Shanthi Iyer, Pavan Kumar Kasanaboina and Jia Li

 5f-1a: North Carolina A&T State University

  5f-c: 1601 E MarKet Street

   Greensboro   NC 27410

Scientific Progress

Technology Transfer

FINAL REPORT

to

ARMY RESEARCH OFFICE

A Study of GaAsSb Nanowires by Molecular Beam Epitaxy for Near IR Applications

Grant No: W911NF-11-1-0223

Period: 06/15/2011- 06/14/2015

Program Manager: William Clark

Shanthi Iyer, Principal Investigator
Department of Electrical and Computer Engineering/
Nanoengineering
North Carolina A&T State University
Greensboro NC 27411

C. Lewis Reynolds, Co-Principal Investigator
Department of Materials Science and Engineering
North Carolina State University
Raleigh, NC 276495

i

APPENDIX

A. **S. Iyer et al., "A Study of Ga Assisted Growth of GaAs/GaAsSb Axial Nanowires by Molecular Beam Epitaxy",** Chapter 3 Nanoscience and Nanoengineering: Advances and Applications, Ajit D. Kelkar, Dan Herr and James G. Ryan; CRC Press.: Boca Raton FL, ISBN 978-1-4822-3119-9, 2013, pages 31-49.

B. **S. K. Ojha et al., "A study of Be-doped GaAs nanowires grown by Ga assisted molecular beam epitaxy",** Not published

C. **P. K. Kasanaboina et al.,** Effect of Growth Parameters and Substrate Surface Preparation for High Density Vertical GaAs/GaAsSb Core-shell Nanowires with Photoluminescence Emission at 1.3 μm", August 2015 (Submitted to Journal of Electronic Materials)

D. **P. K. Kasanaboina et al., "**Tailoring of GaAs/GaAsSb core-shell structured nanowires for IR photodetector applications**,** Proc. SPIE 9373, Quantum Dots and Nanostructures: Synthesis, Characterization, and Modeling XII, 937307 -1 to 937307-9 (February 27, 2015); doi:10.1117/12.2080572.

E. **P. K. Kasanaboina et al., "**Bandgap Tuning of GaAs/GaAsSb Core-Shell Nanowires Grown by Molecular Beam Epitaxy**,** Semiconductor Science and Technology, (Sept. issue 2015) in print.

F. **S. K. Ojha et al., "**Effects of Sb variation in Ga assisted GaAs/GaAsSb/GaAs axial heterostructure nanowires**, draft copy.**

G. **S. K. Ojha et al., "**Study of Be doping in GaAs core & core-shell nanowires using photoluminescence and Raman spectroscopy", manuscript under preparation.

H. P. K. Kasanaboina et al., "Self-catalyzed growth of dilute nitride GaAs/GaAsSbN/GaAs core-shell nanowires by molecular beam epitaxy", Appl. Phys. Lett. 107, 103111 -5(2015).

I. S. Iyer et al., Invention disclosure NC A&T Ref # EN00950915 "Band Gap Tuning up to 1.3μm in GaAsSbN NWs grown by Ga assisted Molecular Beam Epitaxy."

A Study of GaAsSb Nanowires by Molecular Beam Epitaxy for Near IR Applications

Grant No: W911NF-11-1-0223

Technical Description

This is the final technical report describing the research activities of the above ARO grant from June 15, 2011 thru June 14, 2015. The focus of this project was on the growth and characterization of high quality Ga-catalyzed GaAsSb/GaAs heterostructure nanowires (NWs) by molecular beam epitaxy (MBE) on (111) Si for optoelectronic applications in the telecommunication wavelength region of 1.3 µm.

Personnel: This program involved the efforts of the PI (Electrical and Computer Engineering and Nanoengineering), two PhD candidates Sai Krishna Ojha and Pavan Kumar Kasanaboina (Electrical and Computer Engineering, (ECE)), one master student Md Shifat Us Sami (Nanoengineering) and one post-doctoral research associate Dr. Jia Li (ECE) from NCA&TSU and Dr. Lew Reynolds, Dr. Tom Rawdanowicz, and Dr. Yang Liu from Department of Material Science and Engineering, NCSU.

The authors would like to acknowledge Dr. Jeffrey White, Army Research Laboratory, MD for helpful discussions on the Raman interpretation, Dr. Madan Dubey for providing the right contacts for research results discussion at the Army Research Laboratory, Professor Yuntian Zhu for the use of his Raman system, Dr. Judith Reynolds for carrying out the Raman measurements on Be doped GaAs samples, Dr. Ryan White for performing the X-ray energy dispersive spectrometry measurements on the FEI Titan G2 at NC State University's Analytical Instrumentation Facility. Dr. Cynthia S Day from Winston Salem University is also acknowledged for allowing us to use their large angle x-ray diffraction system and assisting us on initial set up of the system.

Finally the authors are thankful to technical monitor Willliam Clark for his critical comments steering the research in the right direction.

Scholarly Output: The work reported has resulted in one publication in Appl. Phys. Lett, (2015), one in print Semicond. Science and Tech, (Sept. issue 2015), one conference proceedings in SPIE (2015) and one book chapter in Nanoscience and Nanoengineering (CRC Press, 2013) and one manuscript currently under review in J. Electron. Mater. 25 student presentations were made in conferences. Presentations in international conferences include MRS Fall Meetings, Electronics Materials Conferences, SPIE Photonics West Conferences and North American Molecular Beam Epitaxy (NAMBE) conferences. Local conferences include annual conferences, namely AVS/ASM/MRS Meeting held at NCSU, Fitzpatrick Institute for Photonics (FIP) Annual Symposium, Nanomanufacturing at Joint School of Nanoscience and Nanoengineering and College of Engineering poster presentation at North Carolina A&T State University.

1.0 Experimental Details

NW growths were carried out in the EPI 930 solid source MBE system with valved As and Sb cracker sources and plasma source for Nitrogen. All the NWs were grown on intrinsic (111) Si substrates. All the growths were Ga-assisted growth in the temperature range of 580˚ C to 620˚ C. The As/Ga flux ratio examined were in the range of 1-20. X-ray diffraction scans (XRD) were performed using Bruker´s D8 Discover instrument with a DaVinci diffractometer in the standard Bragg-Brentano para-focusing configuration at Winston Salem University. X-rays from the Cu Kα source were not filtered and thus contained both $K\alpha_1$ and $K\alpha_2$ components. Scanning electron microscope (SEM) imaging was carried out using a Carl Zeiss Auriga-BU FIB FESEM Microscope with an attached energy dispersive x-ray spectrometer for compositional analysis. The STEM analysis was performed on an aberration-corrected (probe) FEI Titan G2 system and the bright field TEM, selected area electron diffraction (SAED), and high-resolution TEM (HRTEM) characterization were carried out on a JEOL 2010F microscope operated at 200 kV at NCSU. The other characterizations include low temperature (4K) micro-photoluminescence (μ-PL) spectra with lock-in techniques using either Si or InGaAs detectors and room temperature Raman measurements, which was carried out at SMIF facility, Duke University.

1.1   Summary of Accomplishments

The major tasks of the project pursued during the different years this period are summarized below.

Year 1

- Au assisted growth of GaAs and GaAsSb NWs: Optimization of the growth parameters were carried out for the growth of NWs on Au catalyst.

- Ga- catalyzed growth of GaAs, GaAsSb/GaAs and GaAs/GaAsSb/GaAs heterostructure NWs: Duration of Ga shutter opening prior to the growth along with other MBE growth parameters were optimized.

Year 2

- Structural and optical properties of Ga-catalyzed segmented growth of GaAsSb NWs: Detailed study of Ga assisted GaAsSb/GaAs heterostructured segmented NWs were carried out for Sb compositions <10%.

- Ga- catalyzed growth of Be doped GaAs NWs: A detailed and comprehensive study of Be doping of the NWs were also carried out. The study provided an insight in the growth of shell configuration and the surfactant effects that can be used advantageously in our ongoing work on GaAsSb/GaAs NW growth as a result of Sb being a well-known surfactant

- Processing of GaAs NW Ensemble: Progress was also made in processing of the NWs to make electrical contact.

The following two pieces of equipment were installed and made operational.

- Ga Sumo Cells from Veeco: The Ga sumo cells were installed in the MBE system.

- An optical closed cycle cryostat system from Montana Instruments: Optical closed cycle cryostat system with an extended sample chamber was acquired and installed.

Year 3

- Effect of Substrate Preparation on NW Density and Orientation: Effect of flux ratio on the density and orientation of the NWs grown on substrate without any substrate preparation and the effect of chemical etching with subsequent oxidation of the substrate on the growth was studied. Latter process allowed accurate control of oxide thickness, which was found to be critical for the growth of high density all vertical NWs.

- Effect of Shell Growth Temperature and Sb Composition on $GaAs_{1-x}Sb_x$/GaAs core shell NWs: The effect of shell growth temperature on the morphological, structural and optical properties of core-shell configured $GaAs/GaAs_{1-x}Sb_x$ nanowires grown by Ga-assisted molecular beam epitaxy (MBE) for different Sb content were studied in detail.

- Equipment installation: Installation and operation of a μ-PL system: Custom made micro-PL system has been set up that would allow 4K measurements on NWs from the visible to 2 µm spectral range. The Micro-PL System included both Si and InGaAs photodetectors.

Year 4

- Study of Ga- catalyzed growth of GaAs/GaAsSb/GaAs multishell NWs on chemically prepared (111) Si substrate: Detailed correlation of Sb composition to the morphology, microstructural quality, optical and vibrational properties was made. Red shift of 4K PL emission up to 1.3 µm was achieved.

- Study of Ga- catalyzed growth of GaAs/GaAsSb/GaAs axial NWs on chemically prepared (111) Si substrates: Detailed correlation of Sb composition to the morphology, microstructural quality, optical and vibrational properties was made. The nanowires were free of any planar defects and red shift of 4K PL emission up to 1.0 µm was achieved.

- Study of Be doping in GaAsSb NWs on chemically prepared (111) Si Substrates: This is a repeat of the work carried out during the year 2 except in this case it was carried out on chemically etched substrate resulting in improved quality of the doped NWs, free of any defect related peak in PL.

- Study of dilute amount of N in GaAsSb multishell NWs grown by Ga assisted MBE on chemically prepared (111) Si substrates: Influence of N incorporation in dilute amount

on the morphology, microstructural quality, optical and vibrational properties were made. Room temperature emission at 1.3 µm on as-grown NWs was achieved.

1.2 Summary of Technical progress

Year 1

The start of this grant unfortunately coincided with the move of our MBE system to a class 1000 clean room facility located in the Joint School of Nanoscience and Nanoengineering building, which is close to the NCA&TSU campus. Hence the system was not operational for almost a year as there were many problems associated with the move and compatibility to the clean room facility became a major issue. The MBE system, being one of the first generation EPI systems, also added to the complexity, as most of the components were not readily available and required almost two to three months wait period. Hence we were unable to begin on this project until almost the end of July 2012, when the MBE became fully operational.

I. Growth of Au assisted and Ga Assisted GaAs, GaAs/GaAsSb and GaAs/GaAsSb/GaAs NWs:

The first year was devoted to development of growth parameters for Au assisted growth of GaAs NWs to GaAsSb NWs and then transitioning to Ga catalyzed growth of these NWs. By the end of the first year we were successful in the growth of good quality heterostructured GaAsSb/GaAs NWs with PL emission ~1.2eV as shown in Fig.1.
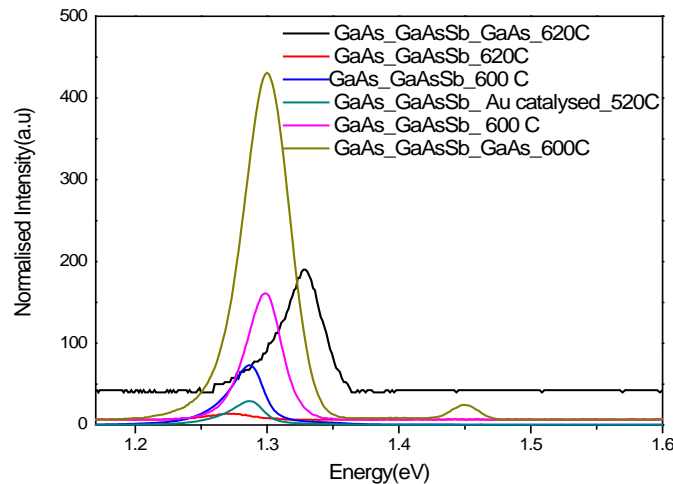

Fig.1. PL spectra of GaAs/GaAsSb and GaAs/GaAsSb/GaAs heterostructures at 10K. The energy peaks lies within the range of 1.28 -1.32 eV. The 1.45 eV peak correspond to the GaAs stem of the wire.
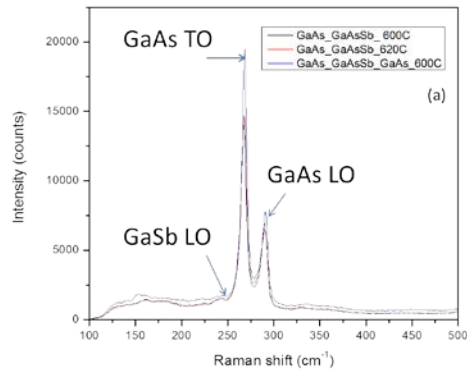
Fig.2. Raman plots of GaAsSb/GaAs NWs grown at two different growth temperatures and GaAsSb NWs with a GaAs cap.

Figure 2 displays the Raman spectra of GaAsSb/GaAs NWs exhibiting GaAs TO and LO phonon modes at 265-267cm^{-1} and at 290.1cm^{-1}, respectively, which is in good agreement with the corresponding bulk GaAs values. The full width half maxima of the TO and LO modes in the GaAs/GaAsSb NWs and the GaAsSb NWs with a GaAs cap are 7.4cm^{-1}/8.7cm^{-1} and 6.4cm^{-1}/9.4cm^{-1}, respectively. These values and the peak positions indicate the good structural quality of the NWs. In addition, the GaSb LO phonon mode at 241cm^{-1} is also observed which is upshifted by about 5cm^{-1} with respect to the bulk GaSb LO mode reported in literature. The high intensity ratio of TO to LO phonon modes of GaAs has been commonly observed in GaAs NWs and is highest for GaAsSb NW with a GaAs cap layers. This is attributed to the LO mode being forbidden from certain surface facets against no such restriction on the TO phonon modes.

II.   Student Participation and Scholarly Output

Sai Krishna Ojha, a Ph.D. candidate was trained on the MBE system.

Year 2

I.   Structural and Optical Properties of Ga-Catalyzed Segmented Growth of GaAsSb NWs.

Structural and optical characteristics of Ga assisted growth of GaAs/GaAsSb/GaAs heterostructured NWs were the focus of study.

Optical characteristics: Scanning transmission electron diffraction (STSEM) and selected area electron diffraction (SAED) analysis revealed the NW tip to be pure ZB phase with randomly

spaced stacking faults present as multiple twins in the upper third to one-quarter of the NW in the form of lamellar parallel to the $(1\bar{1}1)$ twin composition plane. Indexing of the SAED pattern confirms the ZB NW crystal growth to be [111] oriented and the twin composition planes (111) oriented. A low FWHM of ~70meV observed in the room temperature photoluminescence (PL) for the double segmented ensemble of NWs with PL peak wavelength of ~1.28eV is indicative of high quality of the as-grown NWs. The low temperature PL behavior appears to be dominated by excitons bound to shallow defects. Two non-radiative channels were identified, one a weakly-bound exciton and the other related to a deep center, which appears to be influenced by the NW configuration. The details of this work was published as Chapter 3 in "Advances in Nanosciences and Nanoengineering", CRC Press 2013 (see Appendix A). This work was also presented by the students in NAMBE and MRS Fall Meeting 2013 conferences.

> The details of this work is published as a Book Chapter3 in "Advances in Nanosciences and Nanoengineering", CRC Press 2013 as included in Appendix A.

XRD analysis of GaAsSb/GaAs NWs: Following is the work on the X-ray diffraction (XRD) rocking curve and pole figure analysis on selected GaAsSb/GaAs heterostructured NWs that were carried out to assess the degree of misalignment, orientation and texture. Figure.3 below shows the rocking curve scan for GaAs/GaAsSb nanowires grown on a Si (111) substrate which exhibits narrow and high intensities peak while Fig. 4 shows the pole figure for the {311} reflection.
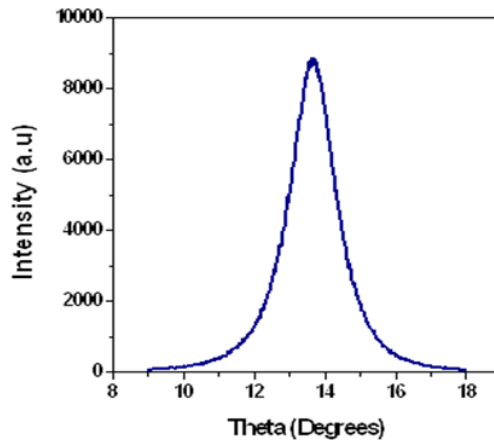

Fig.3 XRD rocking curve scan of GaAs/GaAsSb nanowires

The narrow full width and half maxima value of the rocking curve peak of 1.4^0 which is comparable to the best values reported in literature on GaAs/GaAsSb NWs and indicative of the excellent crystal quality of these well aligned NWs. This work was also presented by the students in NAMBE and MRS Fall Meeting 2013 conferences.
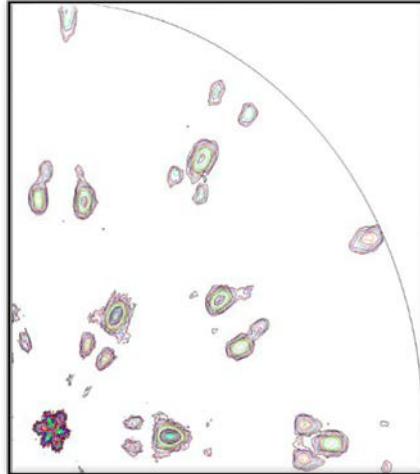
Fig.4. A segment of the pole figure for {311}

Texture data were collected on the {220} and {311} reflections as they exhibited the highest intensity next to the {111} plane. Figure 4 shows the one quarter segment of XRD scan for {311} reflection planes, showing different constant intensity contours for χ=30˚-40˚ and φ=25˚-35˚.At the center of the contour is shown the highest intensity of the diffracted beam with different color for a small segment pole figure.
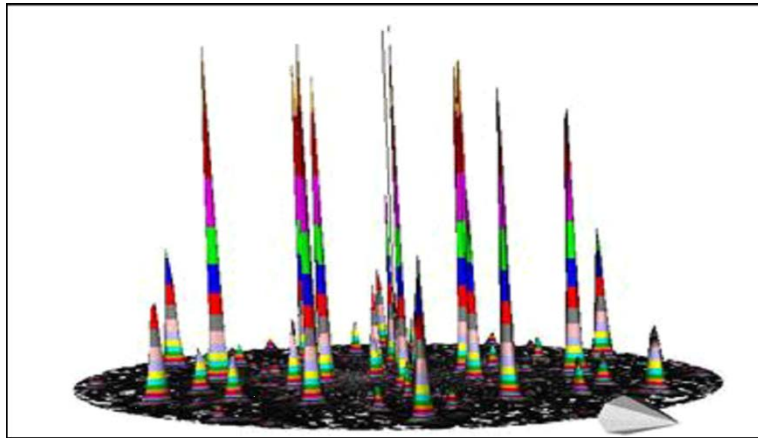

Fig.5. illustrates a 3D view of a full scan pole figure for {220} reflection of the nanowire sample at φ=90 ˚, χ=360 ˚ and 2θ=43.27 ˚. The 3D view of the pole figure encompasses the diffraction peaks of varying intensity which is color coded. The radius of the peak is representative of the width of each peak and variation in the intensity is color coded

.

Figure 5 displays the XRD full scan pole figure for {220} reflection plane at χ=90˚, φ=360˚ and 2θ=43.27˚ for the GaAs/GaAsSb (111) nanowire. The {220} reflection exhibited 50% of the maximum intensity while {311} planes were only 30% of the maximum intensity of the {111}

reflection plane. The value of 2θ for reflection plane {220} is 43.27°, step size has taken 3° in φ and χ with a count time of 10 seconds. The value of 2θ for reflection plane {311} is 51.60°, step size has taken 5° in φ and χ with a count time of 10 seconds. Finally, an abbreviated pole figure from the GaAs/GaAsSb {220} reflection was collected before each run in order to align the sample rotation, (The 2θ zero point and sample height, z, were aligned using the standard direct-beam approach.).

Thus in conclusion, the low full width half maxima obtained on the x-ray rocking curve of the (111) plane reveal high crystalline quality of the grown NWs. XRD full scan pole figures for the {220} and {311} reflections exhibited a threefold symmetry. Large intensity and low full width at half maxima further attest to the high crystal quality of the textured GaAs/GaAsSb NWs.

II.　　Ga- Catalyzed Growth of Be doped GaAs NWs

Doping incorporation in NWs is significantly more complex in comparison to the 2 dimensional and bulk structures due to the additional variants that influence the NW properties which are not existent in the higher dimensional structures. These are the effects of supersaturation in the seed melt, shell configuration with a different growth mechanism than that of the core and the structural dependence of the NW on the NW diameter. Although a dopant study was not part of the original proposal, we focused on this for two reasons. One is to demonstrate the feasibility of a photodetector structure before the expiration of this grant and secondly due to unexpected problems that we encountered in the MBE system. As mentioned above, we lost considerable time due to a defective Ga Sumo cell and also due to relocation of the MBE system. The substrate manipulator was slightly misaligned which led to substrate dropping from the substrate manipulator, blocking the Sb cell during one of the growth run. Further, as low temperature micro-PL measurements was to be operational by the end of October, an important tool for optical studies, it was decided to continue the work without the Sb cell and focused on the study of Be-doped GaAs NWs.

> Very detailed work was carried out on the Be doped NWs as described in Appendix B which has not been published as the NW density were low in the $10^7 cm^{-2}$ and the quality was not great as attested by the presence of a PL peak at 1.3 eV associated with As defect.

However, salient growth parameters for dopant optimization were identified and documented in Sai Krishna Ojha's dissertation, and the results have been used later in Year 4 to get high quality Be doped layers on chemically prepared substrates as discussed later.

This work was presented by the students in NAMBE4 and MRS Fall5 conferences 2013.

III.   Processing of GaAs NW Ensemble

Following is our preliminary work on processing of the NW ensemble that could be used for I-V measurements in order to determine the effective resistance of the doped NWs and also towards future detector fabrication. For this preliminary work intrinsic (111) Si substrates were used in an axial heterostructure configuration of Be-doped NWs. Fig. 6 (a) and (b) show SEM images of flat and top views of as-grown NWs of height of ~3-5µm. NWs were planarized using polymethlmethacrylate (PMMA) polymer with molecular weight (MW) of 950,000 with 6% anisole.
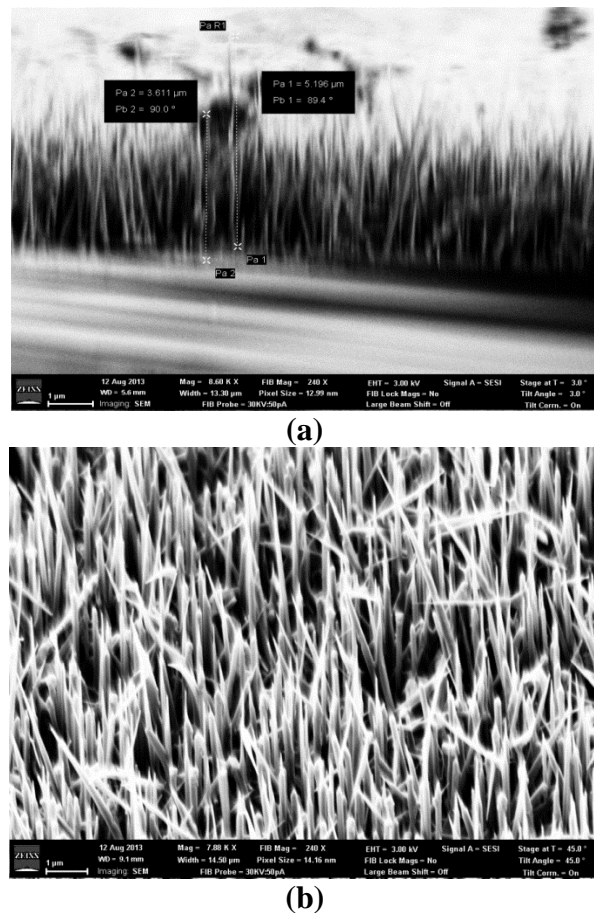

(a)

(b)

Fig.6. SEM images of NW (a) directly after growth, flat view and (b) top view.

Figure.7 shows the dependence of PMMA film thickness determined from ellipsometry with spinning speed (rpm) at 1000, 2000, 3000, and 4000 rpm for 30 seconds. The polymer was first dispensed onto the sample and was allowed to sit for 2-3 min for the polymer to seep through the NWs to spread uniformly across the surface. Based on the above data on spinning speed, PMMA was spin coated at an rpm of 1000 for 30 seconds and cured at 90°C for 1 min.
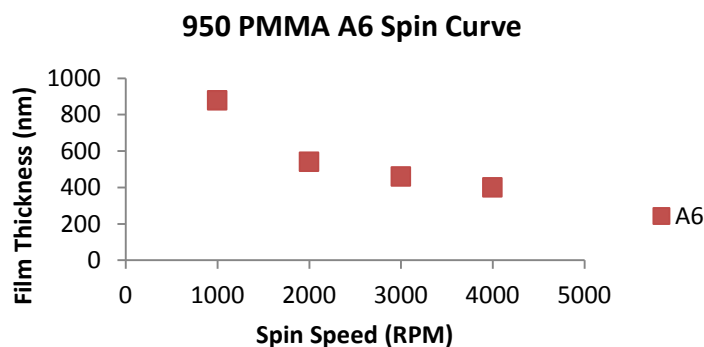
950 PMMA A6 Spin Curve

Fig.7. Spin curve showing polymer thickness with various spinning speed.

After spin coating the polymer, SEM was used to measure the thickness of the polymer. As seen in Fig.8 (a), the height of the PMMA film was found to be ~2.5-2.8μm. Thereafter, the sample was sonicated in DI water for 2 hours to remove the NW on top to achieve complete planarization as shown in Fig.8 (b). How long the sample was sonicated depends on how much of the NW is left after dispensing the polymer.

Following sonication, the sample was than underwent reactive ion etching (RIE) to expose a length of NWs for the metal contact as shown in Fig.9. The sample was plasma etched for 12 minutes with an 0_2 flow of 15sccm, pressure of 210mtorr, and a RF power of 200W. The parameters for RIE can vary depending on the NW length to be exposed to make the subsequent metal contacts.

Metal contacts were then deposited by electron beam evaporation as shown in Fig.10 (a) and (b). The top contact of Ti/Au (10/240nm) was deposited through a mask to create discrete contact pads and to prevent short circuits at the sample edges.

This was a test run to optimize all the processing parameters prior to carrying out on the actual samples of doped NWs which is currently under progress.
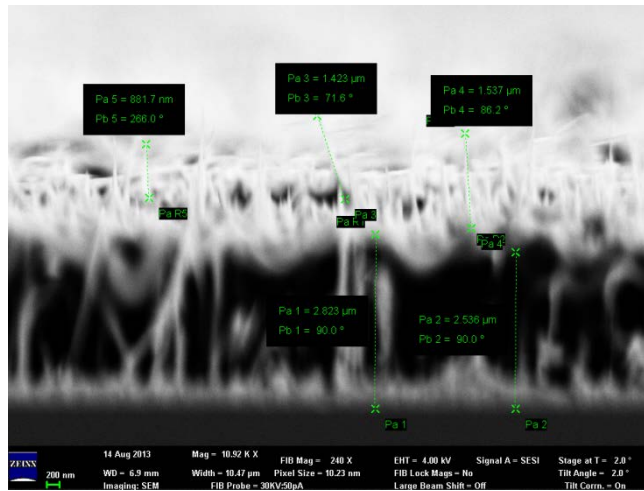
(a)
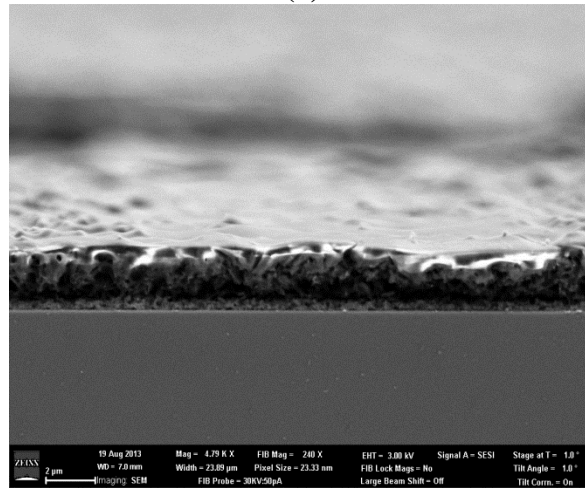
(b)

Fig.8. SEM images after (a) spin coated with PMMA and (b) after sonication in DI water.
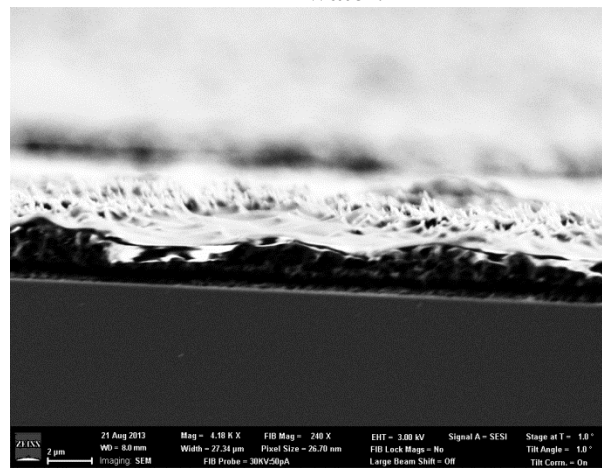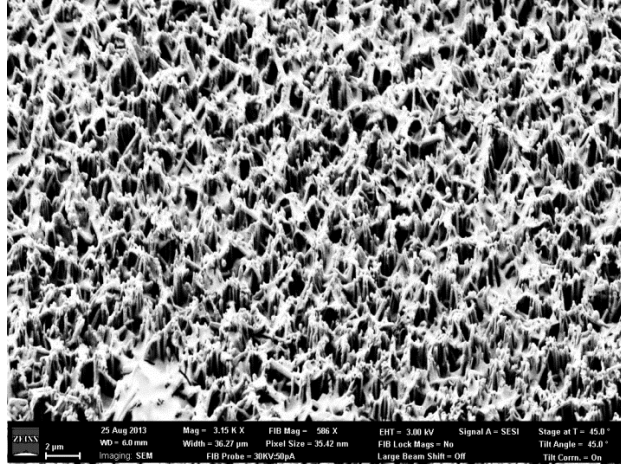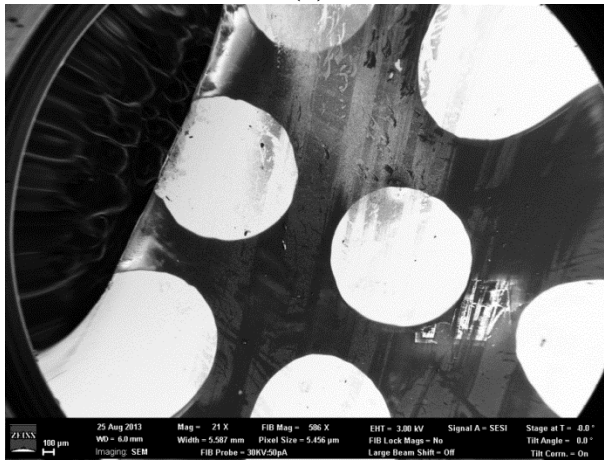

Fig.9 SEM images of PMMA after RIE etching

(a)

(b)

Fig.10 SEM images after contact deposition

IV. Equipment Installation

Installation of Sumo Cell

A Sumo cell that was purchased had a defective crucible installed in the cell, and the crucible broke that necessitated it being sent for repair. Veeco repaired it for no charge; however, as a result the system was out of commission for almost four months as the defective crucible manifested in faulty temperature readings of the cell and also in poor vacuum. So a significant amount of time was spent on troubleshooting. Shipping, repair time and repeated opening and baking of the system added to the downtime of the system. Finally the MBE system with the Sumo cell installed was operational by the middle of this year. The growth rate tremendously improved and also the quality of the NW as attested by the presence of bright reflection high energy electron diffraction (RHEED) spotty patterns as well as enhanced low temperature PL signal. The presence of the bright RHEED spots always resulted in NWs while the absence of a RHEED pattern resulted in very few or absence of NWs.

Acquisition of an Optical Closed Cycle Cryostat System and a Fiber Coupled Confocal Microscope for MicroPL Measurement of NWs

The optical closed cycle cryostat system from Montana Instruments with the sample chamber extended away from the cryostat was installed, that would allow interfacing with low working distance optical microscope for conducting µ-PL measurements. Besides this the system is specified to have low vibrations ~5nm and has a small footprint as shown in the Fig.11 with multiple optical access. Further, the sample holder can be oriented over 360 degrees and the system is user friendly for loading and replacement of the optical windows.
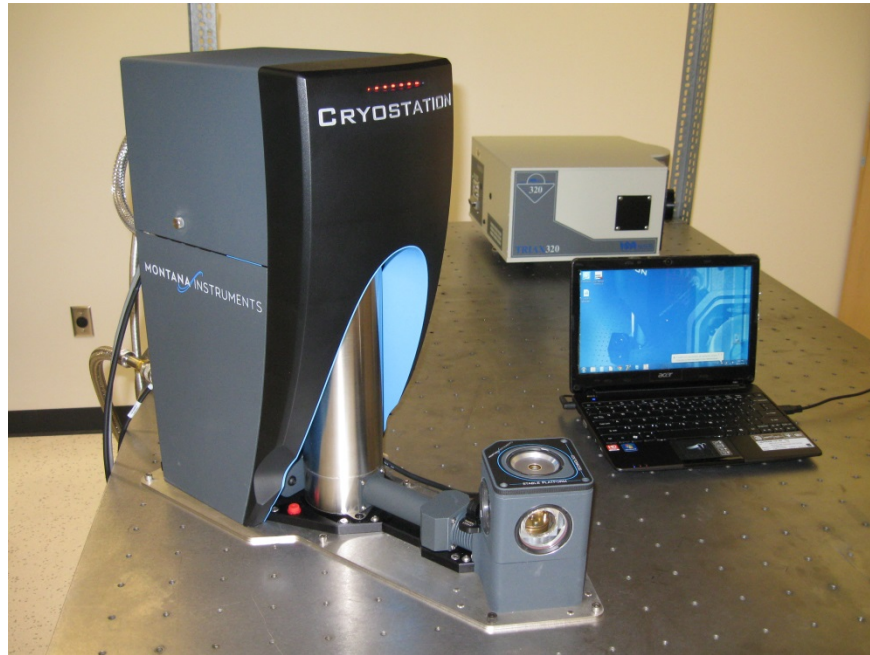

Fig.11 Photograph of optical closed cycle cryostat from Montana Instruments installed in the laboratory

V.   Student Participation and Scholarly Output

Sai Krishna Ojha, Ph.D. candidate completed his second year working on the axial segmented GaAsSb NW portion of the project. Pavan Kumar Kasanaboina who joined the PhD. program was trained on the MBE system. The above work resulted in one manuscript which has been published as a book chapter in a CRC press publication. One student presentation was made in AVS/ASM/MRS meeting 2012.

Year 3

One of the major problems that we encountered was that the NWs thus far grown were not all vertical and the NW density was low in the range of 10^7cm^{-2}. Hence one of the major focus during this grant period was a systematic study of the substrate preparation and its impact on the

vertical alignment and NW density. After the successful completion of this task, the focus of the studies reverted back to study of the effect of Sb composition on GaAsSb/GaAs core shell structures and shifting the wavelength to 1.3µm, a wavelength of great interest.

The major tasks of the project during this period are summarized below.

I. Effect of Substrate Preparation on NW Density and Orientation

For the Ga-assisted molecular beam epitaxial growth of vertical, dense and uniform GaAs core nanowires on Si (111), the effect of substrate surface preparation in combination with the growth parameters variation were examined. On an epiready substrate without any surface preparation both initial Ga shutter opening duration and V/III beam equivalent pressure (BEP) ratio play a vital role in achieving almost all vertical nanowires with moderate density $\sim 10^7 \text{cm}^{-2}$. Although a NW density as high as $3 \times 10^8 \text{cm}^{-2}$ could be achieved, not all the nanowires were vertical. Also the spatial uniformity of the nanowires was poor. Substrate surface preparation by chemical cleaning followed by oxidation in air led to highly vertical and uniform nanowires with high density (8×10^8 cm^{-2}).

> This work is currently under review with J. Electronic Materials and the manuscript is included in Appendix C.

II. Effect of Shell Growth Temperature and Sb Composition on $GaAs_{1-x}Sb_x$/GaAs core shell NWs

The morphology, structural and optical properties of the nanowires were found to be strongly influenced by the shell growth temperature and Sb% in the nanowires. The nanowires exhibit planar defects such as twins and stacking faults with more stacking faults and micro-twins found at the top section. Optical characteristics of the nanowires as measured by 4K photoluminescence (PL) exhibit a red shift to 1.2eV with increasing Sb incorporation up to 12%. The Raman spectra of reference GaAs nanowires show TO and LO modes representative of the zinc blende structure at 291cm^{-1} and 267.8cm^{-1}, respectively. Red shifts of both modes in conjunction with corresponding asymmetrical peak broadening observed in X-ray diffraction with increasing Sb incorporation are attributed to enhanced strain and disorder within the nanostructures. Nanowires of similar Sb composition but grown at different shell temperatures reveal straight nanowires with improved microstructural and optical quality when grown at higher growth temperatures. The presence of GaAs passivation layer significantly enhanced the PL intensity such that PL was observed even at room temperature.

> This work was presented in SPIE conference 2015 and was published in SPIE proceedings.2015. The reprint is included in Appendix D.

III.   Equipment Installation

Setting up of micro-PL system using Si and InGaAs photodetectors

A custom made μ-PL set up has been installed comprised of a low vibration optical cryostat from Montana Cryostation with the sample chamber extended away from the cryostat, which is interfaced with a fiber coupled confocal microscope from Horiba Jobin Yvon, Inc. The entire system has been custom designed for a working distance as low as ~310μm. It is equipped with a charge coupled device and a color TV camera for simultaneous viewing of the sample and the laser spot. Synergy software is used for data acquisition and data mining for PL measurements. The entire PL set is shown in Fig. 12(a). The NW's are excited using a 633nm He-Ne laser with a maximum power of 35.0mW. The laser (spot size estimated to be roughly about 3μm) focused on a few (2~4) NWs using an objective lens (50X, NA=0.9 Zeiss optics) as shown in Fig.12(b). The PL from the NWs is collected by the same lens, dispersed by a spectrograph (Horiba iHR 320) having a focal length of 320mm with a spatial resolution of 0.06nm. The spectra are collected by either a Si photodetector in the range of 200 to 1000nm or an InGaAs detector in the range of 900 nm to 1800 nm, which are attached to the two ports of the monochromator.

MicroPL measurements were set up which consisted of a standalone confocal microscope with an objective lens having a working distance ranging from 10.6mm to 0.21mm. This is integrated to the under white light illumination and enables visualizing the laser spot simultaneously reproducing images in the LabSpec software. It was fiber coupled to the existing monochromator in the laboratory.

(a)   (b)
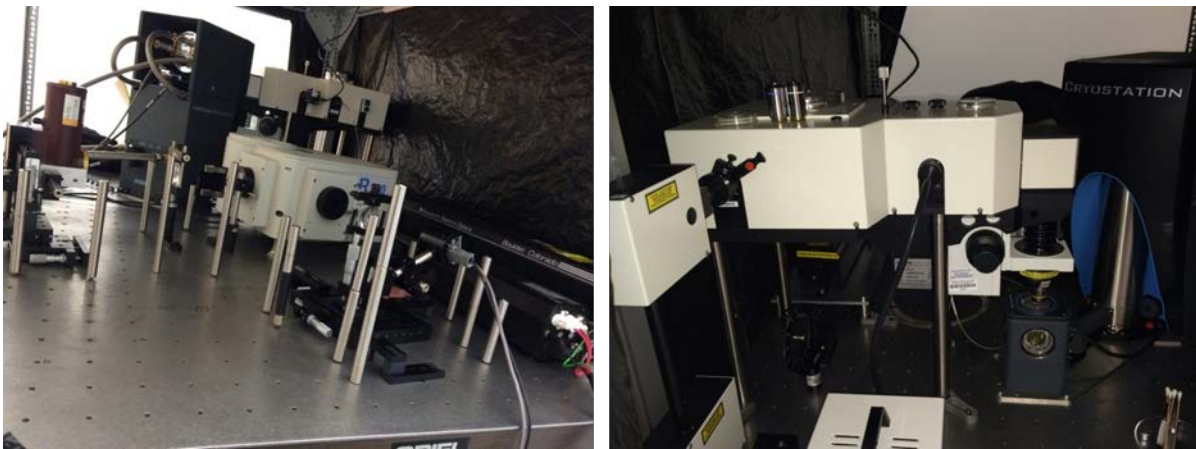
Fig.12 (a) Optical μ-PL set up, (b) Microscope setup used for focusing laser on sample

IV.   Student Participation and Scholarly Output

Sai Krishna Ojha and Pavan Kumar Kasanaboina continued to work on this project focusing on axial and core-shell GaAsSb NW growths, respectively. One more MS student, Md Shifat Us Sami, joined the group and was trained on the PL system and other characterization systems.

Nine student oral and poster presentations were made in the conferences, which include AVS/ASM/MRS Meeting 2013 at NCSU, NC; Material Research Society (MRS) Fall Meeting 2013 at Boston, MA; and Electronics Materials Conference at Santa Barbara, CA.

The work on GaAsSb segmented NW was published as book Chapter 3 in Nanoscience and Nanoengineering: Advances and Applications, Ajit D. Kelkar, Dan Herr and James G. Ryan; CRC Press.: Boca Raton FL, ISBN 978-1-4822-3119-9, 2013, pages 31-49.CRC press publication

Year 4

I.   Study of Ga- catalyzed growth of GaAs/GaAsSb/GaAs multishell NWs on chemically prepared (111) Si substrate

Abstract: In this work we present the band gap tuning up to 1.3µm in GaAs/GaAsSb core-shell nanowires, by varying the Sb content using Ga-assisted molecular beam epitaxy. Increase in Sb content leads to strain accumulation in the shell manifesting in rough surface morphology, multifaceted growths, curved nanowires and deterioration in the microstructural and optical quality of the nanowires. The presence of multiple PL peaks for Sb compositions ≥12 at% and degradation in the nanowire quality as attested by broadening of Raman and X-ray diffraction peaks reveal compositional instability in the nanowires. Transmission electron microscope (TEM) images show the presence of stacking faults and twins. Based on PL peak energies and their excitation power dependence behavior, an energy band diagram for GaAs/GaAsSb core-shell nanowires is proposed. Optical transitions are dominated by type II transitions at lower Sb compositions and a combination of type I and type II transitions for compositions ≥12 at.%. Type I optical transition as low as 0.93eV (1.3µm) from the GaAsSb for Sb composition of 26 at.% has been observed. The PL spectrum of single nanowire is replicated in the ensemble nanowires demonstrating good compositional homogeneity of the latter. A double shell configuration for passivation of deleterious surface states leads to significant enhancement in the PL intensity resulting in the first observation of room temperature emission, which provides significant potential for further improvement with important implications for nanostructured optoelectronic devices operating in the near infrared regime.

> The details of the above work have been accepted in Semicon. Science and Tech. and is scheduled to appear in the Sept. 2015 issue. The proof of the paper is included in the Appendix E.

II. Study of Ga- catalyzed growth of GaAs/GaAsSb/GaAs axial NWs on chemically prepared (111) Si substrates

Abstract: In this work we report on the effect of Sb on the optical and structural properties of GaAs / GaAs$_{1-x}$Sb$_x$ /GaAs axial NWs which were grown on (111) Si substrate by Ga assisted molecular beam epitaxy (MBE). The Sb composition in the ~3µm GaAsSb segment was varied up to 8.5 at%, which was verified by energy dispersive x-ray spectroscopy (EDXS). All the NWs exhibited a zinc blende (ZB) crystal structure and the high quality of the NWs was attested by the lack of any defects in the GaAsSb segment with mixed wurtzite and zinc blende phases towards the top of the NW as ascertained by high resolution transmission electron microscopy (HR-TEM) imaging. The vertical alignment of the NWs gradually changed to curved with increasing Sb concentration and has been attributed to increased strain in the NW. 4K micro-photoluminescence (PL) shows a red shift to 1.07eV with increasing Sb to 8.5% with a corresponding reduction in PL intensity with increasing Sb. The excitation power dependent PL of these NWs displayed a blue shift of ~15-20meV, which is characteristic of a type-II transition. With increasing Sb, the LO mode of the Raman spectra is shifted towards lower wavenumbers and also the spectra broadens. Both decreased PL intensity and broadening of PL and Raman spectra with increasing Sb suggest degradation of optical quality of the NWs.

The details of the above work in the form of a manuscript to be submitted to a suitable journal are currently under preparation and a draft copy of the manuscript is included in Appendix F.

III. Study of Be doping in GaAsSb NWs on chemically prepared (111) Si substrates Study of dilute amount of N in GaAsSb multishell NWs grown by Ga assisted MBE on chemically prepared (111) Si substrates

Abstract: The doping of Be in GaAs core and core-shell nanowires grown by Ga assisted molecular beam epitaxy have been investigated by µ-photoluminescence and Raman scattering. The band to acceptor (e, A) transition was observed in the NWs with a variation in the doping concentration. For core-shell NWs, both band to acceptor (e, A) and band to band (B, B) transitions were observed which eventually merged at higher concentration of Be (~8.2×10^{19}cm^{-3}). The incorporation of Be seems to be higher in case of higher V/III ratio of core-shell which is attested with red shift of the LO GaAs peak in Raman scattering. The presence of the peak at 1.49eV at 4K photoluminescence along with a reduction of the ILO/ITO peak ratio indicates enhanced Be doping at a Be cell temperature of 990˚C which is consistent with the linear and symmetric I-V characteristics.

The details of the above work is currently under preparation and is included in the Appendix G. It is to be noted that Be doping work as detailed in Appendix B was

repeated on chemically prepared substrate and high quality NWs were achieved as attested by PL and Raman data

IV.   Study of dilute amount of N in GaAsSb multishell NWs grown by Ga assisted MBE on chemically prepared (111) Si substrates

Abstract: Bandgap tuning up to 1.3μm in GaAsSb based nanowires by incorporation of dilute amount of N is reported. Highly vertical GaAs/GaAsSbN/GaAs core-shell configured nanowires were grown for different N contents on Si (111) substrates using plasma assisted molecular beam epitaxy. X-ray diffraction analysis revealed close lattice matching of GaAsSbN with GaAs. Micro-photoluminescence (μ-PL) revealed red shift as well as broadening of the spectra attesting to N incorporation in the nanowires. Replication of the 4K PL spectra for several different single nanowires compared to the corresponding nanowire array suggests good compositional homogeneity amongst the nanowires. A large red shift of the Raman spectrum and associated symmetric line shape in these nanowires have been attributed to carrier localization at point defects. Transmission electron microscopy reveals the preponderance of stacking faults and twins in these nanowires. The lower strain present in these dilute nitride nanowires, as opposed to GaAsSb nanowires having the same PL emission wavelength, and the observation of room temperature PL demonstrate the advantage that the dilute nitride system offers in the nanowire configuration, providing a pathway for realizing nanoscale optoelectronic devices in the telecommunication wavelength region.

The detail of the above work is published in Appl. Phys .Lett. and is included in the Appendix H.

This work also resulted in local invention disclosure and is included in the Appendix I.

V.   Student Participation and Scholarly Output

Sai Krishna Ojha and Md Shifat Us Sami completed their PhD dissertation entitled "Self-Catalyzed growth of Axial GaAs/GaAsSb Nanowires by Molecular Beam Epitaxy for Photodetectors" and MSNE Thesis entitled "Micro-Photoluminescence (μ-PL) Study of Core-Shell GaAs/GaAsSb Nanowires grown by Self-Assisted Molecular Beam Epitaxy", respectively. Pavan Kumar Kasanaboina continued working on the core-shell NWs and is near the completion stage of his dissertation.

The work carried out during this period resulted in two publications Appl. Phys. Lett. (2015) and Sem. Science and Tech (September issue, 2015) and one SPIE Proc. (2015).

Three student presentations in international conferences namely Electron. Mater. Conf. 2015, SPIE Photonics West Conference, Feb. 2015, NAMBE conference Sept 2014 and eight presentations in the local conferences which include Fitzpatrick Institute for Photonics (FIP) Annual Symposium, Duke University, Durham, NC (March 9-10, 2015), MRS/ASM/AVS

Meeting Joint Symposium. Nov. 2014, Nano manufacturing-2014, Joint School of Nanoscience and Nanoengineering, Greensboro, Sept. 2014,

2.0. Overall Summary

By the end of this grant growth of high quality, vertical orientation and high density GaAs/GaAsSb/GaAs axial and core-shell NWs were achieved. A systematic and comprehensive study of these NWs was made which provided deeper insight into the growth and effect of the Sb composition on the crystalline and microstructural, morphological and optical properties of the NWs. P-type doping of the GaAs was also a subject of investigation. Effect of N in dilute amount in GaAsSbN materials in red shifting the wavelength was also examined in detail. These studies enabled successful shift of bandgap to 1.3µm in both GaAsSb and GaAsSbN material system in the core shell configuration of the NWs. These results have shown that GaAsSb(N) NWs have significant promise for nanophotonic applications in the near-IR regime of the electromagnetic spectrum.

The laboratory served as an excellent training ground for the students and one of the students already is progressing very successfully at different levels of the interview process at Intel. The grant funds also allowed us to upgrade the MBE facility and develop the infrastructure for NW characterization.

Appendix A

S. Iyer, L. Reynolds, T. Rawdanowicz, S. Krishna Ojha, P. Kumar Kasanaboina and A. Bowen;." A Study of Ga Assisted Growth of GaAs/GaAsSb Axial Nanowires by Molecular Beam Epitaxy". Chapter 3 Nanoscience and Nanoengineering: Advances and Applications, Ajit D. Kelkar, Dan Herr and James G. Ryan; CRC Press.: Boca Raton FL, ISBN 978-1-4822-3119-9, 2013, pages 31-49.

3 A Study of Ga-Assisted Growth of GaAs/GaAsSb Axial Nanowires by Molecular Beam Epitaxy

Shanthi Iyer, Lew Reynolds, Thomas Rawdanowicz,
Sai Krishna Ojha, Pavan Kumar Kasanaboina,
and Adam Bowen

CONTENTS

3.1 INTRODUCTION

The microelectronics revolution has given rise to the concept that smaller device dimensions provide enhanced performance with an increased number of components in a circuit, higher operating speeds, and lower power consumption at a reduced cost [1]. This research has led to the vast range of semiconductor electronic and photonic devices and phenomena with which we are familiar today, such as high electron mobility and complementary metal oxide field effect transistors (FETs), lasers, light-emitting diodes (LEDs), and quantum Hall effects. Their beneficial

impact on society in general and the military in particular thus provides motivation for further downscaling to nanometer dimensions. It has been suggested that the new phenomena associated with novel nanoscale materials and devices offer the opportunity for engineering unique material properties and bottom-up assembly and to serve as the building blocks for the next generation of integrated nanosystems. In nanometer-scaled structures, radial and longitudinal quantum confinement in conjunction may also provide the ability to realize the control of electronic, optical, and magnetic properties of the materials in functional devices. Further, the relaxation of the lattice mismatch constraints, a major impediment encountered in thin-film heterostructures, provides the flexibility to integrate nanoscale heterostructures of a wide range of materials with engineered features that could lead to a new class of multifunctional devices, having high impact on the optoelectronic, nanoelectronic, and energy applications.

The current state of the art for photonic devices, namely lasers and detectors, is based on either III–V or II–VI compound semiconductors. The integration with Si-based devices poses problems, due to the large lattice mismatch, differences in thermal expansion coefficients, and polar/nonpolar issues between the two material systems. Although there are methods that permit the integration of the two different systems, the techniques are quite involved and add expense. Relaxed mismatch requirements, in conjunction with high-quality quantum heterostructures that can be synthesized in the nanowires (NWs), lend themselves to the integration of compound semiconductor-based optical devices with Si-based microelectronics, providing a multitude of functionalities, potentially leading to efficient, inexpensive, tunable infrared (IR) lasers for IR countermeasures, integrated sensor/detection systems, and other areas of photonics. That is, nanostructures enable the management of stresses and strains that allow fabrication of integrated materials systems that otherwise might not be possible.

3.2 DISTINGUISHING FEATURE OF NWs OVER THE BULK

NWs are particularly attractive for altering the physical properties of semiconductor materials in view of the high surface-to-volume ratio and the possible quantum confinement effects. Phonon transport is significantly degraded in Si NWs with diameters less than the phonon mean-free path. The measured thermal conductivity is two orders of magnitude less than that of the bulk, and more importantly, it departs from the Debye T^3 law for boundary scattering as NW dimensions become <40 nm [2]. While reduced lattice thermal conductivity may impede progress toward nanoelectronic applications, it could be an advantage for thermoelectric materials [3–5]. Higher strength and stiffness of NWs compared to bulk materials, attributed to a lower density of line defects with decreasing lateral dimensions, may have unique applications as sensors and actuators based on nanoscale cantilevers. The size dependence of the melting temperature in crystals with grains <50 nm is a well-known phenomenon [6], one, which may imply that annealing temperatures required for NWs are a small fraction of that required for bulk materials. This may be particularly relevant to dopant activation in material systems such as p-type GaN.

Quantum confinement in semiconductor structures manifests itself in a size dependence of the band gap. While a simple particle-in-the-box model predicts a d^{-2} dependence of the shift in band gap above the bulk value for semiconductor materials, InP NWs have exhibited a $d^{-1.45}$ dependence [7]. Thus, a higher effective band gap can be achieved in quantum-confined NWs with larger surface-to-volume ratios. A polarization dependence of light absorption/emission has also been observed in NWs in which the PL intensity is maximized in a direction parallel to the long axis [8]. Crystallographic direction-related luminescent characteristics have been reported for GaN NWs [9]. Furthermore, NW lasers have been achieved in both ZnO [10] and GaN [11] systems.

Charge transport in one-dimensional nanostructures is a developing research area and it has been suggested that Si NWs become insulated at sufficiently small diameters. On the other hand, GaN NWs with diameters up to ~18 nm still display semiconductor behavior. N-doped InP NWs have exhibited linear I–V behavior at room temperature and zero-bias suppression of conductance at low temperatures, which is indicative of coulomb-blockade transport [12]. Rectifying behavior has been observed in single GaN NWs with an internal p–n junction [13]. Cross-NW p–n junctions have led to the fabrication of FETs in numerous material systems, as well as LEDs, logic gates, resonant tunneling diodes, and a memory effect [1,14]. Huang et al. [15] reported an NW photonic LED array in which the emission wavelength could be tuned from 350 to 700 nm by using NWs fabricated from semiconductors of the appropriate material composition. In addition, they reported an NW-integrated optoelectronic circuit, in which an Si NW FET was employed for the drive current of a GaN-based LED. Qian et al. [16] have fabricated a tunable InGaN-based LED from a core-shell NW. Recently, a GaAs/AlGaAs core-multi-shell NW-based LED integrated on an Si substrate for operation in the near-IR region has been reported [17].

On the basis of data available in the literature for a host of material systems, from Si to III-nitrides, for example, it is clear that nanostructures offer considerable opportunities for altering the properties of bulk materials and for fabricating novel optoelectronic devices, multifunctional devices, and smart sensors.

3.3 GROWTH MECHANISM OF NWs

Among the different growth mechanisms, the vapor–liquid–solid (VLS) mechanism, originally reported by Wagner and Ellis for the growth of Si whiskers [18], is the most commonly used growth mechanism. Central to this process is the liquid metal catalyst on which the desired component of the source semiconductor in the vapor phase is soluble. The solubility of the species of interest in the liquid creates a concentration gradient in the liquid. The transport of these solutes to the metal–substrate interface causes supersaturation, leading to nucleation and subsequent NW growth. The droplet size defines the diameter of the NW growth and hence, any parameter that affects the equilibrium composition of the droplet would naturally influence the droplet size. The two important parameters that have been found to affect the droplet size are the growth temperature as well as the vapor pressure of the constituent source species [19]. When the reactant species are incorporated as the catalyst, a one-dimensional NW grows. By changing the reactant species, one can grow axial

or radial heterostructures by altering the growth conditions to achieve preferential incorporation on the catalyst or uniformly along the surface of the growing NW [20].

Among the several metals that have been used as the catalyst, Au has been the most common. However, the deep trap formation along with the high diffusivity of Au in most of the semiconductors leads to contamination of the NW and in addition, the trend toward the elimination of Au in most of the device processes in the electronics industry makes it unattractive. Hence, recently, there has been an increasing interest on the self-catalyzed growth of NWs using the low melting point of the source element as the catalyst such as Ga melt for GaAs NWs [19].

The growth of thin NWs is more desirable as it is rich in novel physics and these unusual properties can be suitably exploited for various applications. However, the downsizing of the NW diameter poses challenges, as the droplet size decreases due to (a) the increasing difficulty in the realization of supersaturation at the droplet NW interface, (b) presence of strong van der Waals interatomic forces, and (c) Ostwald ripening favoring larger-diameter droplets [21]. In addition, in the case of GaAs and InAs, there is an added complexity due to the very small internal energy difference between their zinc-blende (ZB) and wurtzite (WZ) structures [22]. Hence, the transformation from one structure to the other in these NWs is found to be a strong function of the NW diameter. Thin GaAs NWs had been grown using Au catalyst, until recently [23] where the growth of thin GaAs NWs with diameters <15 nm have been demonstrated using self-catalyzed Ga under high As vapor pressure.

The following section is a brief review of the ongoing work on Sb-based NWs with emphasis on the GaAsSb NWs, which covers an important wavelength region of communication near 1.3 μm, as this region corresponds to low losses in the optical fiber.

3.4 BACKGROUND OF Sb-BASED BINARY NWs AND GaAsSb NWs

The low band gaps associated with InSb (0.17 eV), GaSb (0.7 eV), and AlSb (1.6 eV) make Sb-based NWs of high interest for IR optical applications and high-speed electronic devices. Vaddiraju et al. [22] reported both GaSb and InSb NWs using self-catalyzed antimonidization/reactive vapor transport methods, resulting in room temperature PL emission of 1.72 μm in GaSb NWs. Chen et al. [24] reported an InSb NW-based IR photodetector grown by Au catalyst-assisted molecular beam epitaxy (MBE).

Recently, GaSb NWs were also synthesized on c-plane sapphire substrates by gold-mediated VLS growth using a metal organic vapor epitaxy (MOVPE) process with a higher growth rate and varying the V/III ratio [25]. They have reported [25] 3.5 K PL emission from 1.5 to 1.65 μm for V/III ratio ranging from 0.5 to 2. These NWs exhibited a ZB structure, as in the bulk, in contrast to the GaAs NWs that occur more commonly in a hexagonal WZ structure, due to the very small internal energy difference between its ZB and WZ structure [26]. The GaAs crystal structure has been shown to change from WZ to ZB by insertion of either GaSb [27] or GaAsSb layers [28,29], when the growth is appropriately tailored. The lower interface of GaAs/GaAsSb is found to be independent of the GaAs structure, while the upper interface of GaAsSb/GaAs is found to consist of either stacking faults or twins, depending on the GaAs structure being WZ [28,29] or ZB [30], respectively.

The band alignment, correspondingly, changed from type II, as in the bulk, with emission at 0.98 µm [28,31] to weak type I [28] with emission at 0.8 µm due to the conduction band edge of the WZ structure being slightly higher in the latter type. The Sb composition in these films was 25%. The low-temperature PL peaks seem to be distributed between 1.275 and 1.45 eV and the peak that is dominant seems to be strongly influenced by the type (ZB or WZ) of GaAs phase present above and below the GaAsSb segment [30]. Dheeraj et al. [30] have also reported on GaAsSb segments, of a few nanometers in length, sandwiched between GaAs segments axially. It is observed that the average growth rate was found to be dependent on the growth sequence of the segment on the axial wire, that is, with that of the third segment being higher than the second segment while the growth rate of the fourth segment is essentially the same or lower than that of the third segment. Similar trends for GaAs segments were observed although the structural phase for the GaAs segment was WZ as opposed to ZB in the case of GaAsSb segment. Low-temperature micro-PL exhibited a weak peak at 1.27 eV, which was attributed by the authors to the type II band alignment between the WZ phase of GaAs and ZB phase of GaAsSb.

The GaAsSb NW by itself [32] grown on a GaAs (111)B substrate, exhibits rotational twins around its (111)B growth axis, with an equal amount of twinned and untwinned orientations. More recently, Plissard et al. [29] demonstrated the growth of a GaAs/GaAsSb core with AlGaAs shell without Au as the catalyst, but instead, using the group III element Ga to induce the NW growth. The Sb composition used in the GaAsSb core was 30%, while in the shell, it was 22%. Unlike other III–V alloys such as AlGaAs, GaAsSb requires more accurate control in the composition due to the presence of the two competing group V species with differing sticking coefficients. For instance, Ga growth rate was reported [33] to affect the Sb incorporation in the NW due to both the differences in the sticking coefficients and the bonding, although its effect on the PL results was not reported. Thus, the composition of GaAsSb alloy not only seems to depend on the flux ratios but also on the individual fluxes.

3.5   STRUCTURAL AND OPTICAL CHARACTERISTICS OF MBE GROWN GaAsSb-SEGMENTED NWs

Although different techniques have been used for the growth of GaAs NWs [34], GaAsSb NWs have been grown by MBE [29], and only chemical vapor transport [35]. MBE is an ideal technique as the low deposition rate as well as rapid opening and closing of the source shutter lead to better control of the growth on an atomic level with abrupt interfaces. In addition, the presence of *in situ* monitors and the fact that the growth process is governed by the surface kinetics allowing the growth to occur under nonequilibrium conditions, makes it an attractive research tool to demonstrate the conceptual ideas prior to commercialization using much less expensive mass production tools.

In this chapter, we present our work on Ga-assisted growth of GaAsSb segments grown on the GaAs NW stems by MBE. GaAsSb/GaAs segments up to three have been realized, although only the work on these growths to two segmented

GaAsSb/GaAs is presented here. Structural and optical properties as a function of the number of segments in the NWs are presented using a variety of characterization techniques.

3.5.1 Experimental Procedure

NW growths were carried out in the EPI 930 solid source MBE system with valved As and Sb cracker sources. All the NWs were grown on EPI ready (111) Si substrates. Ga-assisted NW growths were initiated by impinging Ga flux on the substrate for 6–8 s prior to the opening of the As flux. The growth temperature for Ga-assisted growth was investigated in the range of 580–620°C. The As/Ga flux ratio was kept constant for all the samples at an As beam equivalent pressure (BEP) of 2.5×10^{-6} Torr. The NWs were characterized using *in situ* reflection high-energy electron diffraction (RHEED) and scanning electron microscopy (SEM) images from a Zeiss EVO 10 for determining NW physical dimensions and surface features. PL measurements were conducted using a He–Ne laser as the excitation source with a 0.32 m double grating monochromator for wavelength dispersion. A Si detector was used with a conventional lock-in amplifier system. A closed-cycle three-stage APD cryogenic system was used to study the variation of PL characteristics in the 10–300 K temperature range. Raman spectroscopy was carried out using HeNe laser with 633 nm excitation wavelength and a Horiba Jobin Yvon LabRam ARAMIS with a spectral resolution of 0.6 cm^{-1} for spectral dispersion. The Raman signal was detected using multichannel air-cooled charge-coupled device and the peak positions were obtained from the Lorentzian fit to the data. NW microstructure investigation and analysis were performed using conventional and high-resolution transmission electron microscopy (CTEM and HRTEM, respectively), as well as scanning transmission electron microscopy (STEM) on a JEOL2000FX and a JEOL2010F. Compositional analysis was performed using x-ray energy dispersive spectrometry (XEDS) with a super X windowless silicon drift detector (SDD) and Bruker AXS multichannel analyzer on an FEI Titan G2 60–300. The TEM sample preparation consisted of creating an NW suspension by sonication in methanol for 1 min and pipetting droplets onto a lacy Formar/carbon copper TEM grid.

The heterostructured NWs consist of a GaAs stem followed by a GaAsSb segment that was then terminated with a GaAs cap. Although the As to Sb flux ratio was 10, the Sb composition fraction was much less than 10% as determined from electron diffraction spectroscopy (EDS) characterization. The growth schematic of GaAs/GaAsSb/GaAs single-segment NWs referred to as N1-620 and N1 for the NWs grown at 620°C and 600°C, respectively, is shown in Figure 3.1a. N2 refers to two segments of GaAsSb sandwiched between GaAs sections as shown in the schematic in Figure 3.1b, grown at 600°C.
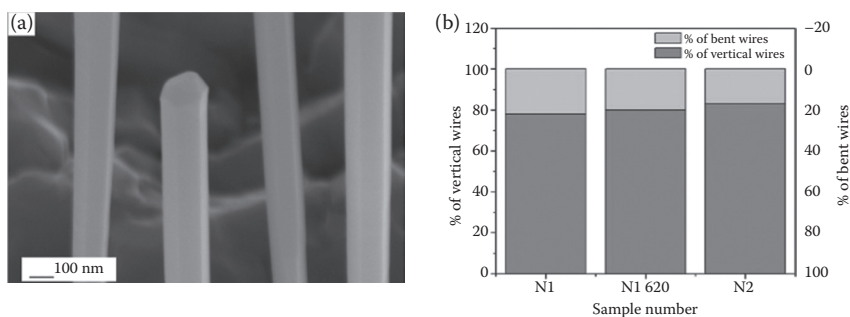
3.5.2 Scanning Electron Microscopy

Figure 3.2a displays the SEM image of NW1-620 NWs exhibiting a hexagonal shape with well-delineated surface planes and terminating with a flat top. Typically, 80% of the wires were found to be vertically oriented to the substrate (Figure 3.2b). Typical
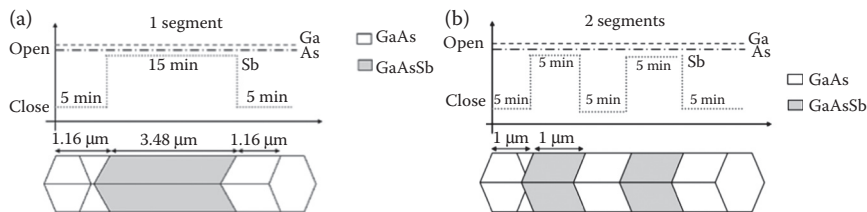
FIGURE 3.1 Growth schematics of (a) one segment and (b) two-segment NWs.

FIGURE 3.2 (a) Hexagonal-shaped GaAs NWs grown on Si substrate and (b) comparison of the percentage of vertical and bent wires in different samples taken over an area of 200 μm^2.

NW diameters were in the range of 150–180 nm and ~4–5.5 μm in length, and the NW density ranged from 4×10^6 to $3 \times 10^7/cm^2$. It is to be noted that to achieve the flat top, the As flux was left "on" after the termination of the NW growth until the substrate temperature reached 500°C.

Simultaneous closing of the As and Ga shutters results in a Ga droplet on the top of the NW as shown in Figure 3.3a. Leaving the As "on" after termination of the growth resulted in a tapered top as shown in Figure 3.3b. Thus, the tip of the NW can be suitably controlled by the As flux caused by varying Ga consumption consistent with the VLS growth mechanism.
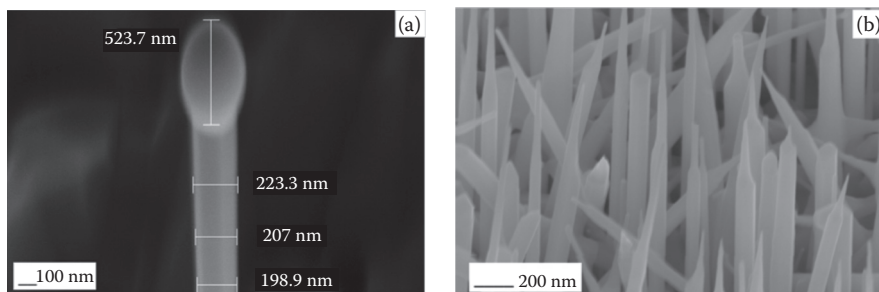
FIGURE 3.3 (a) N1 wire with Ga droplet on the top and (b) NWs with tapered top.

3.5.3 TRANSMISSION ELECTRON MICROSCOPY

Transmission electron microscope (TEM) images and associated selected area electron diffraction (SAED) patterns of NW N1-620 with a single GaAsSb segment as depicted in Figure 3.1 are shown in Figure 3.4. This NW with Ga droplet formation at the NW tip exhibited pure ZB phase verified by SAED (see Figure 3.4b) with randomly spaced stacking faults present as multiple twins in the upper-third to one-quarter of the NW in the form of lamellar parallel to the $(1\bar{1}1)$ twin composition plane. This lamellar twinned region corresponded to the cessation of
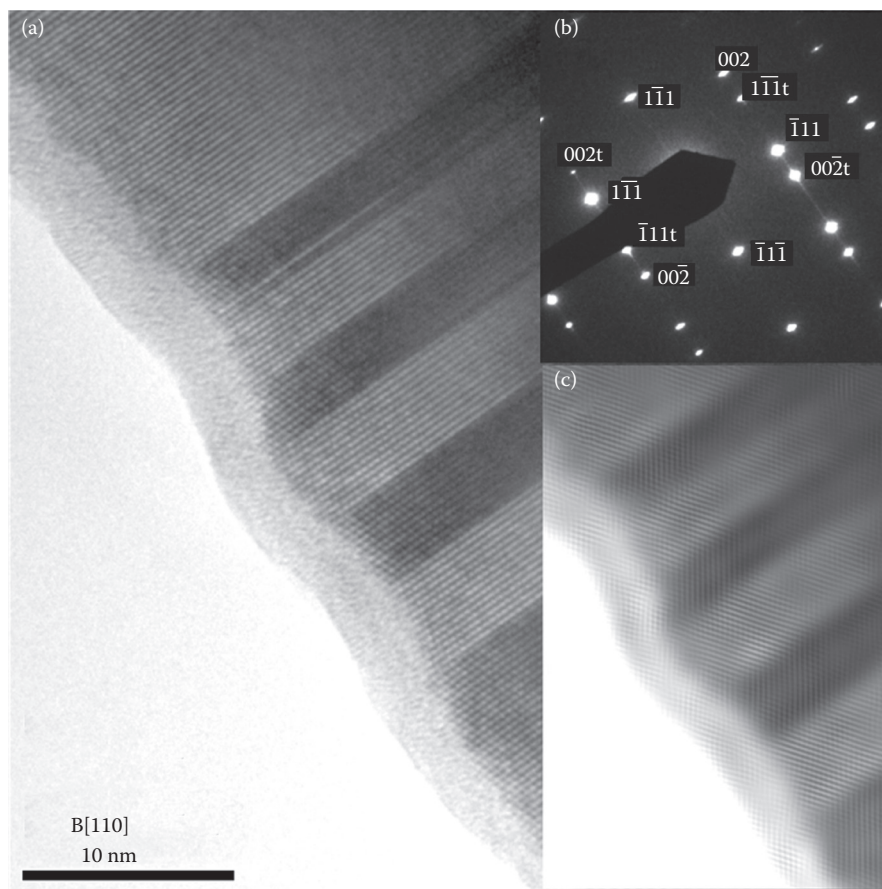
FIGURE 3.4 TEM image (a) of NW N1-620 consisting of pure ZB phase along with multiple twin boundaries. The HRTEM image (b) of twin boundaries with SAED pattern (inset) at the twin (111) plane. Fast Fourier filter of HRTEM image (c) applied to the (002) reflections of both ZB twin phases illustrates the mirroring of the (002) and (002t) planes across the twin boundary.

Sb incorporation. SAED pattern indexing confirms the ZB NW crystal growth to be [111] oriented and the twin composition planes (111) oriented.

For these GaAs/GaAsSb NWs, the twin boundary separates the crystal domains by rotation about the composition plane symmetry axis. Since the GaAs ZB crystal structure is in the F$\bar{4}$3 m space group, the [111] symmetry axis belonging to the $\bar{4}$3 m point group is parallel to the NW crystal growth zone axis. Subsequently, the ZB phases mirror one another across the twin boundary with the ZB zone axes [1$\bar{1}$1] and [$\bar{1}$1$\bar{1}$] changing directions across the twin composition plane. For ZB GaAs, the symmetry operation for a rotation about the [111] axis is a triad. Thus, the twinning operation may be a 60°, a 180°, or a 240° rotation about the twin axis. However, it is conventional to describe the twinning operation as a rotation of 180°.

For the N1-620 NWs exhibiting Ga droplets at the tip, there was no evidence of a WZ phase at any point along the NW. However, for the N1 and N2 NWs in which the tips were devoid of Ga droplets, a region of WZ phase would occur just below the tip, as shown in Figure 3.5. However, at the tip, these NWs without Ga droplets consistently terminated in the ZB phase.

The XEDS line scan shown in Figure 3.6 confirms the incorporation of Sb alloying in the NW. The Sb composition and location along the N1-620 NW was established using STEM and XEDS elemental mapping of the entire NW. This enabled quantification of the atomic weight percent of Ga, As, and Sb in selected regions with
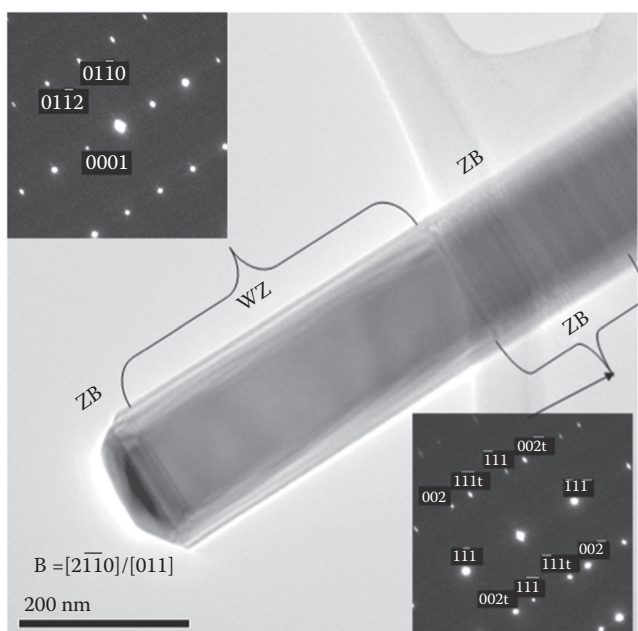
FIGURE 3.5 N2 NW without a Ga droplet at the tip and with a 400 nm region with a WZ structure just below the tip. The very tip end itself and the remaining NW below the WZ region are pure ZB with multiple twinning.

Reg3	Region 2	Region 1	
51%	51%	51%	At.wt% Ga
48%	45%	49%	At.wt% As
1%	4%	<1%	At.wt% Sb
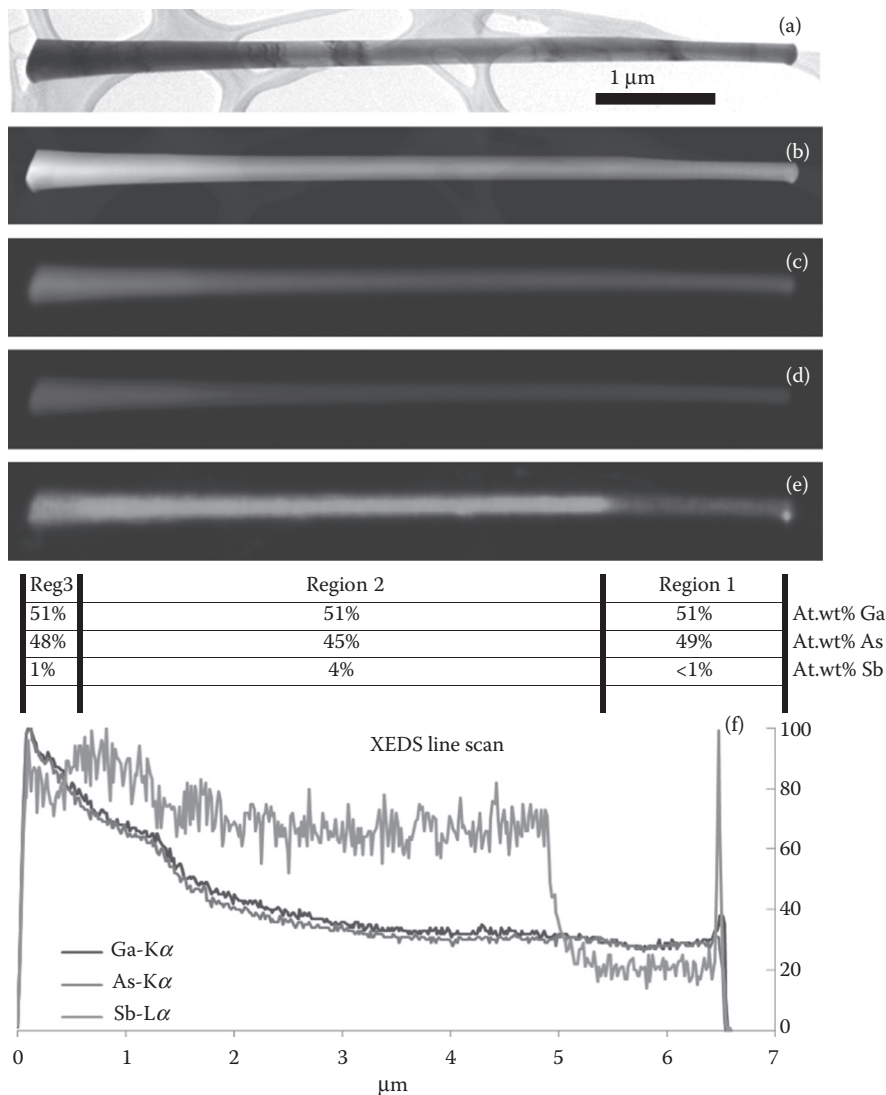
FIGURE 3.6 (See color insert.) A NW with a single GaAsSb band (Region 2 (e)) imaged with TEM (a), HAADF–STEM (b), and XEDS–STEM mapping (c) through (e) of Ga, As, and Sb, respectively. An XEDS line scan (f) shows the relative elemental x-ray count distribution along the NW axis. The collective x-ray count increases with NW diameter in the direction of the NW base.

and without intentional Sb incorporation. Although Sb was not intended to be present in Region 3 of Figure 3.6e, XEDS quantification reveals the presence of Sb due to coaxial deposition during the growth of GaAsSb segment in Region 2. One should note that the growth rate of both GaAs and GaAsSb in the NWs is ~20–25% greater than anticipated compared to the schematic in Figure 3.1a.

3.5.4 Photoluminescence

Photoluminescence is a powerful tool to investigate the optical properties of the NWs, which are greatly influenced by the surface and morphological effects due to the inherent large surface-to-volume ratio. For instance, the WZ–ZB interface in GaAs is reported to yield PL peak energies lower than the corresponding poly-types due to the two phases at the interface forming a type II band alignment [36]. Similarly, the presence of defect levels often leads to luminescence at energies below that of the band gap at low temperatures. Thus, a clear interpretation of lumines-cence spectra of these NWs requires more detailed investigations. The temperature dependence of photoluminescence determines the nature of defects and nonradia-tive recombination centers and hence is indicative of the lifetime of the carriers. In this work, we have carried out a detailed study of the temperature dependence of the PL spectra for the three NWs. Figure 3.7a displays the low-temperature PL of all the three NWs. The N2 sample exhibits the highest PL peak intensity with the spectra having a slightly asymmetric line shape with a relatively sharp high-energy cutoff.

In Figure 3.7b, the temperature dependence of the PL peak energy is displayed for all the samples. In the low-temperature regime, single-segment wires exhibit a slight red shift with decreasing temperature compared to the double-segmented NW.

The temperature dependence of the PL peak position was fitted using the Varshni equation

$$E_g(T) = E_g(0) - \frac{\alpha T^2}{\beta + T} \tag{3.1}$$

where T is the absolute temperature, $E_g(0)$ is the band gap at 0 K, and α and β are the fitting parameters. The values of these parameters for all the three samples are listed in Table 3.1. The values of α and β of the NWs are comparable to those of GaAs NWs reported in the literature. An excellent fit is obtained with the Varshni formula
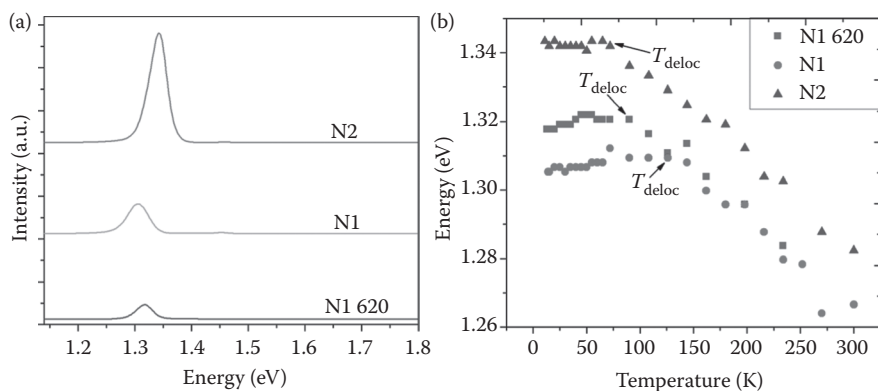
FIGURE 3.7 (a) 11 K PL spectra of the NWs and (b) temperature dependence of PL peak energy.

TABLE 3.1

Summary of Samples and Pertinent PL Parameters

Sample	Segments	Growth Temperature (°C)	α (eV/k)	β (k)	E_g (eV)	Energy at 11 K	E_a (meV)	E_b (meV)	E_{local}^{max} (meV)	T_{deloc} (°C)
N1-620	1	620	3.87×10^{-4}	251	1.328	1.31	51.4	4.5	9.8	90
N1	1	600	3.75×10^{-4}	247	1.326	1.31	47.6	6.8	20	172
N2	2	600	3.7×10^{-4}	230	1.345	1.34	84.7	10.8	0	72

for sample N2 over the entire temperature range, while for the single-segmented samples, there is considerable difference between the experimental values and those obtained using Varshni's formula for temperatures below about 110 K. That is, in these latter samples, the temperature-independent portion that is normally observed at the lowest temperatures extends to considerably higher temperatures.

In Table 3.1, we also list the values of E_{loc}^{max} and T_{deloc}, which are defined as the maximum localization energy measured as the largest energetic difference between the experimental PL peak energy and the value of the energy predicted by the Varshni relation, and the temperature at which delocalization of the carriers is complete, respectively.

These quantities are shown in Figure 3.8. The values achieved are comparable in the two single-segmented NWs, but they are considerably lower for the double-segmented NW. To understand the nature of the recombination mechanisms, the temperature dependence of the total integrated PL intensity (I_{PL}) was also measured in these samples, as shown in Figure 3.8. The integrated intensity rapidly decreases with increasing temperature, in particular, for temperatures above 80 K. A best fit to the temperature dependence of the I_{PL} was obtained using the following phenomenological expression [37]:

$$I_{PL}(T) = \frac{I_0}{1 + A\exp(-(E_a/kT))} \tag{3.2}$$

in which the presence of only one nonradiative recombination channel has been assumed in a given temperature range of investigation. I_0 is the PL intensity at $T = 0$ K and E_a represents the thermal activation energy of the first nonradiative channel, respectively.

The values of I_0, E_a, and E_b that resulted in the best fit to the experimental data in all three samples are also listed in Table 3.1. The values of E_a and E_b in the N1 and N1-620 are comparable, but are ~45% smaller than those for the double-segmented
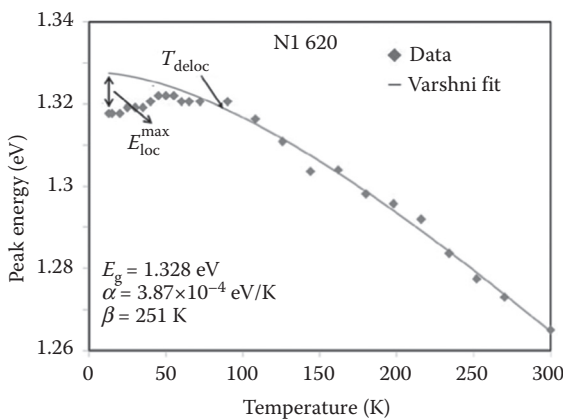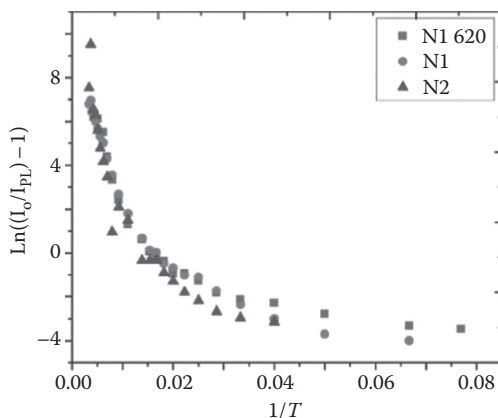

FIGURE 3.8   Varshni fit for the data of sample N1-620.

FIGURE 3.9 Temperature dependence of the integrated intensity.

sample N2. The difference between the experimental values and Varshni-predicted PL peak energy, as well as the invariance of the PL peak energy with temperature from 11 up to 80–100 K and the corresponding very-low-temperature variation of the full width half maxima (FWHM) (see Figure 3.9) in this temperature range, can be considered as a strong evidence for exciton localization. The variation in the PL peak energy as a function of temperature in these NWs can be quantitatively explained as follows: At low temperatures, the excitons are localized either at the defects induced in the NWs by surface irregularities or impurities or at the band-tail states in the density of states (DOS). The latter is more likely as the FWHM significantly varies with temperature.

As the temperature is increased above the exciton localization energy identified as T_{deloc}, the excitons become delocalized due to dissociation into electron–hole pairs. Above this, the emission energy decreases as a function of temperature due to the band gap shrinkage following the Varshni-like relation. The differences in the PL peak energies observed at low temperature (10 K) and at room temperature in all these samples seem to be similar, ~55–60 meV, and, thus, independent of the GaAsSb segment length. These values are somewhat smaller than 76 meV reported by Chiu et al. [38] in GaAsSb quantum wells (QWs) and 81 meV from the bulk values. Thus, our data suggest that downsizing radially reduces the temperature-induced band gap variation.

The delocalization temperature is the lowest for the double-segmented NW with the smallest localization energy and the effect of axial confinement results in opening of the band gap, blue shifting the PL peak energy in the entire temperature range.

The value of the FWHM of an excitonic transition in these NWs is representative of the quality of the alloy segments, as well as the extent of the interface roughness [32]. The FWHM of the N2 is the lowest in the entire temperature region, which is an indication of better optical quality of these NWs. The observed variation of the FWHM with temperature in these NW structures can be qualitatively explained as follows: At low temperatures, FWHM reflects the energy distribution of the exciton

states in the localizing potentials. As the temperature is raised, the excitons begin to become delocalized. For temperatures above T_{deloc}, almost all the excitons have become delocalized and the exciton–optical phonon interaction becomes dominant with the value of the FWHM increasing with temperature. As shown in Figure 3.9, the variation in FWHM with temperature is less and T_{deloc} is smaller in sample N2 due to the smaller range of values of the localization energies. In sample N1, the FWHM exhibits a small inverted S-curve, that is, a mild dip in the FWHM curve as the temperature approaches T_{deloc}, which is a signature of strong exciton localization normally observed in dilute nitride system [39–41]. The T_{deloc} is considerably larger for this sample. The large value of T_{deloc} is consistent with the large E_{loc}^{max} also observed in this sample.

We have analyzed the variation of I_{PL} as a function of temperature using Equation 3.2 and the values of the various fitting parameters for all three samples are listed in Table 3.1. We find that the values of E_a and E_b are comparable for the two single-segment wires, but are considerably larger for the N2 sample. For the sample N1-620, the E_b is 4.5 meV, which is in excellent agreement with exciton binding energy in GaAs. The low activation energy (E_b) and the high activation energy E_a correspond to nonradiative channels that are responsible for determining the quenching of PL intensity at temperatures below 100 K and higher than 100 K, respectively. The low values of 4–10 meV for E_b indicate that the weak excitons are bound to shallow defects. Higher E_a at 77 meV has been observed in GaAs NWs grown by Au-assisted catalyst and has generally been assigned to a deep center associated with Au-induced defects [42], which cannot be the case in our NWs since our NWs are Ga catalyzed. Such a deep center has been observed in CdS NWs [43]. The observation of such a deep exciton suggests the presence of the defect complexes in these NWs.

The room temperature PL is realized for the samples grown at 600°C and also, the low-temperature PL peak intensity was considerably higher; particularly, the N2 exhibited the highest PL peak intensity almost threefold higher than the next largest PL intensity observed in N1. Sample N1-620 had the lowest PL intensity. The lowest FWHM and smallest variation in the FWHM observed for the double-segmented wire is consistent with the better quality of this NW. Conversely, N1-620 showed significant variation in FWHM with temperature and is characterized by low PL peak intensity.

The foregoing discussion of the behaviors of the PL peak energy, excitonic linewidth, and integrated PL intensity as a function of temperature in our samples suggests that among the three NWs investigated, the double-segmented GaAsSb NW is the better quality NW with reduced defect density of localized states and of nonradiative recombination centers. The temperature dependence of the PL can be well described by a Varshni-like relation for temperatures above 100–150 K. The low-temperature behavior appears to be dominated by excitons bound to shallow defects and two nonradiative channels were found, one weakly bound exciton related and the other related to a deep center, which appears to be influenced by the NW structure.

3.5.5 Raman Spectroscopy

Raman spectra were taken at different locations and representative Raman spectra are shown in Figure 3.10 and summarized in Table 3.2 for the NWs N1 and N2 and
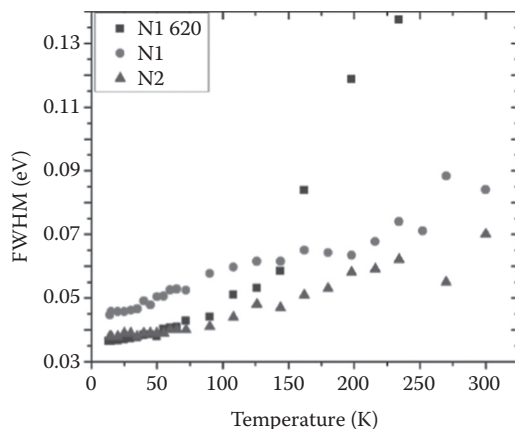
FIGURE 3.10 Temperature dependence of FWHM.

a reference GaAsSb thin film grown on a (001) GaAs substrate. For the reference sample, one should note that the GaAs-like longitudinal optical (LO) and transverse optical (TO) modes occur at 279 and 255 cm^{-1}, respectively, and the intensity of the LO mode is greater than that of the TO mode. This is not unexpected since the TO mode is forbidden for the (100) surface. Its presence is most likely associated with relaxation of the selection rules due to the presence of defects. Very weak GaSb-like TO and LO modes are also observed at 227 and 240 cm^{-1} in this reference sample. In the NW samples, the spectra exhibit GaAs-like TO and LO phonon modes at 266 and at 289 cm^{-1}, respectively, which are in good agreement with the corresponding bulk GaAs values. Compared to the reference epitaxial film, however, the GaAs-like TO and LO modes in the NWs are shifted upward by 10–11 cm^{-1}, which are opposite to the downshift in energy reported [44] in GaAs NWs. The FWHM of the GaAs-like TO and LO modes in NWs N1 and N2 are 8/8 cm^{-1} and 8/11.1 cm^{-1}, respectively. These values and the peak positions indicate good optical quality of the NWs. In addition, the GaSb-like TO and LO phonon modes were also observed at 222 and 237 cm^{-1}, respectively, in reasonable agreement with the corresponding bulk values for GaSb. Note that the GaSb-like modes are downshifted in energy 3–5 cm^{-1} compared to the reference sample. The GaSb peak intensity scales to the anticipated

TABLE 3.2

Raman Mode Data for N1, N2, and the Reference GaAsSb Epilayer Grown on GaAs

Sample	GaAs TO (cm^{-1})	GaAs LO (cm^{-1})	GaSb TO (cm^{-1})	GaSb LO (cm^{-1})	GaAs TO/ LO	GaSb TO/ LO
N1	266	289	222	235	2.2	0.8
N2	266	289	223	237	1.6	0.73
Reference	255	279	227	240	0.73	0.94
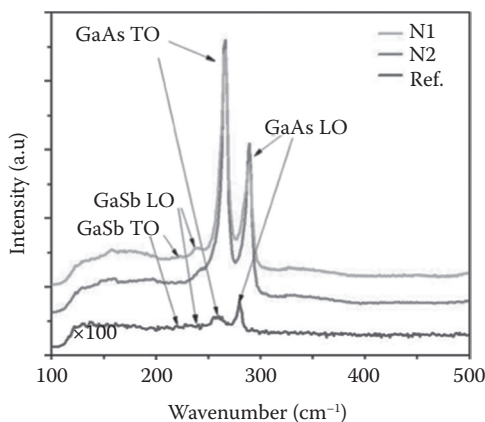
FIGURE 3.11 Raman spectra depicting the GaAs- and GaSb-like modes of NWs N1 and N2 compared to an epitaxial $GaAs_{0.95}Sb_{0.05}$ epitaxial film reference.

thickness of the GaAsSb layers in the NWs. The high-intensity ratio of TO to LO phonon modes of GaAs has been commonly observed in GaAs NWs, being the highest for N1 and is attributed [45] to the LO mode being forbidden from certain surface facets as opposed to no such restrictions imposed on the TO phonon modes. A relatively low TO/LO GaAs phonon peak ratio as well as a lower FWHM of these two in NW N2 is also indicative of better quality layers consistent with the PL data discussed earlier (Figure 3.11).

3.6 CONCLUSIONS

Segments of GaAsSb NWs on GaAs stem have been successfully grown by MBE, using a Ga-catalyzed VLS technique. The two-segmented GaAsSb NWs were found to be of excellent optical and structural quality as attested by low FWHM and their temperature variation in the corresponding PL spectra, as well as low TO/LO ratio observed for both GaAs and GaSb peaks. TEM of these NWs revealed both GaAs and GaAsSb to be of ZB phase for the wire terminating without any Ga droplet. The stacking faults and twins were found to be present in all the NWs. These are preliminary data, and further growth optimization will be initiated. Hence, a fairly good optical and structural quality of the GaAsSb NWs grown so far show great promise for applications in the 1.3 µm region and longer wavelength for optical communications.

ACKNOWLEDGMENTS

REFERENCES

1. J. X. Serge Luryi and A. Zaslavsky, *Future Trends in Microelectronics: The Nano Millennium,* (Wiley-IEEE Press, New York, 2002).
2. D. Li, Y. Wu, P. Kim, L. Shi, P. Yang, and A. Majumdar, *Appl. Phys. Lett*. 83(14), 2934–2936, 2003.
3. M. Law, J. Goldberger, and P. Yang, *Annu. Rev. Mater. Res*. 34, 83–122, 2004.
4. L. J. Lauhon, M. S. Gudiksen, and C. M. Lieber, *Phil. Trans. Roy. Soc. Lond. A* 362, 1247, 2004.
5. Y. Xia, P. Yang, Y. Sun, Y. Wu, B. Mayers, B. Gates, Y. Yin, F. Kim, and H. Yan, *Adv. Mater*. 15(5), 353–389, 2003.
6. K. F. Peters, J. B. Cohen, and Y.-W. Chung, *Phys. Rev. B* 57(21), 13430, 1998 and references therein.
7. H. Yu, J. Li, R. A. Loomis, L.-W. Wang, and W. E. Buhro, *Nat. Mater*. 2(8), 517–520, 2003.
8. J. Wang, M. S. Gudiksen, X. Duan, Y. Cui, and C. M. Lieber, *Science* 293(5534), 1455–1457, 2001.
9. T. Kuykendall, P. J. Pauzauskie, Y. Zhang, J. Goldberger, D. Sirbuly, J. Denlinger, and P. Yang, *Nat. Mater*. 3(8), 524–528, 2004.
10. M. H. Huang, S. Mao, H. Feick, H. Yan, Y. Wu, H. Kind, E. Weber, R. Russo, and P. Yang, *Science* 292(5523), 1897–1899, 2001.
11. J. C. Johnson, H.-J. Choi, K. P. Knutsen, R. D. Schaller, P. Yang, and R. J. Saykally, *Nat. Mater*. 1(2), 106–110, 2002.
12. S. De Franceschi, J. A. van Dam, E. P. A. M. Bakkers, L. F. Feiner, L. Gurevich, and L. P. Kouwenhoven, *Appl. Phys. Lett*. 83(2), 344–346, 2003.
13. G. Cheng, A. Kolmakov, Y. Zhang, M. Moskovits, R. Munden, M. A. Reed, G. Wang, D. Moses, and J. Zhang, *Appl. Phys. Lett*. 83(8), 1578–1580, 2003.
14. C. Thelander, H. A. Nilsson, L. E. Jensen, and L. Samuelson, *Nano Lett*. 5(4), 635–638, 2005.
15. Y. Huang, X. Duan, and C. M. Lieber, *Small* 1(1), 142–147, 2005.
16. F. Qian, S. Gradecak, Y. Li, C.-Y. Wen, and C. M. Lieber, *Nano Lett*. 5(11), 2287–2291, 2005.
17. K. Tomioka, J. Motohisa, S. Hara, K. Hiruma, and T. Fukui, *Nano Lett*. 10(5), 1639–1644, 2010.
18. R. S. Wagner and W. C. Ellis, *Appl. Phys. Lett*. 4, 89, 1964.
19. X. Sun, S. Wang, J. S. Hsu, R. Sidhu, X. G. Zheng, X. Li, J. C. Campbell, and A. L. Holmes, *IEEE J. Sel. Top. Quantum Electron.* 8(4), 817–822, 2002.
20. L. J. Lauhon, M. S. Gudiksen, D. Wang, and C. M. Lieber, *Phil. Trans. R. Soc. Lond. A* 420, 57–61, 2002.
21. P. W. Voorhees, *J. Stat. Phys*. 38(1–2), 231–252, 1985.
22. S. Vaddiraju, M. K. Sunkara, A. H. Chin, C. Z. Ning, G. R. Dholakia, and M. Meyyappan, *J. Phys. Chem. C* 111(20), 7339–7347, 2007.
23. G. E. Cirlin, V. G. Dubrovskii, Y. B. Samsonenko, A. D. Bouravleuv, K. Durose, Y. Y. Proskuryakov, B. Mendes et al., *Phys. Rev. B* 82(3), 035302, 2010.
24. H. Chen, X. Sun, K. W. C. Lai, M. Meyyappan, and N. Xi, Traverse City, MI, United States, 2009 (unpublished).
25. R. Burke, X. Weng, M.-W. Kuo, Y.-W. Song, A. Itsuno, T. Mayer, S. Durbin, R. Reeves, and J. Redwing, *J. Electron. Mater*. 39(4), 355–364, 2010.
26. C. Y. Yeh, Z. W. Lu, S. Froyen, and A. Zunger, *Phys. Rev. B* 46(16), 10086, 1992.
27. M. Jeppsson, K. A. Dick, J. B. Wagner, P. Caroff, K. Deppert, L. Samuelson, and L.E. Wernersson, *J. Cryst. Growth* 310(18), 4115–4121, 2008.
28. A. F. Moses, T. B. Hoang, D. L. Dheeraj, H. L. Zhou, A. T. J. van Helvoort, B. O. Fimland, and H. Weman, *IOP Conf. Ser.: Mater. Sci. Eng*. 6, 012001, 2009.

29. S. Plissard, K. A. Dick, X. Wallart, and P. Caroff, *Appl. Phys. Lett*. 96, 121901, 2010.
30. D. L. Dheeraj, H. L. Zhou, A. F. Moses, T. B. Hoang, A. T. J. van Helvoort, B. O. Fimland, and H. Weman, ISBN 978-953-7619-79-4, pp. 414, 2010.
31. D. L. Dheeraj, G. Patriarche, H. Zhou, T. B. Hoang, A. F. Moses, S. Grnsberg, A. T. J. Van Helvoort, B.-O. Fimland, and H. Weman, *Nano Lett*. 8(12), 4459–4463, 2008.
32. D. L. Dheeraj, G. Patriarche, L. Largeau, H. L. Zhou, A. T. J. Van Helvoort, F. Glas, J. C. Harmand, B. O. Fimland, and H. Weman, *Nanotechnology* 19(27), 27505, 2008.
33. J. Todorovic, H. Kauko, L. Ahtapodov, A. F. Moses, P. Olk, D. L. Dheeraj, B. O. Fimland, H. Weman, and A. T. J. van Helvoort, *Semicond. Sci. Technol*. 28, 115004, 2013.
34. K. A. Dick, *Prog. Cryst. Growth Ch*. 54, 138–173, 2008 and references therein.
35. K. J. Kong, C. S. Jung, G. B. Jung, Y. J. Cho, H. S. Kim, J. Park, N. E. Yu, and C. Kang, *Nanotechnology* 21, 435703(6pp), 2010.
36. C.-Y. Yeh, Z. W. Lu, S. Froyen, and A. Zunger, *Phys. Rev. B* 46(16), 10086, 1992.
37. T. Torchynska, J. Aguilar-Hernandez, M. M. Rodriguez, C. Mejia-Garcia, G. Contreras-Puente, F. G. B. Espinoza, B. M. Bulakh et al., *J. Phys. Chem. Solids* 63, 561–568, 2002.
38. Y. S. Chiu, M. H. Ya, W. S. Su, and Y. F. Chen, *J. Appl. Phys*. 92, 5810, 2002.
39. J. Li, S. Iyer, S. Bharatan, L. Wu, K. Nunna, W. Collis, K. K. Bajaj, and K. Matney, *J. Appl. Phys*. 98(1), 13701–13703, 2005.
40. K. Nunna, S. Iyer, L. Wu, J. Li, S. Bharatan, X. Wei, R. T. Senger, and K. K. Bajaj, *J. Appl. Phys*. 102(5), 053106, 2007.
41. S. Bharatan, S. Iyer, K. Nunna, W. J. Collis, K. Matney, J. Reppert, A. M. Rao, and P. R. C. Kent, *J. Appl. Phys*. 102(2), 23501–23503, 2007.
42. S. Breuer, C. Pfuller, T. Flissikowski, O. Brandt, H. T. Grahn, L. Geelhaar, and H. Riechert, *Nano Lett.* 11, 1276–1279, 2011.
43. T. B. Hoang, L. V. Titova, H. E. Jackson, and L. M. Smith, *Appl. Phys. Lett*. 89, 123123, 2006.
44. N. Begum, A. S. Bhatti, M. Piccin, G. Bais, F. Jabeen, S. Rubini, F. Martelli, and A. Franciosi, *Adv. Mater. Res*. 31, 23, 2008.
45. N. Begum, M. Piccin, F. Jabeen, G. Bais, S. Rubini, F. Martelli, and A. S. Bhatti, *J. Appl. Phys*. 104, 104311, 2008.

Reg3	Region 2		Region 1	
51%	51%		51%	At.wt% Ga
48%	45%		49%	At.wt% As
1%	4%		<1%	At.wt% Sb
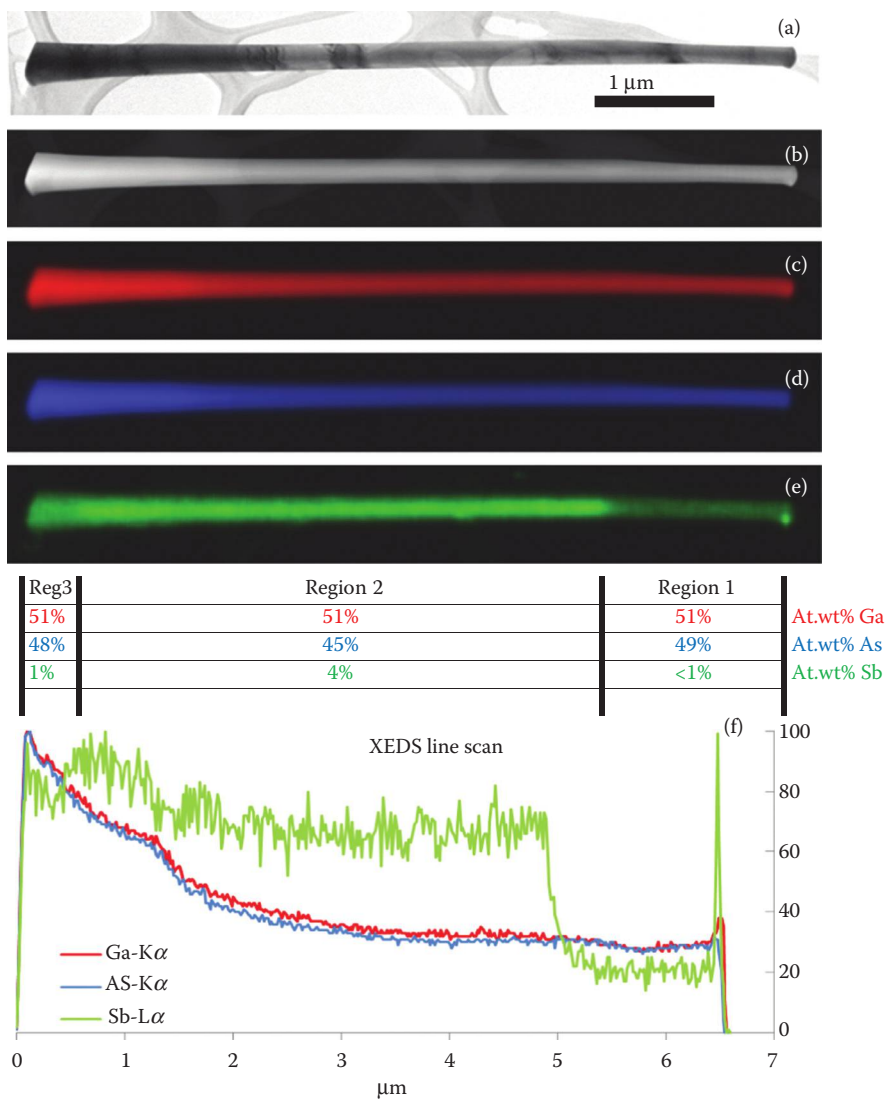
FIGURE 3.6 A NW with a single GaAsSb band (Region 2 (e)) imaged with TEM (a), HAADF–STEM (b), and XEDS–STEM mapping (c) through (e) of Ga, As, and Sb, respectively. An XEDS line scan (f) shows the relative elemental x-ray count distribution along the NW axis. The collective x-ray count increases with NW diameter in the direction of the NW base.

Appendix B

Sai Krishna Ojha, Pavan Kumar Kasanaboina, C Lewis Reynolds.Jr, Thomas A Rawdanowicz, Ryan M White and Shanthi Iyer

" A study of Be-doped GaAs nanowires grown by Ga assisted molecular beam epitaxy"

Not published

A study of Be-doped GaAs nanowires grown by Ga assisted molecular beam epitaxy

Sai Krishna Ojha[a], Pavan Kumar Kasanaboina[a], C Lewis Reynolds.Jr [b], Thomas A Rawdanowicz[b], Ryan M White[b] and Shanthi Iyer [a,c,*]

a Department of Electrical and Computer Engineering, North Carolina A&T State Univerity, 1601,E Market St,Greensboro, NC 27411,USA
Author 1email:sojha@aggies.ncat.edu,Author 2 email: pavan.kmm@gmail.com
b Department of Materials Science and Engineering, North Carolina State University, 911 Partners Way
Engineering Building I, Raleigh, NC 27606, USA
Author 3 email: lew_reynolds@ncsu.edu, Author 4 email: tarawdan@ncsu.edu, Author 5 email: rmwhite@ncsu.edu
cDepartment of Electrical and Computer Engineering/Nanoengineering, NCA&T State University, 1601 E Market st Greensboro, NC, 27411,USA

*Corresponding Author 6 email:sni0124@gmail.com Tel: +1 3362853710; Fax number: (+1) 336-500-0115

Abstract

Effective implementation of doped nanowires (NWs) in nanoscaled devices requires controlled and effective dopant incorporation. A catalyst free Ga-assisted approach for producing Be-doped GaAs NWs grown by molecular beam epitaxy is reported. A systematic and a comprehensive study is reported using a variety of characterization techniques to determine the impact of growth variants on the NW ensemble properties and thereby identify the relevant growth parameters that lead to enhanced Be incorporation. The NWs are characterized by two photoluminescence (PL) emission peaks that are attributed to Be- related near band edge (~ 1.48 to 1.51 eV) emission and surface defects (~1.35-1.39 eV). The dominance of the former, a signature of enhanced Be incorporation, is found to occur for shell configured nanowires at a lower V/III ratio and at a higher Be cell temperature of 990°C. The enhanced GaAs TO/LO Raman peak ratio exhibited by these NWs further attest to the effective Be incorporation. The NWs exhibit a mixture of zinc blende (ZB) and wurtzite (WZ) structures although terminating always in a ZB structure.

1. Introduction

Over the last decade, semiconductor nanowires (NWs) have generated great interest due to their flexibility in bandgap engineering, crystal phase, and material design. This is brought about by their one dimensional (1D) nature and high aspect ratio leading to relaxation of lattice mismatch constraints with the substrate. The realization of these NWs in technological applications requires successful controlled doping. Doping incorporation in NWs is much more complex in comparison to two dimensional structures and bulk semiconductors due to the additional pathways for doping as well as growth variants that influence the NW doping which are non-existent in higher dimensional structures. These are the effects of supersaturation in the seed melt, differing growth mechanisms of the core and the shell configuration, quantum confinement

and crystal structure dependence on NW diameter, large defect compensation caused by the huge surface to volume ratio and to a lesser extent the III-V flux ratio as well as the actual value of flux.

In bulk GaAs, Be, Zn, and C are some of the typical dopants used for p-type doping [1-3]. Amongst these, Be is the commonly used p-type dopant in molecular beam epitaxy as it has a high diffusion coefficient[4] and less memory effects[5]. Additionally, high carrier lifetime[6] and carrier concentrations [7] have been demonstrated in the layers. There have been several previous investigations on Be doping in NWs that have been reported in the literature [4, 8-10]. Hilse et al.[10] found that Be incorporation in GaAs is limited by Be interstitials, Be_I, and the ability to achieve p-type conductivity relies on incorporating Be substitutionally on Ga lattice sites (Be_{Ga}). In a core–shell structure, the Be concentration is found to be enhanced in the shell configuration compared to the simple core-only configuration due to the reduction in the depletion layer width caused by the pinning of the Fermi level at surface defects[2]. Yee et al.[11] reported the influence of Be concentration on the growth rate and attributed this behavior to the change in the droplet's chemical potential. Studies of I-V characteristics and carrier mobilities[12] have been carried out, and the absence of Coulomb blockade in heavily doped NWs[13] has been demonstrated.

As is evident from this brief literature survey, the previous studies have been focused on single NWs, and the results are somewhat scattered. For effective implementation of NWs in miniaturized devices, a study of NW ensemble is more meaningful, and a good understanding of the effect of various growth variants on doping is important in order to synthesize reproducible NWs with the desired doping. In this work, a systematic and comprehensive approach is adopted to gain further insight on the effects of growth parameters, namely Be cell temperature, V/III flux ratio, and NW core/shell configuration, on the morphological, structural, and optical

characteristics of Be-doped GaAs nanowires using characterization techniques, such as scanning electron microscopy (SEM), low temperature photoluminescence (PL), Raman spectroscopy, and scanning transmission electron microscopy (STEM). This has enabled us to identify the relevant growth parameters that strongly influence Be incorporation in the NWs.

2. Experimental details

Be-doped GaAs NWs were grown in an EPI 930 solid source MBE system equipped with a Ga SUMO cell, Be effusion cell and an As valved cracker as described in reference[14] ENREF_16. The Ga-assisted NW growth was carried out on epiready Si (111) substrates. Growth was initiated by opening the Ga cell's shutter for 8 seconds prior to simultaneous opening of As and Be shutters. The core GaAs NW growth was carried out at 600°C and was grown for 4 minutes. Growth was terminated by closing the Ga and Be shutters simultaneously, while the As shutter was closed after the growth temperature reduced below 500 °C. However, for the shell growth, the growth was again initiated with the opening of the Ga and Be shutters along with As at the substrate temperature of 465°C for 4 minutes. Flowchart 1 lists the samples reported in this work adopted for easy identification of the samples with varying Be cell temperature and V/III ratio.
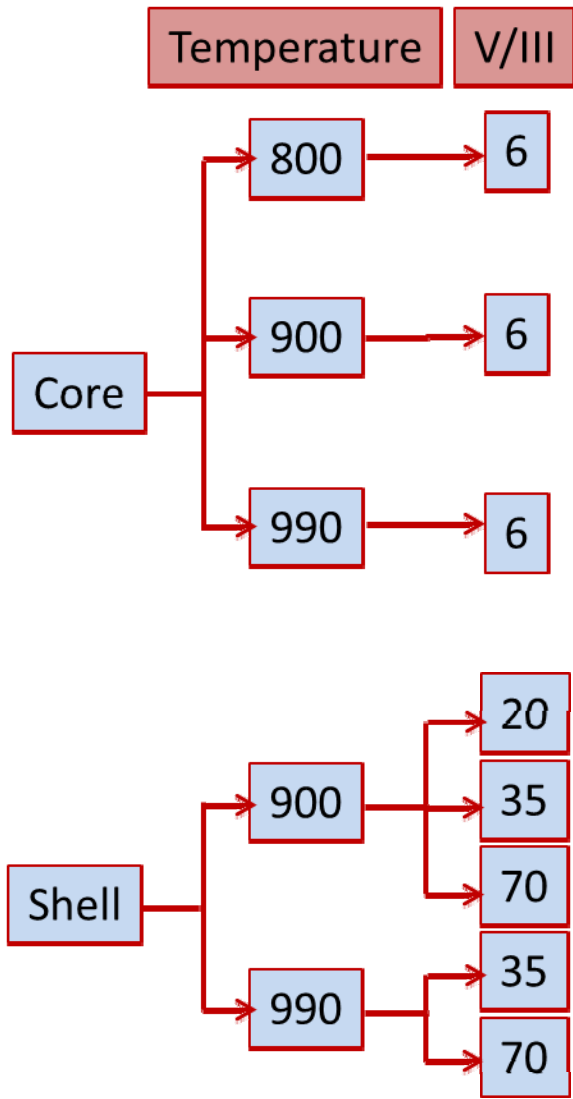
Flowchart 1: Summary of the growth parameters of the Be-doped NWs where the samples are identified based on the core/shell configuration, Be cell temperature (ºC) and V/III ratio.

PL measurements were conducted using a He-Ne laser as the excitation source with a 0.32 m double grating monochromator for wavelength dispersion. A Si detector was used with a conventional lock-in amplifier system. A closed cycle three stage APD cryogenic system was used to carry out the measurements at 10K. Raman spectroscopy was carried out in a Renishaw Ramascope using an Ar ion laser with a 514.5 nm excitation wavelength. The Raman signal was detected using a multichannel air-cooled charge-coupled device. Scanning electron microscope

(SEM) imaging was performed using a Carl Zeiss Auriga-BU FIB FESEM Microscope. The STEM analysis was performed on an aberration-corrected (probe) FEI Titan G2 system.

3. Results and discussion

3.1 Scanning Electron Microscopy and STEM

The core NWs were grown at 600˚C with a Be cell temperature of 900˚C for different V/III ratio. Figure 1 displays the variation of NW density and diameter with V/III ratio during core growth. A V/III ratio of 6 was found to be optimum for obtaining high density of NWs with minimal parasitic layer growth (two dimensional(2D) planar layer) and high photoluminesnce intensity at 10K. Typical lengths of the NWs studied were in the 1-1.5 µm range and typical axial and shell growth rates were 300 nm/min and ~ 2.00 nm/min, respectively. It is to be noted that these are typical growth rates as they were found to be a function of both the growth temperature and V/III ratio.
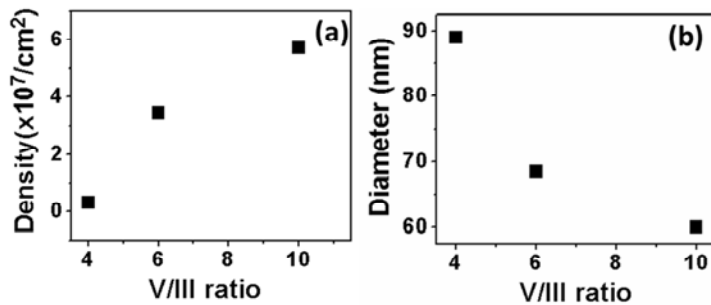
Fig. 1. Variation of (a) NW density and (b) diameter as a function of V/III ratio during core growth.

Widely different growth rates of the axial and radial growth are indicative of two different growth mechanisms being responsible in the two regimes, namely vapor liquid solid (VLS) and vapor solid solid (VSS) mechanisms, respectively.
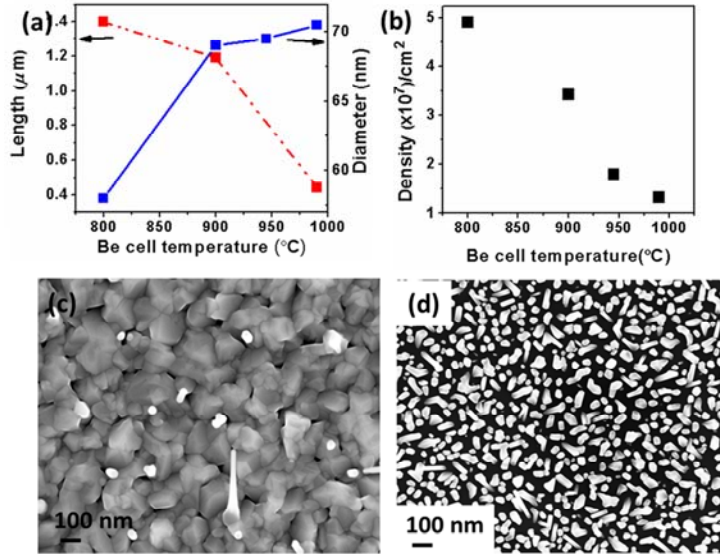
Fig. 2. : Variation of (a) length and diameter and (b) density of the Be doped GaAs NWs with increasing Be cell temperature from 800˚C to 990˚C.

As shown in Fig. 2, the axial growth rate depends on Be cell temperature. With an increase in the Be cell temperature from 800˚C to 990˚C, the axial growth rate and density of the NWs are reduced with simultaneous enhancement in the NW diameter as shown in Fig. 2 (a) and (b). This Be cell temperature dependence can be explained based on the surfactant nature of the Be dopant. The surfactant suppresses Ga adatom surface diffusivity due to a surfactant/adatom exchange mechanism [12, 17]. The decrease in Ga adatom diffusion length is thus responsible for the decrease in axial growth rate and for promoting Volmer-Weber growth which results in islanding as observed in Fig. 2 (c) and 2(d) at Be cell temperature of 800˚C and 990˚C.
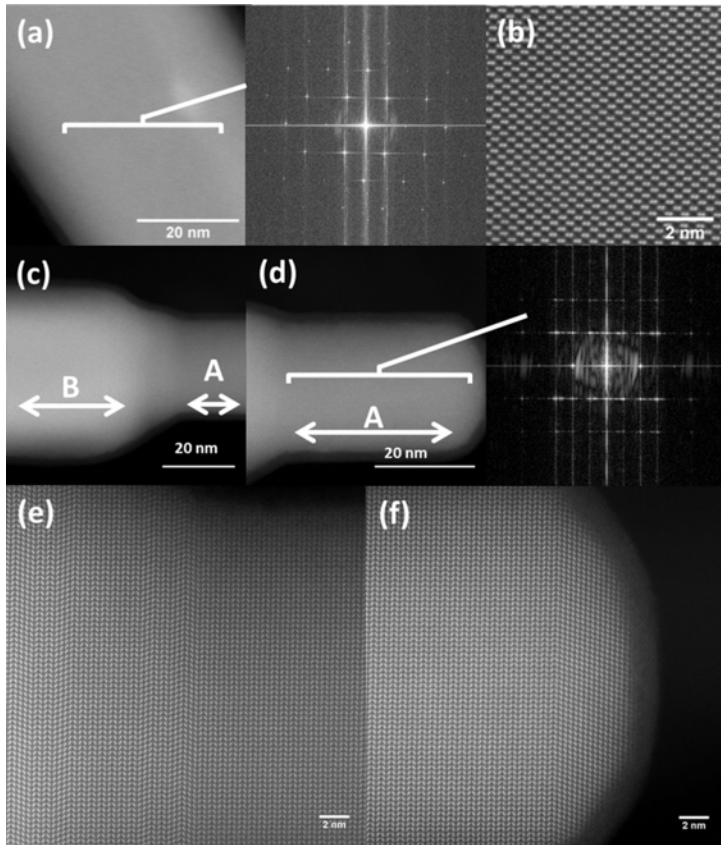
Fig. 3. (a) and (b) displays the zinc blende GaAs with GaAs dumbbells clearly visible as viewed from the [011] zone axis. (c). Image showing necking down near the NW tip from a sample with the core doped with Be at 800˚C. (d) Inset FFT of WZ region in the NW tip viewed along the [2-1-10] zone axis. WZ growth direction is <0001>. (e) Shows a transition from ZB to WZ with random twinning present. (f) The tip end of the GaAs structure is shown transitioning back to ZB.
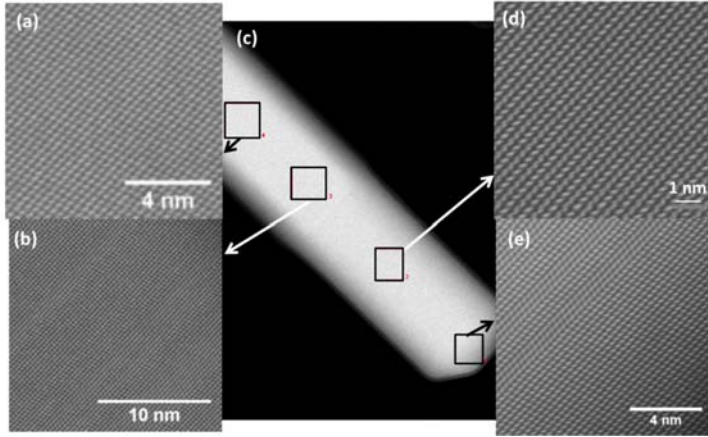
Fig. 4.(a) HAADF STEM image of NW sample C90 with Be cell temperature of 900 ˚C and V/III ratio of 6, viewed along the [011] ZB zone axis indicating a predominantly ZB region. (b) viewed along the [2-1-10]∥[011] (WZ∥ZB) zone axes indicating a transition region from twinning ZB to polytype WZ congruent with NW diameter reduction (c) HAADF STEM image with selected areas annotated for region identification and correlation of subsequent images viewed from different axes, d) viewed along the [2-1-10] WZ zone axis indicating predominantly polytype wurtzite crystal structure and e) viewed along [2-1-10]∥[011] (WZ∥ZB) zone axes at the NW tip terminating in a ZB structure.

STEM micrographs as shown in Figs. 3 and 4, of core NWs grown at different Be cell temperatures of 800 ˚C and 900 ˚C exhibit a combination of both WZ and ZB crystal structures. At the very tip of these NWs, the WZ structure transitions and terminates in a ZB structure, as shown in Figs. 4(a) and 4(e). The reduced diameter region associated with a necking phenomenon occurring near the tip of sample for 900 ˚C exhibits predominantly a WZ structure. The necking of the NW is observed only in nanowires in which the cores are doped and is not observed in undoped NWs (not shown). This behavior can be attributed to termination of the Be flux while the As flux remains "on". In the absence of Be, supersaturation is increased and with

the availability of As flux, the wire continues to grow albeit with a smaller diameter, which strongly favors the WZ structure[13, 15].

3.2. Photoluminescence and Raman analysis

Figure 5(a) shows PL spectra of two different nanowire core samples exhibiting lower 2D layer thickness with higher NW density (area coverage) and vice versa. Figure. 5(b) shows the PL of the NWs before and after sonication. The higher intensity observed in lower 2D layer thickness and higher NW density, along with vanishing of the PL signal on the samples which were sonicated strongly suggest that the PL signal originates from the NWs themselves with a higher density of nanowires providing higher PL intensity.
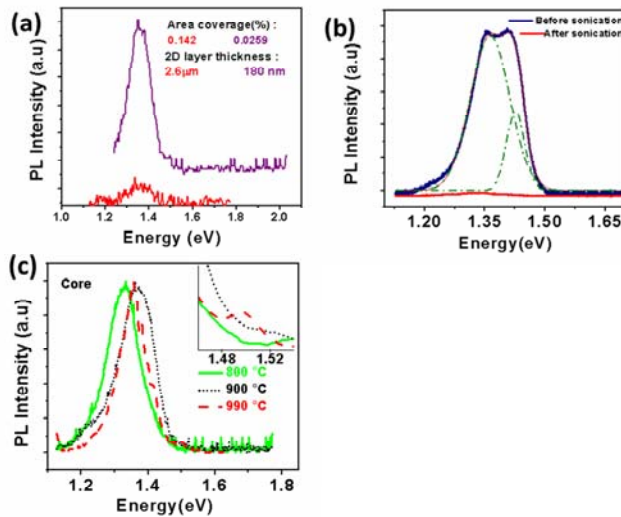
Fig. 5.(a) PL spectra for core only nanowires of two different samples with variation in NW density and 2D layer thickness for NWs grown at a Be cell temperature of 900 $^{\circ}$C. (b) PL spectra of a nanowire sample grown at 900˚C with shell III/V ratio of 70 before and after sonication and (c) PL spectra of NWs grown at different Be cell temperatures.

Figure 5(c) represents PL spectra of core NWs that were grown at different Be cell temperatures. A dominant and broad peak is observed in the range of 1.35-1.39 eV. This PL peak will hitherto be referred to as A and is associated with deep impurities and defects commonly attributed [16] to the presence of two complexes, $As_{Ga} - Si_{Ga}$ and $Si_{As} - V_{As}$. We previously reported that this is caused by diffusion of Si atoms from the Si substrate[14]. The PL peak shifted to higher energy with an increase in Be cell temperature from 800 ˚C to 900 ˚C, and no significant additional shift was observed with a further increase in Be cell temperature. Hence, extensive characterization was carried out on the NWs grown with a Be cell temperature of 900 ˚C and for the highest Be cell temperature of 990 ˚C, which exhibited a more narrow PL signal. A small peak was also observed at ~1.5 eV in all the samples except the one grown at 800 ˚C Be cell temperature. This peak becomes more well defined for NWs grown at a Be cell temperature of 990 ˚C. The PL shape of the NWs grown at 800 ˚C exhibited a long tail on the high energy side of the emission peak in contrast to that on all other samples, which showed a tail on the low energy side.
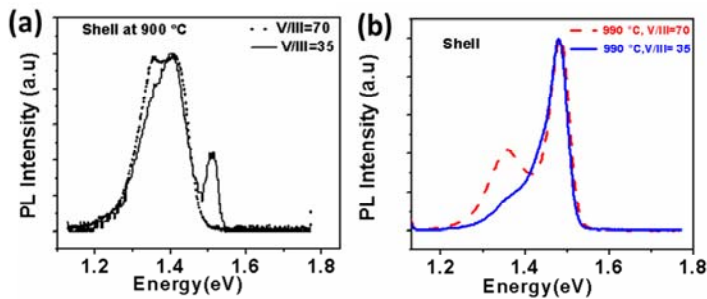

Fig. 6. PL spectra of core/shell NWs grown at Be cell temperatures of (a) 900 ˚C and (b) 990 ˚C for different V/III ratios of the shell.

In the case of core/shell NW structures for a Be cell temperature of 900 ˚C, as shown in Fig. 6(a), a blue shift in PL peak energy is observed with decreasing V/III ratio, which was achieved by

increasing Ga flux. There was no discernable PL emission for a shell V/III ratio of 20. At higher cell temperature of 990 ˚C (Fig. 6(b)), grown otherwise under identical conditions, the PL spectra indicate clear suppression of defect related peak A with the higher energy peak referred to as B shifting towards 1.5 eV. Lowering of the V/III ratio to 35 results in peak B becoming more dominant with peak A appearing as a shoulder.

Raman spectra of core and shell configurations are shown in Figs. 7(a) and 7(b), respectively, which reveal three prominent peaks at 267.7 cm^{-1}, 290.7 cm^{-1} and 521.3 cm^{-1}, corresponding to GaAs (TO), GaAs (LO) and Si (LO) peaks, respectively. Figures 7(c)-7(e) display the variation of the full width half maxima (FWHM) of the GaAs (LO) peak, GaAs LO peak intensity and TO/LO intensity ratio as a function of Be cell temperature. It is observed that all three are a strong function of Be cell temperature and are only weakly dependent on NW configuration. With increasing cell temperature, the GaAs (LO) FWHM increases while the LO intensity decreases with a corresponding increase in the TO/LO ratio. Amongst the 990 ˚C grown NW samples, the highest FWHM of the LO peak was exhibited by the shell configuration. This sample also exhibits a weak additional peak at 391 cm^{-1} as shown in Fig. 7(a), which is close to the 384 cm^{-1} observed at 77K by Hilse et al.[10] on their Be-doped NWs grown by MBE and was assigned to Be_i-Be_{Ga} clusters.
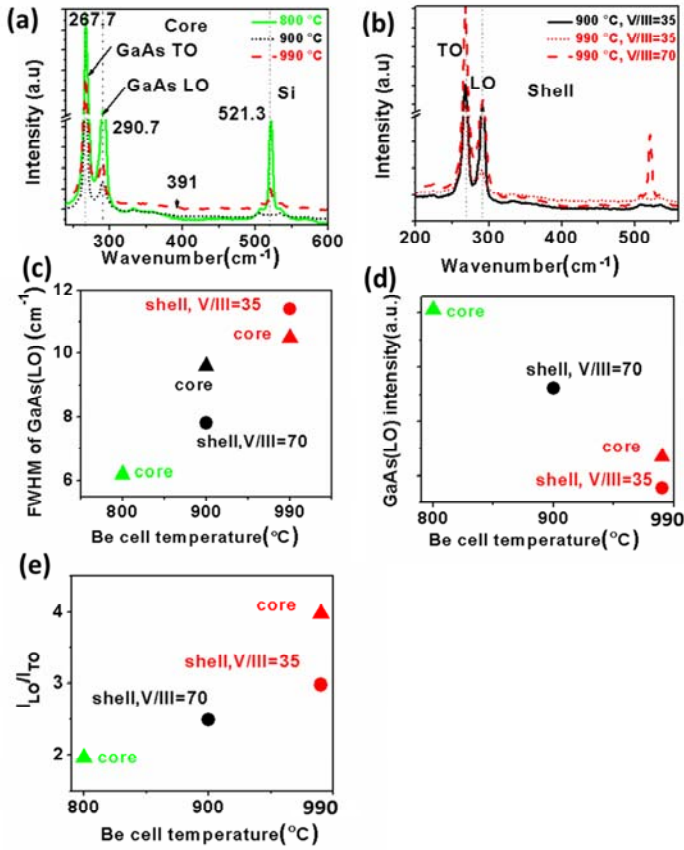
Fig. 7. Raman plots of the (a) NW core grown at different Be cell temperatures and (b) core/shell configurations. Variation of (c) FWHM of LO modes of GaAs and their (d) intensities (LO) and (e) I_{TO}/I_{LO} for the GaAs peaks as a function of Be cell temperature for core and shell configured NWs.

On the basis of the data presented above, the structural, vibrational and optical characteristics of these MBE grown Be-doped GaAs NWs exhibit a strong dependence on the Be cell temperature. For the core configuration, the NW characteristics for the Be cell temperature of 800 ºC are quite distinct from those grown at higher Be cell temperatures: i) PL peak A is slightly blue shifted and the shape is somewhat different being sharper on the higher energy side (that is, tail on the low energy side) and ii) exhibiting the highest GaAs Raman LO peak accompanied with the

14

lowest TO/LO peak intensity ratio. At the other extreme, Be-doped GaAs NWs grown at a Be cell temperature of 990 °C are characterized by: i) observation of a well-defined small peak near band edge (~1.495 eV) in addition to a more narrow defect-related PL peak A and ii) a high GaAs TO/LO Raman peak ratio as well as a high FWHM of these two individual peaks. An additional Raman peak observed at 391 cm^{-1} can be assigned to the interstitial Be, as reported [10] to be present only at high Be concentrations. The PL peak beyond 1.49 eV near the band edge is known to occur in the bulk doped layers only for the Be concentration exceeding $1 \times 10^{19}/cm^3$ [15]. The carrier concentration determined from Hall measurements on Be-doped GaAs thin films grown on a GaAs substrate at a Be cell temperature of 900 °C was $\sim 10^{20}/cm^3$. Thus, it is reasonable to consider the onset of the band edge peak near 1.49 eV to correspond to carrier concentrations in the NWs to be above $10^{19}/cm^3$. The evolution of the higher energy peak B may thus be considered as a signature of Be incorporation, which is consistent with reports in literature [16]. Thus, PL and Raman characteristics are indicative of enhanced Be incorporation in these NWs with increasing Be cell temperature. To the contrary at low Be cell temperatures, a low concentration of Be is reported[2] to pin the Fermi level at the surface due to dominance of surface defects. This in turn leads to a doping profile induced electric field quenching of low energy photons [17], which is consistent with the distinct PL behavior of this sample.

In the shell configuration, the second PL peak B in the range of 1.48 eV to 1.51 eV becomes more pronounced as shown in Fig. 6. The ratio of the peak intensity of B to A was observed to increase with a decrease in V/III ratio as well as an increase in Be cell temperature. A V/III ratio of 35 was found to be the optimum below which the PL signal vanishes. The Raman peak intensity ratio of TO/LO increases with an accompanying reduction in the individual peak intensity and broadening of the peaks for the shell configured NWs in comparison to the core

(see Fig. 7). The Si peak at 521 cm^{-1} is also reduced. Also, amongst the shell configuration all the above discussed Raman features are more accentuated with an increase in the cell temperature and for the V/III ratio of 35. All these observations suggest that Be preferentially incorporates through side facets as opposed to soluble Be within the Ga melt, which is in excellent agreement with the conclusions by Casadei *et al.* [2] on their Be-doped shell configured single NW based on electrical conductivity measurements. Further, the extended growth period resulting from the temperature ramping and shell growth also likely contribute to the continued diffusion of Be within the volume of the core [4]. It has been reported that Be atoms diffuse predominantly via a kick-out diffusion mechanism [18] in which lower As/Ga ratio promotes diffusion [19, 20]. Further variation in the As/Ga ratio from 70 to 35 was found to increase the radial growth rate by 3x. These observations provide insight on the As/Ga ratio dependence of the shell configuration on our PL and Raman data.

4. Conclusion

A detailed and comprehensive investigation on the effects of NW configuration, V/III flux ratio, and cell temperature on Be incorporation in MBE grown Be-doped GaAs NWs have been presented. Presence of PL emission in the 1.48 eV to 1.51 eV energy range and high ratio of this peak to a defect-related peak in the 1.35-1.39 eV range are signatures of enhanced Be incorporation. Be incorporation is found to be preferentially incorporated through side facets. Be cell temperature and V/III ratio of the shell strongly influence dopant incorporation.

A14-0011-001). The authors would like to acknowledge Professor Yuntian Zhu for the use of his

Raman system and Dr. Judith Reynolds for performing the Raman measurements.

REFERENCES

[1]   S. Lee, C. Fetzer, G. Stringfellow, D. Lee and T. Seong, J.Appl.Phys., 85, 3590 (1999).
[2]   A. Casadei, P. Krogstrup, M. Heiss, J.A. Rohr, C. Colombo, T. Ruelle, S. Upadhyay, C.B. Sørensen, J. Nygard and A. Fontcuberta i Morral, Appl. Phys. Lett., 102, 013117 (2013).
[3]   J.S. Lee, S. Brittman, D. Yu, H. Park, J. Am Chem. Soc., 130, 6252 (2008).
[4]   M. Tejwani, H. Kanber, B. Paine, J. Whelan, Appl. Phys. Lett., 53,2411 (1988).
[5]   J. Nagle, R.J. Malik, D. Gershoni, J. Cryst. Growth, 111, 264 (1991).
[6]   W. Walukiewicz, J. Lagowski, L. Jastrzebski, H.C. Gatos, J. Appl. Phys., 50,5040 (1979).
[7]   A.J. Moll, K.M. Yu, W. Walukiewicz, W.L. Hansen, E.E. Haller, Appl. Phys. Lett., 60 2383(1992).
[8]   K. Tomioka, J. Motohisa, S. Hara, K. Hiruma, T. Fukui, Nano lett., 10,1639 (2010).
[9]   H. Wang, L.A. Zepeda-Ruiz, G.H. Gilmer, M. Upmanyu, Nat. comm., 4 (2013).
[10]   M. Hilse, M. Ramsteiner, S. Breuer, L. Geelhaar, H. Riechert, Appl. Phys. Lett., 96 193104 (2010).
[11]   R. Yee, S. Gibson, V. Dubrovskii, R. LaPierre, Appl. Phys. Lett., 101, 263106 (2012).
[12]   Y. Cui, Q. Wei, H. Park, C.M. Lieber, Science, 293, 1289 (2001).
[13]   Y. Cui, X. Duan, J. Hu, C.M. Lieber, The J. Phys. Chem. B 104,5213 (2000).
[14]   S. Iyer, L. Reynolds, T. Rawdanowicz, S.K. Ojha, P.K. Kasanaboina, A. Bowen, Nanoscience and Nanoengineering: Advances and Applications (2014), pp 31, 50.
[15]   Y.M. Makita, Masahiko and Ohnishi,Nobukazu and Phelan,Paul and Taguchi,Takashi and Sugiyama,Yoshinobu and Tacano,Munecazu, MRS Proceedings 102 (1987).
[16]   O.M. Lysov A, Gutsche C, Regolin I, Topaloglu S, Geller M, Prost W, Tegude FJ., Nanotechnology, 22, 085702 (2011).
[17]   H.M. Jeong T, Kim J, Lim K and Youn C, Journal of the Korean Physical Society 46 , 968 (2005).
[18]   T. Tan, U. Gösele, in: P. Heitjans, J. Kärger (Eds.), Diffusion in Condensed Matter, Springer Berlin Heidelberg, 2005, pp 165.
[19]   H.P. Komsa, E. Arola, J. Pakarinen, C.S. Peng, T.T. Rantala, Phys. Rev. B 79, 115208 (2009).
[20]   R. Mosca, S. Franchi, P. Frigeri, E. Gombia, A. Carnera, M. Peroni, Mater. Science and Eng. B 80, 32 (2001).

Appendix C

Pavan Kumar Kasanaboina, Sai Krishna Ojha, Shifat Us Sami, Lewis Reynolds, Yang Liu and Shanthi Iyer, "Effect of Growth Parameters and Substrate Surface Preparation for High Density Vertical GaAs/GaAsSb Core-shell Nanowires with Photoluminescence Emission at 1.3 μm", August 2015 (Submitted to Journal of Electronic Materials)

Effect of Growth Parameters and Substrate Surface Preparation for High Density Vertical GaAs/GaAsSb Core-shell Nanowires with Photoluminescence Emission at 1.3 µm

Pavan Kumar Kasanaboina[1], Sai Krishna Ojha[1], Shifat Us Sami[2], Lewis Reynolds[3], Yang Liu[3] and Shanthi Iyer[1,2,*]

1. Department of Electrical and Computer Engineering, North Carolina A&T State University, Greensboro, NC 27411
2. Nanoengineering, Joint School of Nanoscience and Nanoengineering, NCA&T State University, Greensboro, NC 27401
3. Department of Materials Science and Engineering, North Carolina State University, Raleigh, NC 27695
* Corresponding author email: iyer@ncat.edu

Keywords: Core-shell nanowires; molecular beam epitaxy; micro-photo luminescence; III-V semiconductors; GaAs/GaAsSb

Abstract:

GaAs/GaAsSb nanowire (NW) arrays are ideally suited to meet the demands of the next generation IR photodetectors with potential for improving the detectivity. Nanowires in the core-shell geometry has the advantage of providing axial direction for long optical path for enhanced optical absorption and short radial path for charge diffusion and collection. For the Ga-assisted molecular beam epitaxial growth of vertical, dense and uniform GaAs core nanowires on Si (111), the effect of substrate surface preparation in combination with the growth parameters variation were examined. On the epiready substrate without any surface preparation both initial Ga shutter opening duration and V/III beam equivalent pressure (BEP) ratio play a vital role in achieving almost all vertical nanowires with moderate density $\sim 10^7$ cm^{-2}. Though NW density as high as 3×10^8 cm^{-2} was also achieved but all the nanowires were not vertical. Also the spatial uniformity of the nanowires was poor. Substrate surface preparation by chemical cleaning followed by oxidation in air led to highly vertical and uniform nanowires with high density (8×10^8 cm^{-2}). The GaAsSb shell was then successfully grown around the highly dense and vertical core GaAs nanowires grown at growth temperatures ranging from 550℃ to 590℃. It was found that growth temperature has a strong influence on Sb incorporation in the nanowires and hence the NW morphology and 4K photoluminescence (PL) spectra. Presence of X-ray diffraction peaks corresponding to (111) reflection only and its higher order reflections attest to the vertical alignment of nanowires. Strain in the nanowires as estimated using the Williamson-Hall isotropic strain model increases with Sb incorporation, which results in bending of the nanowires with increasing Sb. Structural properties of these nanowires using scanning transmission electron microscopy (STEM) are also presented. The temperature

dependence PL of the nanowires exhibited "S-curve" behavior, well known signature of localized exciton, with room temperature band edge PL emission occurring at ~1.3 µm.

Introduction:

Recent progress in the development of semiconductor nanowires shows a great potential to significantly impact the next generation electronic and optoelectronic devices, namely light emitting diodes [1], solar cells [2], photodetectors [3, 4], lasers [5, 6] and gas sensors [7] etc. The one dimensional nature of NW also enables unique architecture for heterostructure formation, namely core-shell configuration, which is difficult to achieve in thin film form. The core-shell configuration presents a distinct pathway for decoupling of vertical light absorption and radial carrier separation. Further, the reduced dimensions of nanowires enable better stress/strain management and provides a platform for heterogeneous integration. Thus the growth of III-V compound semiconductor nanowires grown on Si (111) provides a pathway for integrating photonics with CMOS electronics on the same substrate.

Among the different III-V alloys, GaAsSb material system in the NW configuration is very attractive due to its ability to cover the important near infrared wavelength region of the electromagnetic spectrum for telecommunications, solar cells and optical interconnects. The presence of two group V elements and surfactant nature of Sb can be strategically used to grow the highly mismatched alloy system in the NW configuration for effective bandgap engineering in the infrared region.

Growth of high density nanowires with vertical orientation and good reproducibility is an essential precursor for mass production and device implementation. Several techniques are reported to control the density of nanowires, which include pre-patterning the substrate [8, 9, 10], droplet epitaxy [11] and use of native oxide [12]. Amongst these, patterning is somewhat complex and still has several challenges [8, 10] to be addressed, while droplet epitaxy typically does not result in 100 % yield of droplet conversion to nanowires and also exhibits secondary nucleation. The control of the native oxide thickness was found to be a better alternative for obtaining all vertical nanowires of high density [12].

In this work, we investigate the effect of substrate surface preparation in conjunction with the growth parameter variation on the orientation, density and uniformity of GaAs nanowires. The optimized surface preparation and growth parameters thus enabled successful growth of core-shell GaAs/GaAsSb nanowires.

Optimization of the growth temperature of the shell resulted in growth of GaAs/GaAsSb nanowires with high Sb content of 24 at.%. The temperature dependence of photoluminescence (PL) of the nanowires revealed emission from localized exciton at low temperature with room temperature PL emission occurring at ~1.3 µm.

Experimental Details:

All the NW growths were carried out on Si (111) substrates in an EPI 930 MBE system equipped with As and Sb cracker sources. Optimization of growth parameters was carried out on GaAs nanowires grown on epiready Si (111) substrates, which had not undergone any surface preparation. A substrate temperature of 620 ˚C was used and Ga assisted self-catalyzed growth was initiated by opening the Ga flux prior to As$_4$ flux. Both initial Ga shutter opening duration and V/III BEP ratio were varied and optimized conditions were determined to achieve all vertical nanowires. The variation in V/III BEP ratio was implemented by changing only the As$_4$ flux. The effect of surface preparation of the substrate prior to the growth was also the subject of study. Substrate surface preparation consisted of complete removal of the native oxide by using a Piranha/HF solution followed by oxidation at room temperature. The thickness of native oxide on Si (111) substrate was controlled by oxidation time. Subsequent growth optimization was carried out for a Ga shutter opening duration of 15 seconds. These optimized parameters were then used for the growth of the GaAs core in a GaAs/GaAsSb core-shell nanowire configuration on Si (111) chemically treated substrate, as discussed above. For the shell growth, the substrate temperature was lowered and variable growth temperatures in the range of 570 ˚C - 590 ˚C were examined. Shell growth was initiated by opening Sb flux. The substrate was held stationary for all the growths. The nanowires were characterized using scanning electron microscopy, X-ray diffraction and µ-PL systems. The details of characterization tools used are given in our previous works [13, 14].

Results and Discussion:

The growths of GaAs nanowires were carried out at a growth temperature of 620 ˚C. The effects of different growth parameters, namely V/III BEP ratio and initial Ga shutter opening duration prior to opening of the As flux for growth on the NW density and maximum yield of vertical nanowires, are summarized in Fig. 1.
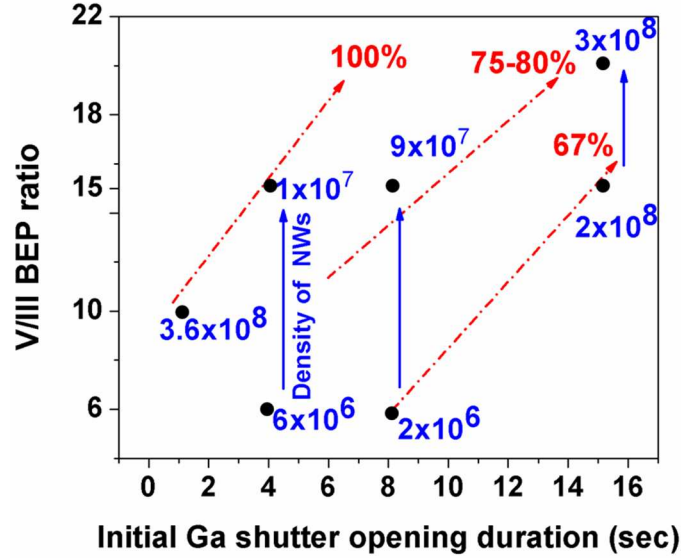
Fig. 1. Variation of NW density with respect to Ga shutter opening duration and V/III BEP ratio. The red dotted lines show the extrapolation for constant percent of vertical nanowires with varying Ga opening duration and V/III BEP ratio.

The data reveal the combination of initial Ga shutter opening duration and V/III BEP ratio for a specified NW density and percent of vertical wires. Though the data is limited, Fig.1 shows a systematic behavior in variation in both NW density and vertical orientation of nanowires with Ga shutter opening duration and V/III BEP ratio. For a constant initial Ga shutter opening duration, higher V/III ratio results in more vertical oriented NW growth with a higher NW density. Conversely, for a constant V/III ratio, there is a threshold Ga opening corresponding to all vertical nanowires and above which the percentage of vertical wires decreases. In Ga-assisted epitaxy, it is well known [15, 16] that Ga is immobilized by the nano-pores created either naturally in the oxide layer or as a result of Ga reacting with the oxide layer. Our observations can be qualitatively explained by understanding the relationship between the shape of the droplet covering the nano-pore to the orientation of the nanowires. Nanowires will grow in a vertical [111] direction only when the NW bottom is epitaxially in contact with Si (111) substrate with the contact angle of the Ga droplet with respect to the surface close to 90° [12]. As all the growth processes were carried out at the same growth temperature in ultrahigh vacuum environment, the oxide layer thickness may be assumed to be the same for all our samples. For a constant V/III BEP ratio used for the growth, if the Ga opening is above or below the threshold then the contact angle deviates from 90° and promotes non-vertical growth. For a constant Ga opening duration and for a lower V/III BEP ratio during the growth, relatively less As adatoms are on the surface impacting

5

the nucleation density and hence reduction in the NW density as well. Conversely, higher V/III ratio implies a larger supply of As adatoms, higher consumption of Ga towards crystallization due to the large supersaturation, thus promoting vertical growth. It also leads to enhanced nucleation sites of the growth resulting in a larger NW density. In our case, we have not attempted to exceed the V/III BEP ratio corresponding to all vertical growth. Increased Ga opening duration leads to more Ga atoms being deposited on the surface prior to the growth, which in turn necessitates higher supersaturation for growth to occur and shifting the condition for similar NW density and all vertical nanowires towards higher a V/III BEP ratio. Thus, the optimized condition corresponding to all vertical nanowires with a density in the high 10^7 cm^{-2} range with reasonable operating growth fluxes and growth rate corresponded to the low Ga opening shutter duration of ~4 sec. Though a NW density as high as 3×10^8 cm^{-2} can be observed for high Ga shutter opening duration of 15 sec, significant percent of nanowires were non-vertical. Thermal annealing for different durations in the ultrahigh vacuum at higher temperatures also did not provide significantly any different result. It is to be noted that, uniformity of the nanowires was poor. This provided a hint that the thermal annealing of the substrate in the ultrahigh vacuum prior to the growth is not sufficient to make the native oxide thin and is likely preventing Ga from contacting the substrate. This may cause the nano-pore size opening to be small.

In order to achieve all vertical nanowires at higher Ga shutter opening durations, larger nano-pore size formation is required, which implies smaller oxide layer thickness [12]. Hence, we investigated the effect of chemical etching of the native oxide followed by oxidation in air of the substrate for the desired duration to yield better control on the oxide layer thickness. A Piranha/HF solution was used to strip off the native oxide from the Si (111) substrate; thereafter, oxidation was carried out in air. All vertical and uniformly distributed nanowires with high density in the range of ~8×10^8 cm^{-2} (Fig. 2) were achieved for a Ga shutter opening duration of 15 sec with a V/III BEP ratio of 20. The oxide layer thickness as determined from ellipsometry was ~9.1±2 Å, which is consistent with the optimized oxide thickness value determined by Matteini et al. [12], on their GaAs nanowires. The length and diameter of the core GaAs nanowires were ~4 μm and 90 nm, respectively. It is to be pointed out that the reproducibility from run to run was good for this substrate preparation procedure and the growth window also was not found to be very stringent.
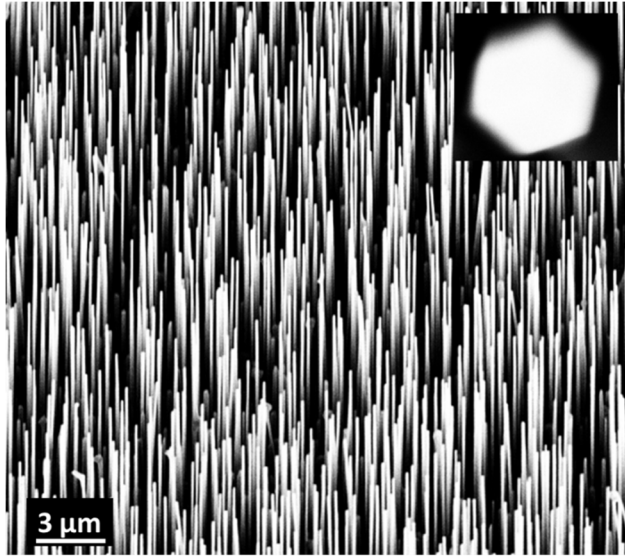
Fig. 2. Tilted view (45 degree) of GaAs nanowires grown on optimized chemically treated Si (111) substrate (inset: top view of the NW).

Thus, we conclude that the substrate preparation prior to growth is highly critical for achieving vertical orientation, uniform distribution and high density nanowires. Chemical treatment and subsequent oxidation of the substrate yields the best results as it enables better control of the native oxide layer thickness on Si (111). Ga opening duration prior to the growth and V/III ratio can then be suitably tailored to achieve vertically oriented nanowires.

This optimized condition for core GaAs growth was then used for GaAs/GaAsSb core-shell NW growth. Figure 3 displays SEM images of core-shell NW growth for shell growth temperatures varying from 570 ˚C to 590 ˚C with the core GaAs growth carried out at 620 ˚C for the same growth duration as that of other GaAs nanowires. All the fluxes were held constant. The typical length and diameter of the core-shell nanowires are ~4 µm and ~200 nm, respectively. Invariant length and increased diameter of the core-shell nanowires confirm the radial growth. For Sb/As BEP ratio of 20, increasing the shell growth temperature from 570 ˚C to 590 ˚C decreases the Sb incorporation in the NW from 12 at.% to 4 at.%, respectively, and the nanowires also became more vertical. With a rise in growth temperature, the increased desorption of Sb lowers the Sb composition. This in turn implies lower mismatch between the core and the shell leading to less accumulated strain in the shell resulting in vertical nanowires. The vertical nanowires are transformed to curved nanowires on doubling the Sb flux (Fig. 3d) with the

growth temperature held constant at 590 ˚C. Direct confirmation of the increased strain in curved nanowires were also borne out by X-ray diffraction analysis.
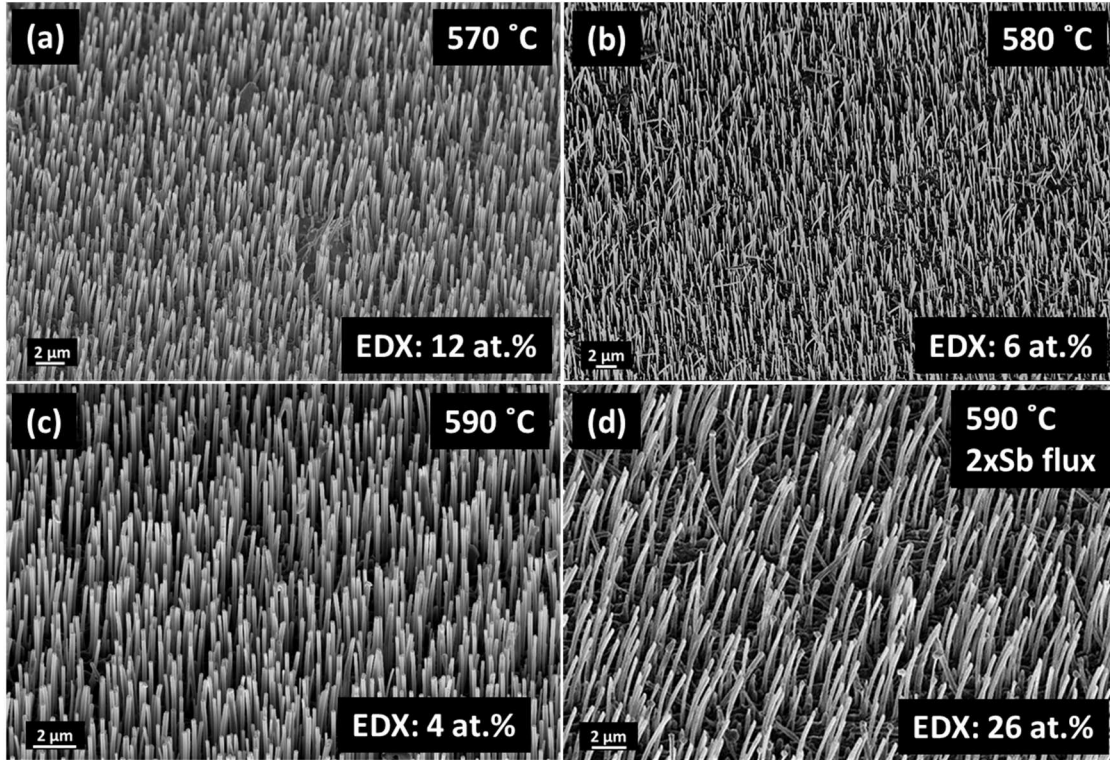
Fig. 3. Effects of growth temperature and Sb flux on GaAs/GaAsSb core-shell nanowires.

X-ray diffraction spectra of all the nanowires displayed reflections corresponding to only GaAs (111), GaAsSb (111) and Si (111) orientations confirming the NW growth along <111> direction (figure not shown). We focused on detailed analysis only on the 4 at.% and 24 at.% nanowires grown at 590 ˚C. The 24 at.% Sb NW displays a distinct broad GaAsSb (111) peak in contrast to 4 at.% NW which exhibited only broadened GaAs (111) peak as shown in our earlier reports [13, 14]. Strain in the GaAsSb shell was estimated by Williamson-Hall analysis using GaAsSb peak broadening [13, 14]. The strain values estimated for 4 at.% and 24 at.% Sb content in the GaAsSb shell are 0.0021 and 0.0076, respectively. The curved nanowires display more strain accumulation compared to vertical nanowires.

Figure 4a illustrates a representative TEM image of $GaAs/GaAs_{0.96}Sb_{0.04}$ core-shell NW. nanowires exhibit zincblende structure as evidenced by high resolution HAADF (High-Angle Annular Dark-Field) STEM image as

shown in Fig.4b. The EDS line scan through the cross-section of the wire revealed non-uniform distribution of Sb concentration across the radius as shown in Fig.4c. This may be attributed to lack of substrate rotation during the growth and any resultant shadowing effect accentuating the Sb composition on one side of the shell in comparison to other. This also may be another likely contributing factor for the curving of the NW at higher Sb concentration.
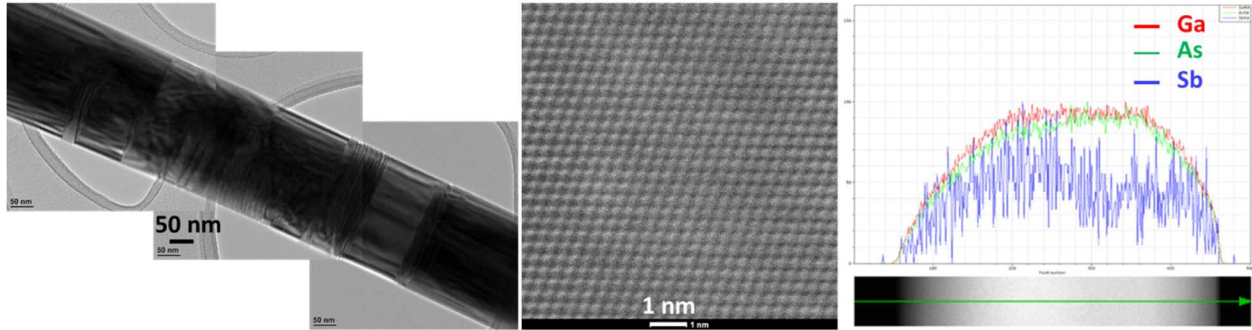
Fig. 4. a) TEM image, b) high resolution HAADF STEM image and c) EDS compositional line scan of GaAs/GaAsSb core-shell nanowires.
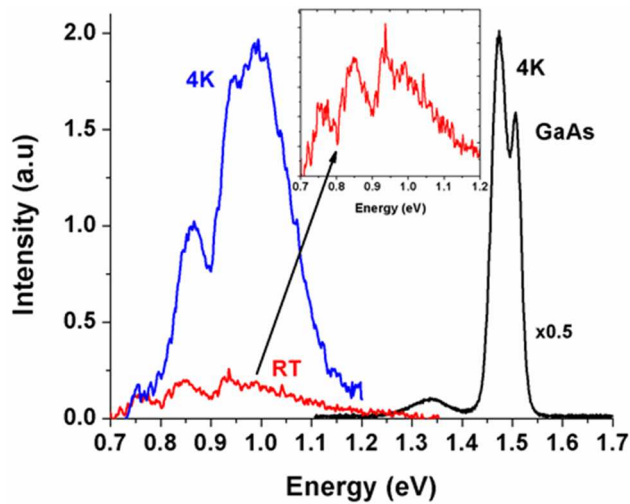
Fig. 5. μ-PL spectra of GaAs/GaAs$_{0.76}$Sb$_{0.24}$ nanowires with room temperature emission ~.1.3 μm along with the reference GaAs nanowires PL spectra.

μ-PL spectra of core-shell nanowires for the highest Sb composition of 24 at.% was carried out (Fig.5) to ascertain the maximum energy shift that can be obtained in this GaAs/GaAsSb system. The reference GaAs nanowires exhibit two closely separated peaks at 1.51 eV and 1.47 eV pertaining to wurtzite (WZ) and zincblende

(ZB) structures, respectively. The GaAsSb shell nanowires' spectra red shifted to 0.99 eV. The increased full width half maximum (FWHM) for GaAs/GaAsSb core-shell nanowires is representative of deterioration in the optical quality of the nanowires. Room temperature PL spectra is also observed in these GaAs/GaAs$_{0.76}$Sb$_{0.24}$ core-shell nanowires at 1.3 μm (0.94 eV) with quantum efficiency of 13%.

The temperature dependence of these nanowires was also carried out to ensure that the PL band is indeed from the band edge emission. Figure 6a illustrates temperature dependent PL spectra of GaAs/GaAs$_{0.76}$Sb$_{0.24}$ core-shell nanowires. The best fit to the curve was obtained following phenomenological Varshni equation at higher temperatures.
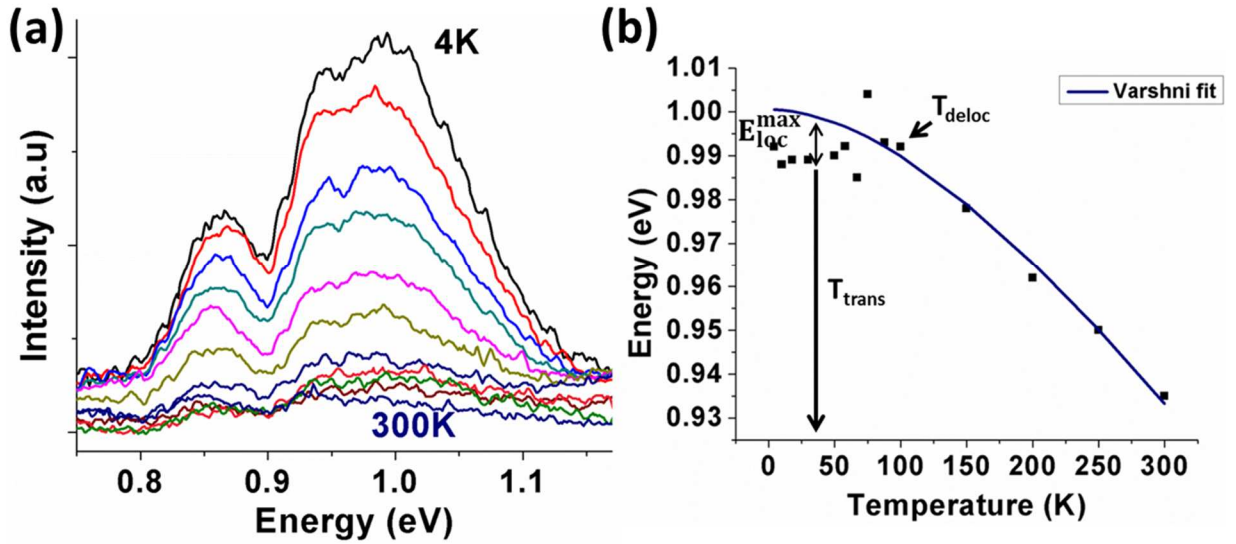
Fig. 6. a) Temperature dependent PL spectra and b) variation of the PL peak energy as a function of temperature in GaAs/GaAs$_{0.76}$Sb$_{0.24}$ core-shell nanowires.

$$Eg(T) = Eg(0) - \frac{\alpha T^2}{\beta + T} \quad (1)$$

where T is absolute temperature, $E_g(0)$ is bandgap at 0K and α, β are fitting parameters. The best fit values of the fitting parameters were found to be 0.5 meV/K and 378 K, respectively. These are somewhat higher than those observed in bulk GaAs. The largest deviation from the Varshni fit is observed at the low temperature corner with a red-blue-red shift in PL peak energy with increasing temperature, characteristic of a well-known "S-curve" behavior. This behavior is commonly attributed to exciton localization in band tail states [17, 18] due to potential

fluctuations. The different contributors to band tail induced states include compositional fluctuations, localized defect states, and inhomogeneous lattice deformation [19]. The S-curve is not observed in GaAsSb thin films and there has been only couple of reports on the observation of S-curve in GaAsSb/GaAs QWs [17, 20, 21, 22]. The contributing factors to the observation of S-curve in our nanowires we believe is due to the growth of highly strained $GaAs_{0.76}Sb_{0.24}$ shell of only few nm thick with a composition in the miscibility gap. Any local compositional fluctuation in the nano-scale can lead to large potential minima similar to quantum dot, forming an excellent trap for the carriers. The three parameters characteristic of the S-shaped curve are T_{trans}, E_{loc}^{max} and T_{deloc} defined as the temperature at which the excitons begin to transfer to higher-energy localized states, the maximum localization energy measured as the largest energetic difference between the experimental PL peak energy and the value of the energy obtained using the Varshni relation, and the temperature at which delocalization of the carriers is complete, respectively. The values of these parameters are found to be ~35 K (T_{trans}), 10 meV (E_{loc}^{max}) and 100 K (T_{deloc}), respectively. The values are consistent with those commonly observed in good quality highly mismatched alloy heterostructure system [17, 22, 23].

In conclusion, all vertical nanowires with NW density in the range of $3x10^8$ cm^{-2} on epi-ready Si (111) substrate has been achieved by optimizing initial Ga opening duration and V/III BEP ratio. Much higher NW density of $8x10^8$ cm^{-2} with uniform distribution on the substrate and all vertically oriented were achieved on chemically cleaned Si (111) substrate with subsequent oxidation in air. Thus, substrate preparation prior to growth is highly critical for achieving vertical orientation, homogeneous, high density nanowires of reproducible quality. For the core shell growth, the shell growth temperature and Sb flux are the determining factor for the Sb incorporation in the shell. All the GaAs/GaAsSb nanowires exhibit ZB structure and maximum redshift of the PL peak energy is observed for Sb content of 24 at.%. The PL temperature dependence of these nanowires exhibited S-curve indicative of exciton localization at low temperatures. Room temperature PL emission at 1.3 μm is observed, thus showing great promise for device operation in the telecommunication wavelength region.

Acknowledgements

References

1. K. Tomioka, J. Motohisa, S. Hara, K. Hiruma, and T. Fukui, Nano Lett. 10, 1639 (2010).

2. E. Garnett and P. Yang, Nano Lett. 10, 1082 (2010).

3. D. Xing, S. Zhang, Z. Wang, G. Adamo, H. Liu, Y. Huang, C. Couteau, and C. Soci, Nano Lett. 14, 2688 (2014).

4. V. J. Logeeswaran, J. Oh, A. P. Nayak, A. M. Katzenmeyer, K. H. Gilchrist, S. Grego, N. P. Kobayashi, S.Y. Wang, N. K. Dhar, and M. S. Islam, IEEE J. Quantum Elect. 17, 1002 (2011).

5. H. Huang, S. Mao, H. Feick, H. Yan, Y.Wu, H. Kind, E.Weber, R. Russo, and P. Yang, Science 292, 1897 (2001).

6. R. Yan, D. Gargas, and P. Yang, Nat. Photonics 3, 569 (2009).

7. P. Offermans, M. Crego-Calama, and S. H. Brongersma, Nano Lett. 10, 2412 (2010).

8. M. Heiss, E. Russo-Averchi, A. Dalmau-Mallorquí, G Tutütüncüoğlu, F. Matteini, D. Rüffer, S. Conesa-Boj, O. Demichel, E. Alarcon-Lladó and A. Morral, Nanotechonology 25, 014015 (2014).

9. A. M. Munshi, D. L. Dheeraj, V. T. Fauske, D. Kim, J. Huh, J. F. Reinertsen, L. Ahtapodov, K. D. Lee, B.Heidari, A. T. J. van Helvoort, B. O. Fimland, and H. Weman, Nano Lett. 14, 960 (2014).

10. S. J. Gibson, J. P. Boulanger and R. R. LaPierre, Semicond. Sci. Tech. 28, 105025 (2013).

11. C. Somaschini, S. Bietti, A. Trampert, U. Jahn, C. Hauswald, H. Riechert, S. Sanguinetti and L. Geelhaar, Nano Lett. 13, 6307 (2013).

12. F. Matteini, T. Gözde, P. Heidi, J. Fauzia, and A. Morral, Cryst. Growth Des. 15 (7), 3105 (2015).

13. P. K. Kasanaboina, S. K. Ojha, S. U. Sami, L. Reynolds, Y. Liu and S. Iyer, SPIE Proc. 9373, 937307-1 (2015).

14. P. K. Kasanaboina, S. K. Ojha, S. U. Sami, L. Reynolds, Y. Liu and S. Iyer, Semicond. Sci. Tech., (2015) (In print).

15. J. Sadowski, D. Piotr, and J. Kanski, arXiv preprint arXiv 0812, 2453 (2008).

16. K. Gas, J. Sadowski, T. Kasama, A. Siusys, W. Zaleszczyk, T. Wojciechowski, J. Morhange, A. Altintaş, H. Q. Xu, and W. Szuszkiewicz, Nanoscale 5, 7410 (2013).

17. M. Baranowski, M. Syperek, R. Kudrawiec, J. Misiewicz, J. A. Gupta, X. Wu, and R. Wang, Appl. Phys. Lett. 98, 61910 (2011).

18. G. Tourbot, B. Catherine, A. Grenier, M. D. Hertog, D. Sam-Giao, D. Cooper, P. Gilet, B. Gayral, and B. Daudin, Nanotechnology 22, 75601 (2011).

19. P. G. Eliseev, P. Perlin, J. Lee, and O. Marek, Appl. Phys. Lett. 71, 569 (1997).

20. M. Dinu, J. E. Cunningham, F. Quochi, and J. Shah, J. Appl. Phys. 94, 1506 (2003).

21. N. Kalyan, S. Iyer, L. Wu, J. Li, S. Bharatan, X. Wei, R. T. Senger, and K. K. Bajaj, J. Appl. Phys. 102, 53106 (2007).

22. J. Li, S. Iyer, S. Bharatan, L. Wu, K. Nunna, W. Collis, K. K. Bajaj, and K. Matney, J. Appl. Phys. 98, 13703 (2005).

23. S. Iyer, L. Reynolds, T. Rawdanowicz, S. K. Ojha, P. K. Kasanaboina and A. Bowen, in Nanoscience and Nanoengineering: Advances and Applications, ed. by A. D. Kelkar, D. C. Herr, J. G. Ryan (CRC Press, 2014), p. 31.

Appendix D

Tailoring of GaAs/GaAsSb core-shell structured nanowires for IR photodetector applications

Pavan Kumar Kasanaboina[1], Sai Krishna Ojha[1], Shifat Us Sami[2], Lewis Reynolds Jr.[3], Yang Liu[3] and Shanthi Iyer[1,2]

1. Department of Electrical and Computer Engineering, North Carolina A&T State University, Greensboro, NC 27411
2. Nanoengineering, Joint School of Nanoscience and Nanoengineering, NCA&T State University, Greensboro, NC 27401
3. Department of Materials Science Engineering, North Carolina State University, Raleigh, NC 27695

ABSTRACT

Ga assisted GaAs/GaAsSb core-shell structured nanowires were successfully grown on chemically etched p-type Si(111) substrate by molecular beam epitaxy (MBE). The morphology, structural and optical properties of the nanowires are found to be strongly influenced by the shell growth temperature and Sb% in the nanowires. The nanowires exhibit planar defects like twins and stacking faults, with more stacking faults and micro-twins found at the top section. Optical characteristics of the nanowires as measured by 4K photoluminescence (PL) exhibit a red shift to 1.2 eV with increasing Sb incorporation up to 12%. The Raman spectra of reference GaAs nanowires show TO and LO modes representative of the zinc blende structure at 291 cm^{-1} and 267.8 cm^{-1}, respectively. Red shifts of both modes in conjunction with corresponding asymmetrical peak broadening observed in X-ray diffraction with increasing Sb incorporation are attributed to enhanced strain and disorder within the nanostructures. Nanowires of similar Sb composition but grown at different shell temperatures reveal straight nanowires with better microstructural and optical quality when grown at higher growth temperatures. The presence of GaAs passivation layer significantly enhanced the PL intensity such that PL was observed even at room temperature.

INTRODUCTION

GaAs$_{1-x}$Sb$_x$ is one of the promising material systems that allow bandgap tailoring in the wavelength range of 1.3 µm-1.55 µm for telecommunication applications. The geometry of nanowires offers potential advantages over their thin film counterparts in terms of increased defect tolerance, reduced reflection, enhanced light trapping, improved band gap tuning and also facilitates strain relaxation [1]. In particular, core-shell structured nanowires, also commonly referred to as radial heterostructures, have several advantages over axial heterostructures in growth, design, optical properties and material composition aspects. For example from a design perspective, core-shell nanowires have optical absorption and charge separation along two orthogonal directions and increases the defect tolerance unlike behavior observed in axial heterostructured nanowires where the optical absorption and charge separation share the same region and thus charge separation is limited to this small region. In addition, the vapor-solid growth mechanism of core-shell configured nanowires allows greater compositional flexibility over the vapor-liquid-solid growth mechanism of axial heterostructured nanowires.

Reports on the growth of axial and core-shell GaAs/GaAsSb heterostructured nanowires have been predominantly focused on structural characterization [2,3,4,5]. Recently, our group [6] and, Todorovic et al [7] investigated the optical properties of axial heterostructured nanowires and tuned the bandgap up to 1.2 eV. To the best of our knowledge, there are no reports on optical properties of GaAs/GaAs$_{1-x}$Sb$_x$ core-shell nanowires. In this work, we report on the effect of shell growth temperature on the morphological, structural and optical properties of core-shell configured GaAs/GaAs$_{1-x}$Sb$_x$ nanowires for different Sb content, that were grown by Ga-assisted molecular beam epitaxy (MBE).

EXPERIMENTAL DETAILS

The nanowires were grown by Ga-assisted MBE on chemically treated P-type Si (111) substrates in an EPI 930 solid source MBE system with valved As and Sb cracker sources. In order to grow GaAs/GaAsSb core-shell nanowires, initially core GaAs nanowires were grown by the vapor-liquid-solid (VLS) mechanism with Ga serving as the catalyst at 620 °C. Ga-assisted nanowire growth was initiated by impinging Ga flux on the substrate for 15 s prior to opening of the As_4 flux with a beam equivalent pressure of 4.8×10^{-6} Torr. After core GaAs nanowire growth, the Ga droplets were solidified by allowing high As_4 flux for 10 min. to prevent axial growth during the subsequent shell growth. The GaAsSb shell was then grown around GaAs core. The shell growth temperature was varied between 550 °C-590 °C while the Sb flux varied from 2.4×10^{-7} to 9.6×10^{-7} Torr.

The morphological features of the grown nanowires were characterized by using Carl Zeiss Auriga-BU FIB field emission scanning electron microscope (FESEM) while an attached X-ray energy dispersive spectroscopy (XEDS) was used to determine the composition of the nanowires. X-ray diffraction (XRD) analysis was carried out using a Bruker D8 Discover instrument with a DaVinci diffractometer, in the standard Bragg-Brentano para-focusing configuration to ascertain the orientation and strain effects in the nanowires. Bright field transmission electron microscopy (TEM) and selected area electron diffraction (SAED) images were obtained on a JEOL 2010F microscope operating at 200 kV. Optical characteristics of the nanowires were measured by μ-photoluminescence (PL) using a 633 nm He–Ne laser as the excitation source with a 0.32 m double grating monochromator for wavelength dispersion and InGaAs detector with a conventional lock-in amplifier system. An Olympus IR 50X lens was used to focus the laser on the nanowires. A closed-cycle optical cryostat from Montana Cryostation with the sample chamber interfaced with a fiber coupled confocal microscope was used to study the variation of PL characteristics in the 4–300 K temperature range. A Horiba Jobin Yvon LabRam ARAMIS Raman microscope was used to determine the vibrational characteristics and hence quality of the nanowires using a He-Ne laser with 633 nm excitation wavelength at room temperature.

RESULTS AND DISCUSSION

GaAs/GaAs$_{1-x}$Sb$_x$ core-shell nanowires with composition varying up to ~12% Sb were grown on chemically etched p-type Si (111) substrate. The morphology and Sb incorporation in the GaAs/GaAsSb core-shell nanowires are
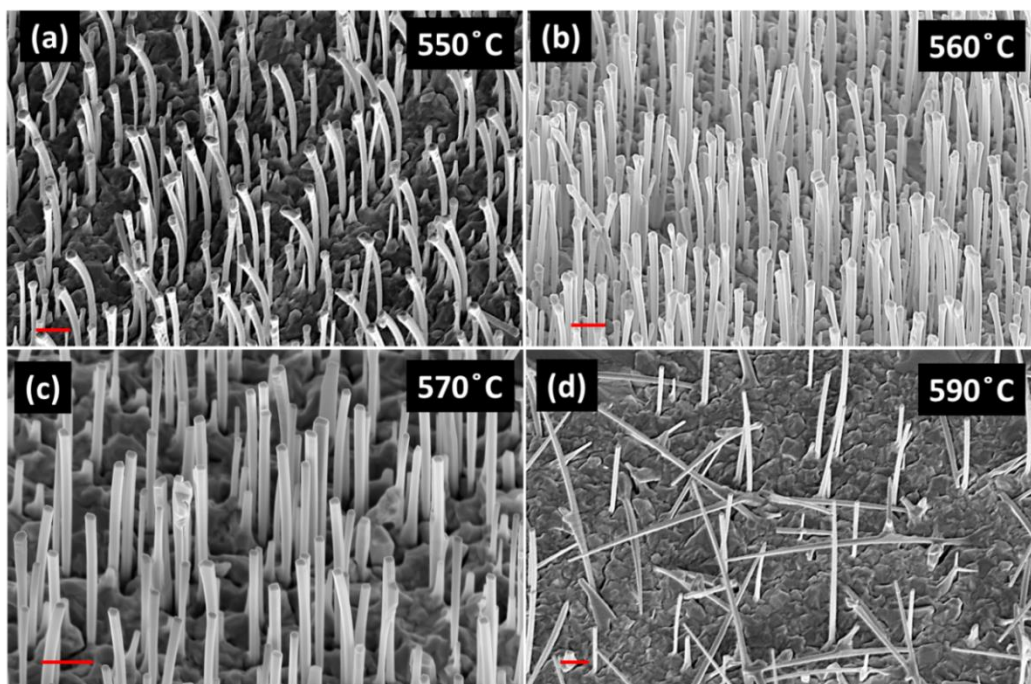

Figure 1. GaAs/GaAsSb core-shell nanowires grown at a) 550 ℃, b) 560 ℃, c) 570 ℃ and d) 590 ℃ (scale bar is 1 μm).

strongly influenced by shell growth temperature as shown in Fig. 1. Sb incorporation decreases with an increase in growth temperature (Fig. 2a), which is attributed to increased Sb desorption from the surface during shell growth as the nanowires also become more vertical. A decrease in nanowire density is also observed.
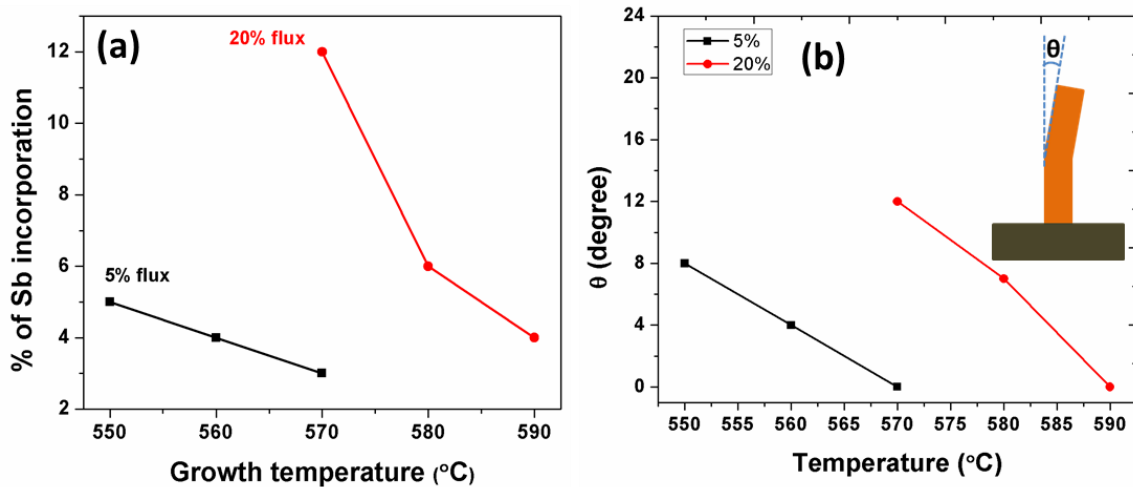

Figure 2. a) Variation in the Sb content of the nanowires with the shell growth temperature and b) degree of nanowire bending as a function of growth temperature.

Beyond a critical temperature, Sb desorbs completely and hence no shell growth was observed. This is found to occur at a critical temperature of 570 ˚C for an Sb flux of 2.4×10^{-7} Torr. However, for this condition the nanowires exhibit perfect hexagonal shape with excellent verticality. Bending of the nanowires occurs below this critical temperature. At higher Sb flux of 9.6×10^{-7} Torr a similar trend was observed with temperature except there was an increase in the critical temperature to 590 ˚C. This indicates that bending of the nanowire is due to the interfacial strain induced between the core and shell with increased Sb incorporation. Overgrown faceted tips and side facets were also observed with increasing Sb content in the nanowire. This is related to the surfactant nature of Sb, in which more Sb on the surface leads to increased strain and likely manifesting in different growth facets [8]. In addition, both length and diameter of the nanowires also increase from 3 µm → 4 µm and 183 nm → 210 nm, respectively, which is indicative of higher axial and radial growth rates with increased Sb content from 3 to 12%.
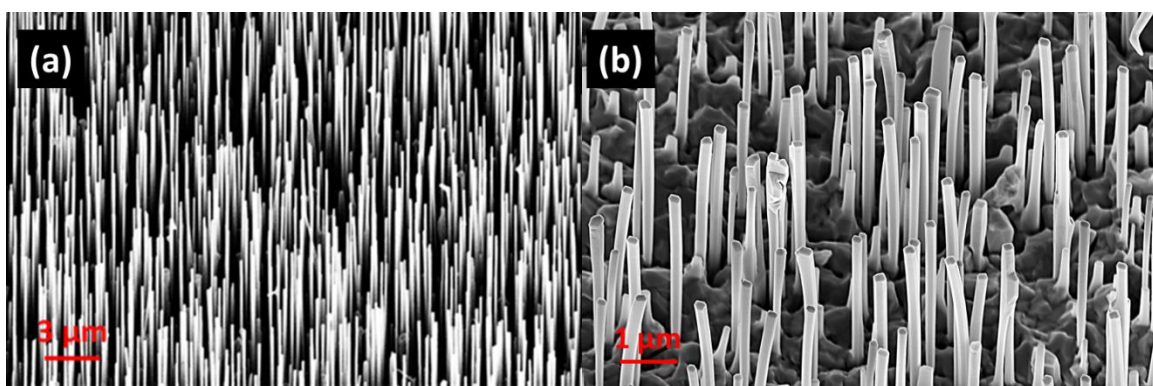
Figure 3. MBE grown a) GaAs core and b) GaAs/GaAsSb core-shell nanowires.

The degree of nanowire bending can be reduced with increasing growth temperature (Fig. 2b), which is consistent with the investigation of Ghalamestani et al [5] on their GaAsSb/GaAs core-shell nanowires. The decrease in

the degree of nanowire bending at elevated growth temperatures at constant Sb flux can be attributed to two strain relaxation mechanisms: either the decrease in Sb content and/or the enhanced probability of migration of atoms to lower energy positions [9]. However, bending of the nanowire is also strongly influenced by Sb content, increasing with Sb content at a specific growth temperature (Fig. 2b). Hence, we conclude that the bending of the nanowires is predominantly due to strain accumulation on the nanowire side facets and ruling out any contribution from the thermal stress component. Figure 3 shows highly vertical GaAs and GaAs/GaAsSb core-shell nanowires grown under optimized growth conditions.

One can further reduce bending of the nanowires by shortening the nanowire, which is related to lower accumulated strain. Figure 4 shows a comparison of 4 µm with 2 µm long nanowires. The former reveals the onset of bending near the middle of the nanowire while 2 µm long nanowire results in predominantly vertical with no evidence of bending in the nanowires.
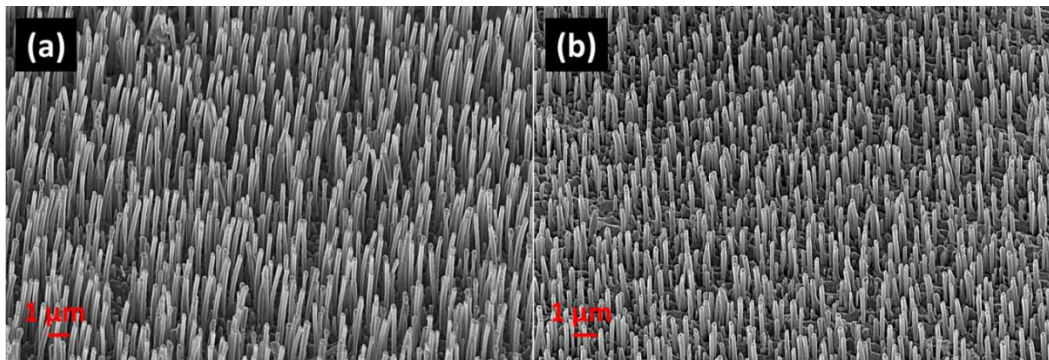
Figure 4. Nanowires grown to lengths of a) 4 µm and b) 2 µm

Figure 5 displays the XRD spectrum of a core-shell GaAs/GaAs$_{0.95}$Sb$_{0.05}$ nanowire, which exhibits only the GaAs (111) and GaAsSb (111) orientation of the zinc blende structure. The absence of other orientation peaks confirms the growth of highly vertical <111> oriented nanowires. The presence of the dominant Si (111) peak is due to the substrate.
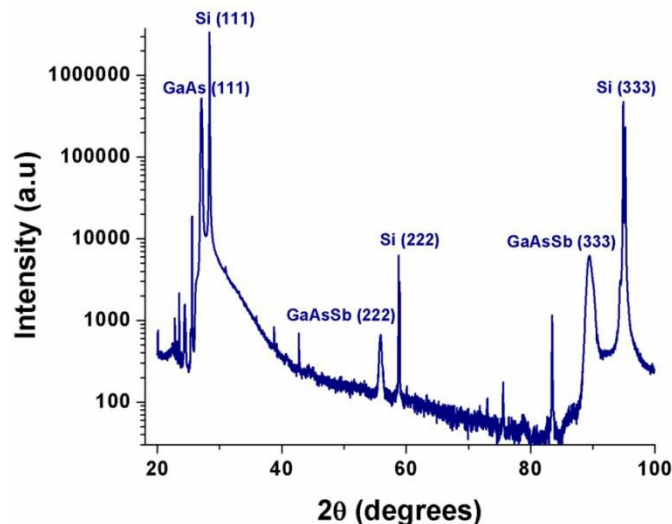

Figure 5. XRD spectrum of core-shell structured GaAs/GaAsSb nanowires.

The lattice strain of the nanowires was estimated by Williamson-Hall isotropic strain model (W-H ISM) from the X-ray diffraction data, assuming the presence of uniform strain throughout the nanowires. The W-H ISM equation for the total peak broadening is given by

$$\beta_r \cos\theta = \frac{K\lambda}{D_v} + 4\eta\sin\theta \qquad (1)$$

where β_r is true width after subtracting instrumental broadening, K is the shape factor, D_v represents the volume weighted crystallite size and η is the strain. The strain in the nanowires is then determined from the slope of the linear fit to the $\beta_r\cos\theta$ versus $4\sin\theta$ linear plot, as shown in Fig.6a for all the samples. On the basis of this analysis, one finds that strain reduces with increasing shell growth temperature (see Fig 6b).
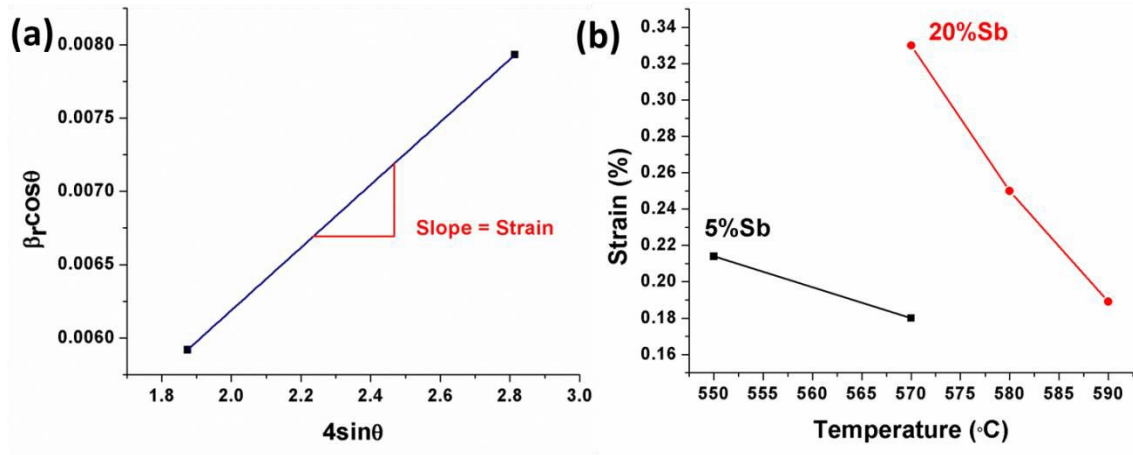
Figure 6. (a) W-H ISM plot of GaAs/GaAs$_{0.95}$Sb$_{0.05}$ nanowire and (b) strain as a function of shell growth temperature for two different Sb %.
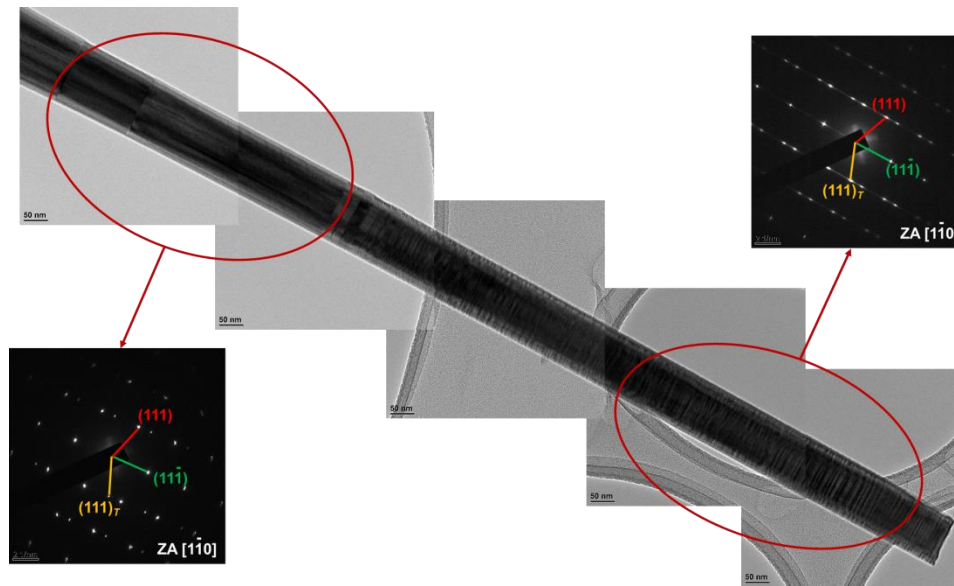
Figure 7. TEM image of GaAs/GaAs$_{0.97}$Sb$_{0.03}$ core-shell nanowire and SAED patterns at different locations.

Proc. of SPIE Vol. 9373 937307-5

Figure 7 shows the TEM image of a GaAs/GaAs$_{0.97}$Sb$_{0.03}$ core-shell nanowire and the associated SAED patterns at different sections along the same nanowire. The SAED patterns confirm the zinc blende (ZB) structure of the nanowire, viewing from zone axis of [110]. Also, twins and stacking faults are observed throughout, with more stacking faults and micro-twins accumulated at the top section of nanowire. The streaky diffraction spots are likely caused by the Sb-induced strain resulting in planar defects [10].

Figure 8 shows the normalized photoluminescence (PL) spectra of nanowires at different shell growth temperatures. The reference PL spectra of GaAs nanowires is characterized by two peaks, ~1.5 eV peak related to the band-to-band transition and a second smaller peak at 1.35 eV, which can be attributed to a surface defect related transition [11]. With a decrease in growth temperature, the band-to-band transition exhibits a red shift with simultaneous broadening of the spectral peaks. This again attests to increased Sb incorporation in the nanowire and the associated strain with a decrease in the substrate temperature, which is consistent with the nanowire morphology and XRD data. Nanowires grown at different shell growth temperatures but similar Sb content revealed that the optical quality is improved when the nanowires are grown at higher shell growth temperature, as evidenced by the lower full width half maximum observed in Fig. 8b for the nanowire grown at 580℃.
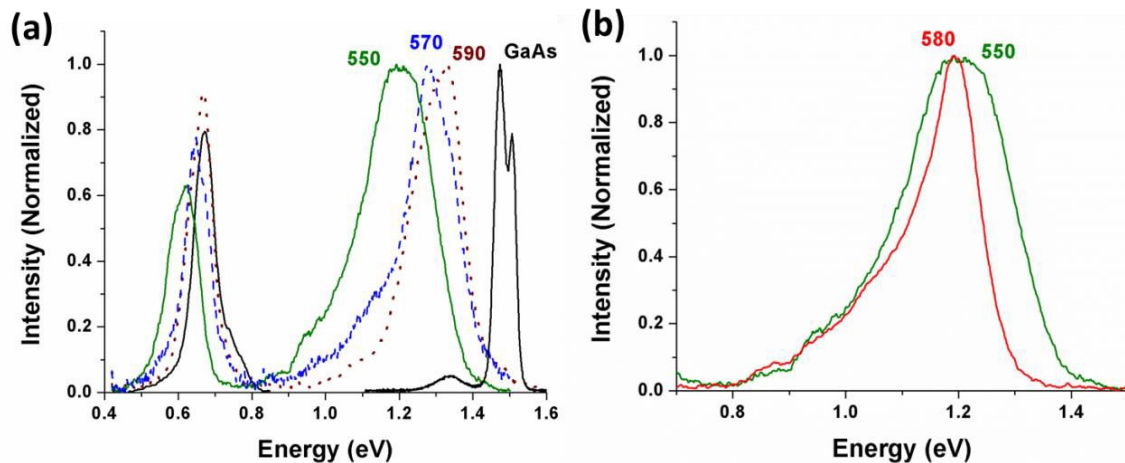

Figure 8. PL spectra of GaAs/GaAsSb nanowires grown at different shell growth temperatures a) for the same Sb flux and b) for similar Sb content in the nanowire.

The second peak at lower energy, ~0.67 eV, also red shifted with decreasing growth temperature. This transition can be assigned to transition from the surface Fermi level, which is known to be pinned close to the middle of the bandgap, to the valence band of GaAsSb.

Figure 9 shows the variation in the PL peak energy with Sb composition for both axial (although not discussed here) and shell configuration grown in our laboratory and are compared with the quantum well (QW) experimental data from Teissier et al [12]. Simulated QW data with well thickness taken to be same as shell thickness using Optel ZB software are also shown. It is to be noted that the values in the latter two cases correspond to relaxed compositions. Although the band gap energies of our GaAsSb nanowires are consistently lower than the quantum well data and simulations, trend of decreasing E$_g$ with increasing Sb is in reasonably good agreement.
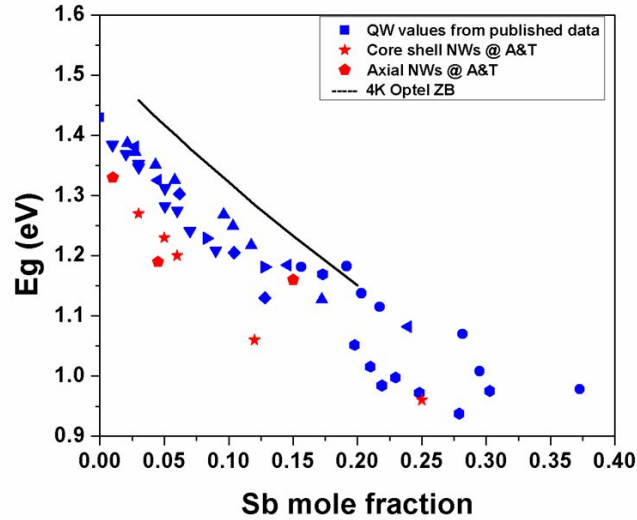
Figure 9. Comparison of band gap energies (E_g) for axial and core-shell nanowires with the respective quantum well (QW) PL peak energies (from the reference [12]) and simulated band gap values of QW using Optel ZB software.
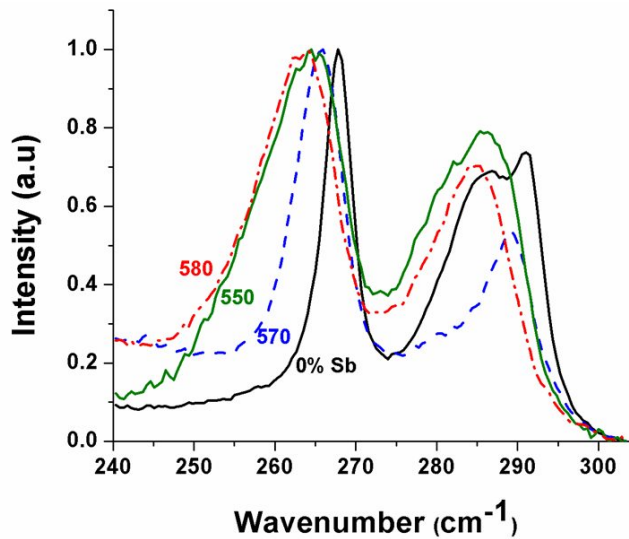

Figure 10. Raman spectroscopy of GaAs/GaAsSb core-shell nanowires at different growth temperatures.

Figure 10 depicts the room temperature Raman spectra of GaAs/GaAsSb nanowires grown at different shell temperatures. The Raman spectra for a reference GaAs nanowire exhibits TO and LO modes at 291 cm^{-1} and 267.8 cm^{-1}, respectively, which is corresponds to the zinc blende structure. Both TO and LO mode peaks are red shifted and broadened with decreasing shell temperature, as shown in Fig. 10. The increased asymmetric broadening of Raman peaks with lower shell growth temperature for a given Sb flux is consistent with respective broadening observed in the PL spectra, and is clear evidence of increased strain and disorder in the nanowire. This results from the increase in the heavier Sb atom content substituting for the smaller and lighter As atoms. However, for nanowires grown at higher shell growth temperature and similar Sb content vertical nanowires are observed, which is accompanied by a reduction in broadening of both the Raman and 4K PL spectra revealing superior nanostructure quality of the nanowires.
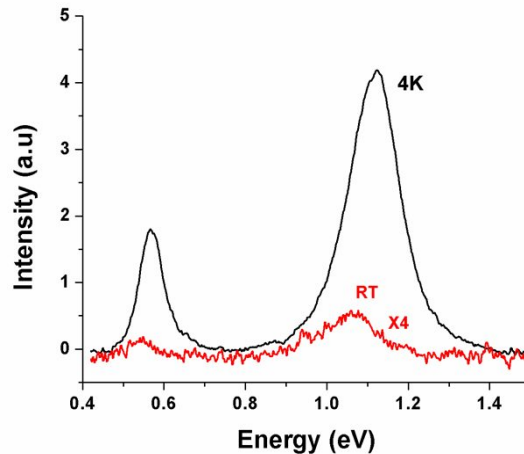
Figure 11. PL spectra of passivated GaAs/GaAsSb core-shell nanowires.

We have extended these results and grown GaAs/GaAsSb/GaAs nanowires; that is, the GaAsSb/air interface is passivated by a confining outer GaAs shell. One observes that the PL efficiency is significantly improved in this double shell configuration as shown in Fig. 11, in which PL emission is observed even at room temperature.

In conclusion, these preliminary investigations show that the growth parameters play vital role in determining the morphology, structural and optical quality of the GaAs/GaAsSb nanowires with potential for further improvement. To the best of our knowledge, the observation of room temperature PL emission in these GaAs/GaAsSb/GaAs core-double shell nanowires is the first to be reported.

ACKNOWLEDGEMENTS

REFERENCES

1. Garnett, E.C., Brongersma, M. L., Yi Cui, and McGehee, M.D., "Nanowire Solar Cells", Annu. Rev. Mater. Res., 41:269–95 (2011).
2. Plissard, S., Dick, K. A., Wallart, X. and Caroff, P., "Gold-free GaAs/GaAsSb heterostructure nanowires grown on silicon", Appl. Phys. Lett. 96, 121901 (2010).
3. Dheeraj, D.L., Zhou, H.L., Moses, A.F., Hoang, T.B., Van Helvoort, A.T.J., Fimland, B.O. and H. Weman, [Nanowires], Book edited by: Paola Prete, ISBN 978-953-7619-79-4, pp. 414, (2010).
4. Kauko,H., Grieb,T., Bjørge,R., Schowalter,M., Munshi,A., M., Weman,H., Rosenauer,A., Van Helvoort,A.,T.,J., "Compositional characterization of GaAs/GaAsSb nanowires by quantitative HAADF-STEM", Micron 44, 254–260, (2013).
5. Ghalamestani,S.G., Munshi,A.M., Dheeraj,D.L., Fimland,B.O., Weman,H., and Dick,K.A., "Self-catalyzed MBE grown GaAs/GaAs$_x$Sb$_{1-x}$ core–shell nanowires in ZB and WZ crystal structures", Nanotechnology 24 , 405601, (2013).
6. Iyer,S., Reynolds,L., Rawdanowicz,T., Ojha,S.K., Kasanaboina,P.K. and Bowen,A., [Nanoscience and Nanoengineering: Advances and Applications], ISBN 9781482231199, CRC Press, Chapter 3, p. 31, (2014).

7. Todorovic,J., Kauko,H., Ahtapodov,L., Moses,A.F., Olk,P., Dheeraj,D.L., Fimland,B.O., Weman,H. and Van Helvoort,A.T.J., "The effects of Sb concentration variation on the optical properties of GaAsSb/GaAs heterostructured nanowires", Semicond. Sci. Technol. 28 115004, (2013).

8. Zhang,L., Tang,H.F. and Kuech,T.F., "Effect of Sb as a surfactant during the lateral epitaxial overgrowth of GaN by metalorganic vapor phase epitaxy", Appl. Phys. Lett. 79, 3059 (2001).

9. Shen,Y., Hong,J.I., Peng,Z., Fang,H., Zhang,S., Dong,S., Snyder,R.L. and Wang,Z.L., "Tuning the Shape and Strain in Micro/Nanowires by a Sideways Physical Deposition Process", J. Phys. Chem. C, 114, 21277–21280, (2010).

10. Maity,T. and Das,J, "Origin of plasticity in ultrafine lamellar Ti-Fe-(Sn) composites", AIP Advances 2, 032175 (2012).

11. Hwang,J.S., Tsai,J.T., Su,I.C., Lin,H.C., Lu,Y.T., Chiu,P.C. and Chyi,J.I., "GaAsSb bandgap, surface fermi level, and surface state density studied by photoreflectance modulation spectroscopy", Appl. Phys. Lett. 100, 222104 (2012).

12. Teissier,R., Sicault,D., Harmand,J.C., Ungaro,G., Roux,G.L. and Largeau,L., "Temperature-dependent valence band offset and band-gap energies of pseudomorphic GaAsSb on GaAs", J. Appl. Phys., Vol. 89, No. 10, 5473, (2001).

Appendix E

Pavan Kumar Kasanaboina, Sai Krishna Ojha, Shifat Us Sami, C. Lewis Reynolds Jr., Yang Liu and Shanthi Iyer, "Bandgap Tuning of GaAs/GaAsSb Core-Shell Nanowires Grown by Molecular Beam Epitaxy", Semiconductor Science and Technology, (Sept. issue 2015) in print.

Bandgap tuning of GaAs/GaAsSb core-shell nanowires grown by molecular beam epitaxy

Pavan Kumar Kasanaboina[1]**, Sai Krishna Ojha**[1]**, Shifat Us Sami**[2]**,**
C Lewis Reynolds Jr[3]**, Yang Liu**[3] **and Shanthi Iyer**[1,2]

[1] Department of Electrical and Computer Engineering, North Carolina A&T State University, Greensboro, NC 27411, USA

[2] Nanoengineering, Joint School of Nanoscience and Nanoengineering, NCA&T State University, Greensboro, NC 27401, USA

[3] Department of Materials Science and Engineering, North Carolina State University, Raleigh, NC 27695, USA

CrossMark

Abstract

Semiconductor nanowires have been identified as a viable technology for next-generation infrared (IR) photodetectors with improved detectivity and detection across a range of energies as well as for novel single-photon detection in quantum networking. The GaAsSb materials system is especially promising in the 1.3–1.55 μm spectral range. In this work we present bandgap tuning up to 1.3 μm in GaAs/GaAsSb core–shell nanowires, by varying the Sb content using Ga-assisted molecular beam epitaxy. An increase in Sb content leads to strain accumulation in shell manifesting in rough surface morphology, multifaceted growths, curved nanowires, and deterioration in the microstructural and optical quality of the nanowires. The presence of multiple PL peaks for Sb compositions $\geqslant$12 at.% and degradation in the nanowire quality as attested by broadening of Raman and x-ray diffraction peaks reveal compositional instability in the nanowires. Transmission electron microscope (TEM) images show the presence of stacking faults and twins. Based on photoluminescence (PL) peak energies and their excitation power dependence behavior, an energy-band diagram for GaAs/GaAsSb core–shell nanowires is proposed. Optical transitions are dominated by type II transitions at lower Sb compositions and a combination of type I and type II transitions for compositions $\geqslant$12 at.%. Type I optical transitions as low as 0.93 eV (1.3 μm) from the GaAsSb for Sb composition of 26 at.% have been observed. The PL spectrum of a single nanowire is replicated in the ensemble nanowires, demonstrating good compositional homogeneity of the latter. A double-shell configuration for passivation of deleterious surface states leads to significant enhancement in the PL intensity resulting in the observation of room temperature emission, which provides significant potential for further improvement with important implications for nanostructured optoelectronic devices operating in the near-infrared regime.

Keywords: nanowires, bandgap tuning, core-shell, molecular beam epitaxy

(Some figures may appear in colour only in the online journal)

1. Introduction

The flexibility offered by the one-dimensional structure of nanowires in band-gap engineering, material design architecture, and the wide choice of substrates have made it an attractive candidate for a variety of device applications. Nanowire (NW) arrays are ideally suited to meet the demands of the third-generation of infrared (IR) photodetectors for imaging with high prospects for improving detectivity, providing better spatial resolution, and offer the potential for multispectral detection by integration of different NW arrays on the same substrate and the possibility of hybrid integration of driver electronics and detectors on the same chip. In particular, wavelengths in the near-infrared region (NIR), 1.3–1.55 μm, have also been of great interest for telecommunications, and there has been continued demand for

improvement in these photodetectors. In recent years, devices with high spatial resolution and single-photon detection have become even more important due to the increasing research interest in quantum networking.

Two ternary material systems that have been extensively investigated in thin-film devices operating at these wavelengths are GaAsSb [1–3] and InGaAs [4, 5]. The GaAsSb (III-V-V) system offers distinct advantages over InGaAs (III-III-V) due to (a) suppressed Auger recombination, (b) longer electron lifetime, and (c) less dependency of the electronic structure on its alloy configuration due to the presence of a single group III element [6]. In nanowires, the advantage of a single group III element is more apparent due to the commonly used vapor-liquid-solid (VLS) growth mechanism for NW growth. Large differences in the In and Ga diffusion rates can lead to considerable compositional inhomogeneity in InGaAs nanowires. Furthermore, the GaAsSb system has the advantage that the surfactant nature of Sb can be exploited to improve the structural and optoelectronic properties.

Several reports have been published on both axial and radial heterostructured growth of gold-assisted and gold-free growth of GaAs/GaAsSb nanowires [7–11]. The focus of the majority of the work has been on crystal structure and insertion of GaAsSb layers in GaAs. Recently, Todorovic *et al* [12] investigated the optical properties of GaAsSb inserts in GaAs nanowires for different lengths of the ternary insert, and band-gap tuning to 1.2 eV was demonstrated by varying Sb composition using Au-assisted molecular beam epitaxy (MBE). Our group reported a similar study with longer inserts and using Ga-assisted MBE [13]. We also recently reported [14] the effect of growth temperature of the shell on the properties of core–shell GaAs/GaAsSb nanowires. Au-free self-catalyzed Ga assisted growth offers the advantage of not only eliminating the Au-induced defects but also suppressing undesirable axial growth during shell growth. It should be noted that a GaAsSb material system belongs to a highly mismatched alloy (HMA) system and the other HMA systems that have been the subject of investigations in the NW configurations are GaP/GaPN [15] and GaAs/GaAsN [16] core–shell nanowires, though the band-gap have slightly higher energy values of 1–2 eV.

The focus of this investigation is a comprehensive understanding of the effects of Sb variation in the Ga-assisted MBE growth of GaAs/GaAsSb in the core–shell configured nanowires for next-generation photodetectors in the telecommunication wavelength range. The impact of Sb variation on morphology, strain, composition, band gap, and band alignment have been studied in detail using a variety of characterization techniques. These are the first reports to our knowledge of achieving PL emission wavelength of 1.3 μm in Ga-assisted GaAsSb core–shell nanowires with prospects of further improvement in PL efficiency demonstrated by passivating the GaAsSb surface via a double-shell configuration.

2. Experimental details

All nanowires were grown on P-type Si (111) substrates using an EPI 930 solid source MBE system with valved As and Sb cracker sources. The growth of GaAs/GaAsSb core–shell nanowires was comprised of two steps. First, core GaAs nanowires were grown using the VLS mechanism with Ga as the catalyst at 620 °C. Ga-assisted NW growth was initiated by impinging Ga flux on the substrate for 15 s prior to the opening of the As$_4$ flux with a beam- equivalent pressure of 4.8×10^{-6} Torr. After growing the core NW for a given duration, the Ga droplets on the tips of the nanowires were solidified to avoid further axial growth during shell growth. GaAsSb shell growth was then initiated after lowering the growth temperature. The shell growth temperature was varied between 550 °C–590 °C and the Sb flux was varied from 2.4×10^{-7} to 2.8×10^{-6} Torr. For the growth of double-shell GaAs/GaAsSb/GaAs nanowires, the Sb flux was terminated prior to the commencement of the second GaAs shell growth.

Scanning electron microscope (SEM) imaging was carried out using a Carl Zeiss Auriga-BU FIB field emission scanning electron microscope (FESEM) with an energy-dispersive x-ray spectrometer for compositional analysis. X-ray diffraction scans (XRD) were performed using Bruker's D8 Discover instrument with a DaVinci diffractometer in the standard Bragg–Brentano para-focusing configuration. X-rays from the Cu Kα source were not filtered and thus contained both K$_{\alpha1}$ and K$_{\alpha2}$ components. The scanning transmission electron microscopy (STEM) analysis was performed on a probe aberration-corrected FEI Titan G2 system operated at 200 kV. The bright-field TEM, selected-area electron diffraction (SAED), and high-resolution TEM (HRTEM) were characterized on a JEOL 2010F microscope operated at 200 kV. Micro-photoluminescence (μ-PL) measurements were conducted in a low vibration closed cycle optical cryostat from Montana Cryostation with the sample chamber extended away from the cryostat. The sample chamber was interfaced with a fiber-coupled confocal microscope from Horiba Jobin Yvon, Inc., with a 633 nm He-Ne laser as the excitation source. The PL signal from the sample was then dispersed using a 0.32 m double-grating monochromator with liquid nitrogen cooled InGaAs detector for detection using conventional lock-in techniques. Raman spectroscopy was carried out at room temperature in a Horiba Jobin Yvon LabRam ARAMIS Raman microscope using a He-Ne laser with 633 nm excitation wavelength. The Raman signal was detected using a multichannel air-cooled charge-coupled device.

3. Results and discussion

Figure 1(a) shows an SEM image of highly vertical core GaAs nanowires on Si (111) substrate with a density in the range of 6–8 μm^{-2}. The nanowires are 4 μm long with diameters ranging from 70–80 nm. Figure 1(b) depicts typical

Q2
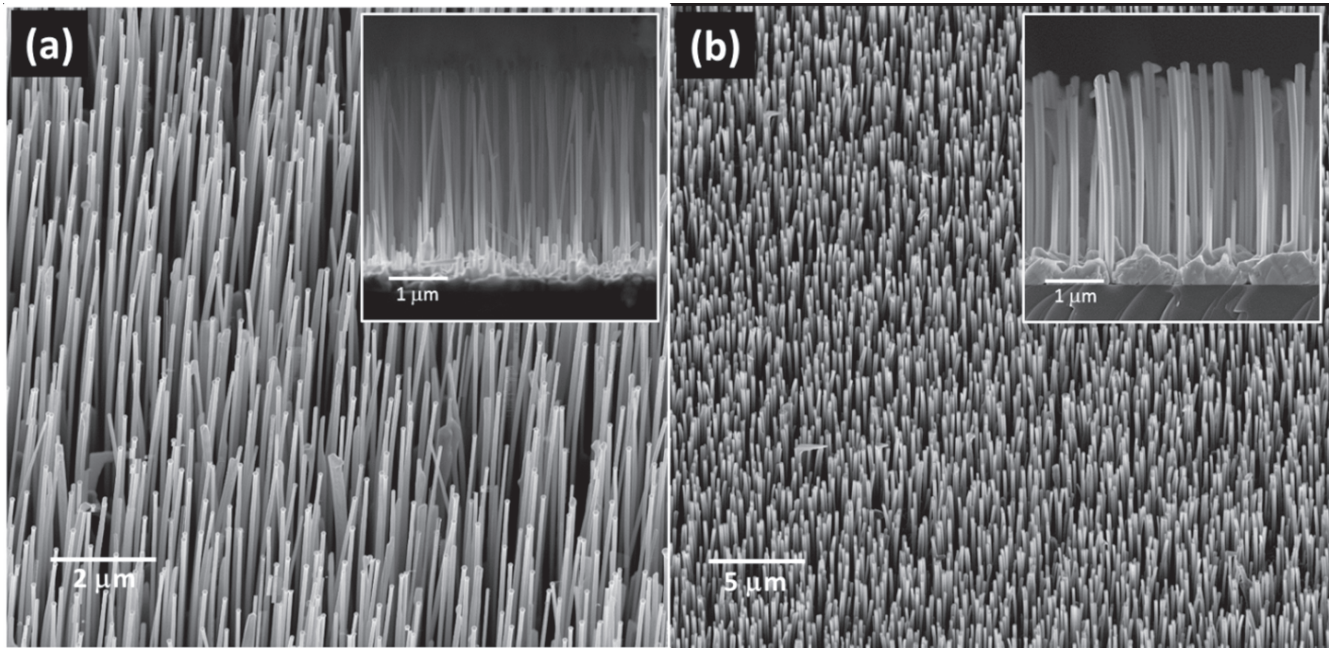
Figure 1. (a) Core GaAs nanowires and (b) core–shell GaAs/GaAsSb nanowires. The insets show the respective side views.
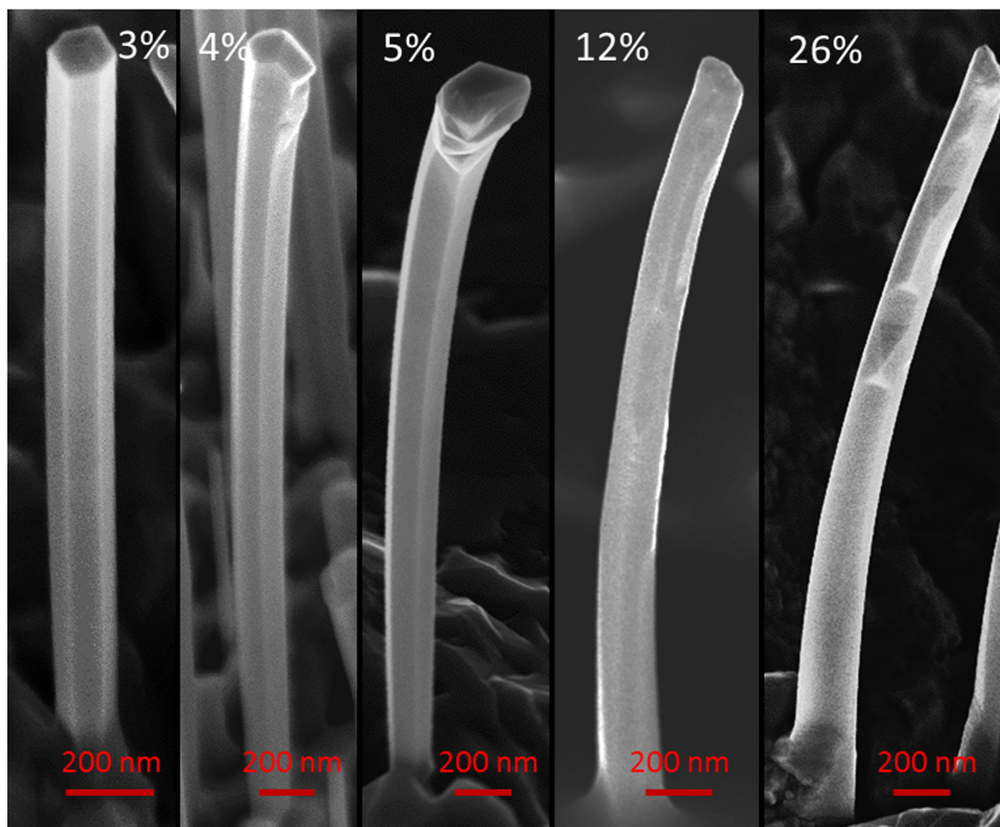

Figure 2. SEM micrographs of single GaAs/GaAsSb core–shell nanowires for different Sb compositions.

GaAs/GaAsSb core–shell nanowires with length and diameters of 4 μm and 180 nm, respectively.

Figure 2 displays the SEM images of the GaAs/GaAsSb core–shell nanowires with increasing Sb incorporation up to 26 at.%. The smooth morphology and well-defined hexagonal faceted top view cross-section observed in nanowires with low Sb content of 3 at.% is transformed to a rougher morphology with different overgrown side facets and elongated hexagonal cross-section with increasing Sb content, as shown in figure 2. The diameter of the NW increases from 183 nm to
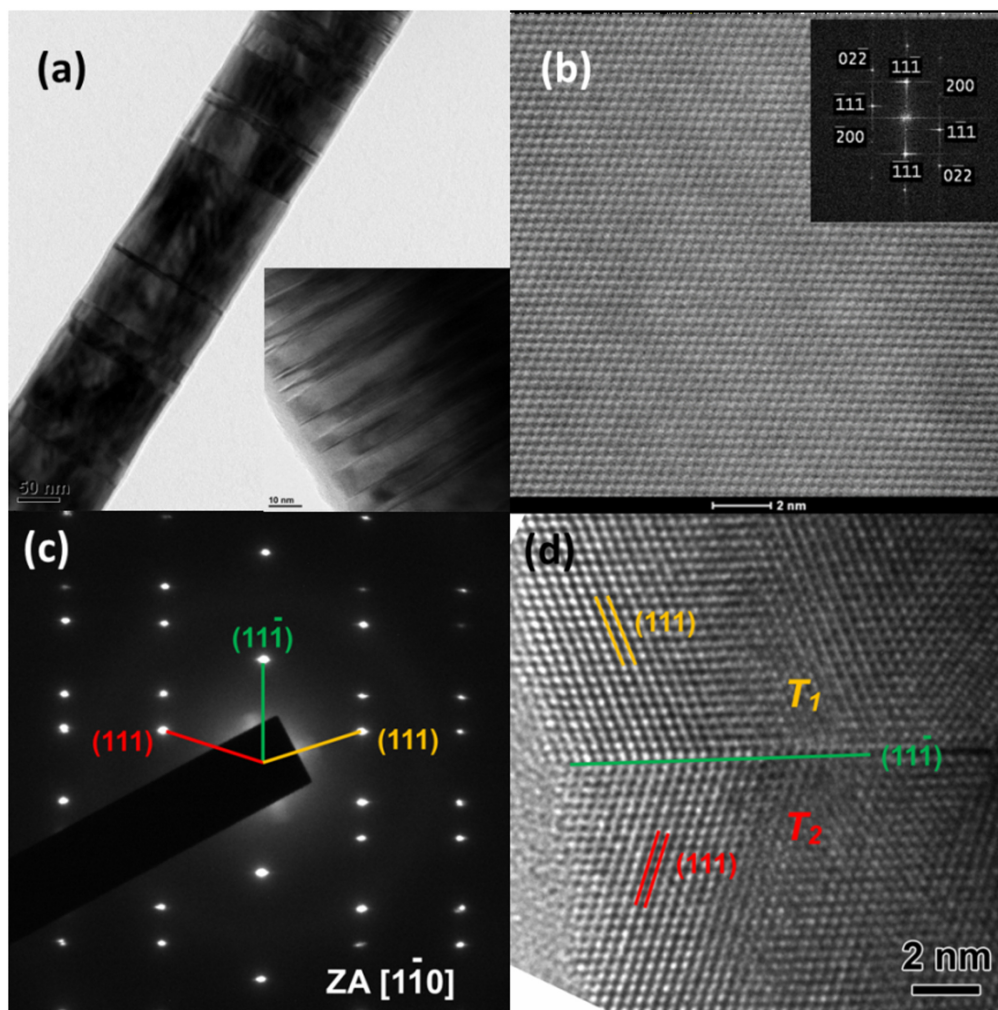
Figure 3. (a) TEM image of core–shell NW, (b) high-resolution STEM image and FFT (inset) acquired using [011] zone axis, (c) SAED pattern shows ZB structure with twins, and (d) HR-TEM image displays the twinning plane (indicated by a green line).

280 nm as the Sb content increases from 3 to 26 at.%, respectively, for similar growth duration. These changes in morphology and diameter are most likely associated with the thermodynamic and kinetic modifications created by the surfactant nature of Sb. Higher Sb flux leads to larger Sb coverage on the surface resulting in the reduction in the free energy of the growth surface, which promotes lateral growth via a vapor solid-growth mechanism. Beyond a certain critical threshold of Sb composition, Sb segregation can occur on the surface [17, 18]. This inhomogeneous Sb coverage on the nanowire surface is likely responsible for the growth of a multitude of side facets at 26 at.% Sb composition and a rough surface morphology.

The alignment of the nanowires also changes from vertical to curved with increasing Sb content. Bending of the NW is strongly influenced by Sb content, increasing with Sb content at a specific growth temperature (figure 2). Hence, it can be inferred that bending of the nanowires is predominantly due to strain accumulation on the NW side facets and thus ruling out any contribution from a thermal stress component as the growth temperature was invariant for the growth. Ghalamestani *et al* [11] also observed similar

behavior on their GaAsSb/GaAs core–shell nanowires. Further evidence of the increased strain with increasing Sb incorporation in the nanowires is also found using XRD measurements, as discussed later.

Figure 3(a) displays the bright field TEM micrograph of a typical GaAs/GaAs$_{0.88}$Sb$_{0.12}$ core–shell nanowire, which exhibits both twins and stacking faults. The lattice resolved HR-STEM image along the [011] zone axis in conjunction with the respective fast Fourier transform (FFT) (figure 3(b)) reveals the zinc-blende (ZB) structure of the NW lattice. The SAED pattern (figure 3(c)) taken along the zone axis [1–10] indicates the twinning structure in the nanowire. The HRTEM image of an isolated twinning plane normal to [11–1] the growth axis is demonstrated in figure 3(d) with the two crystal structures mirrored along the (11-1) plane.

Figure 4 depicts the x-ray diffraction patterns of core–shell GaAs/GaAsSb nanowires with varying Sb content. All diffraction peaks were identified using the JCPDS standard database. The nanowires exhibit only GaAs (111), GaAsSb (111), GaSb (111), and Si (111) Bragg peaks, and their respective higher-order reflections. The absence of other orientations further attests to the growth of highly vertical
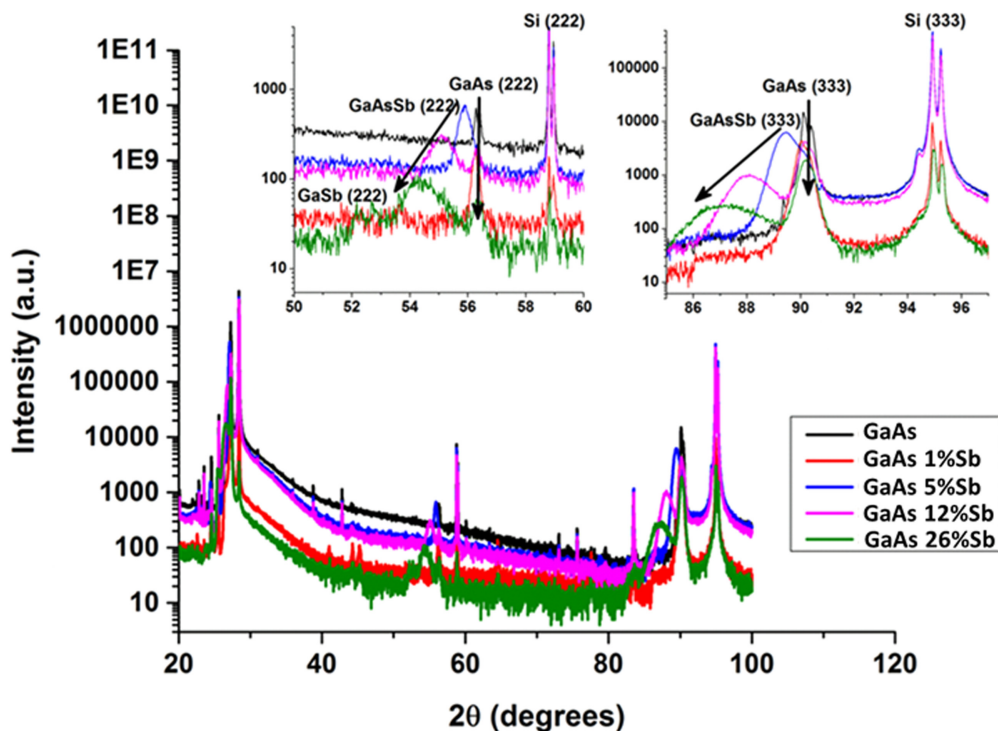
Q3

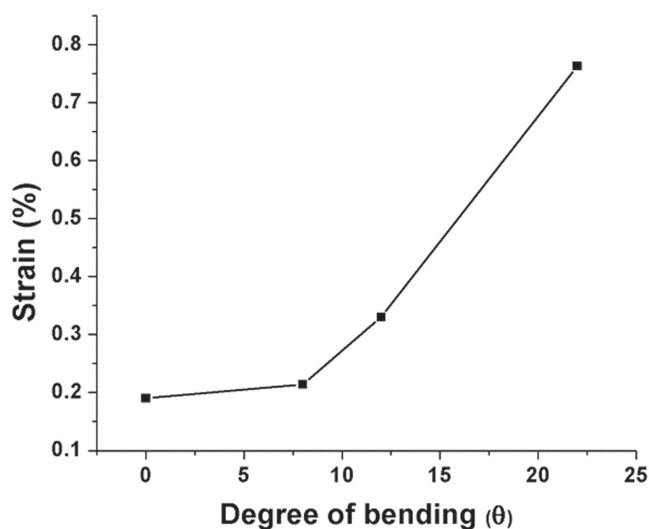**Figure 4.** X-ray diffraction patterns of GaAs/GaAsSb nanowires with different Sb compositions.

Figure 5. Variation of strain in GaAsSb shell with degree of bending.

<111> oriented nanowires. With increasing Sb composition, the GaAsSb (222) and GaAsSb (333) Bragg peaks shift toward lower angles and are accompanied by significant broadening of the peak as shown in the inset of figure 4. At the highest Sb composition of 26 at.%, pure GaSb phase was observed, which is indicative of the presence of segregated Sb as described above.

Due to close proximity of the first-order (111) peaks of GaAs and GaAsSb in conjunction with the use of an unfiltered Cu K_{α} source, broadening of the higher-order (222) and (333) GaAsSb reflections was used for estimation of the overall strain in the GaAsSb shell. The strain calculations were estimated by the Williamson–Hall isotropic strain model (W–H ISM) [19, 20] using the total peak broadening. The strain thus calculated was found to increase monotonically with increasing degree of bending as shown in figure 5. These data confirm our earlier conjecture that bending of the nanowires is associated with enhanced strain accumulation in the shell. There are two factors that are likely contributors to this increase in strain. With increasing Sb composition, mismatch between the core and the shell is increased and the shell thickness also increases. Both these lead to increased strain in the shell. Although the Williamson–Hall model has often been used in the literature for determination of the strain in nanowires [19, 21], its applicability for core–shell nanowires is debatable due to non-uniform strain distribution in the shell [22]. As a consequence, while the strain value may not be an absolute value, it provides an overall trend of the strain accumulation in the shell with increasing Sb composition.

Figure 6 shows the normalized micro-photoluminescence (PL) spectra of core–shell nanowires at 4 K for different Sb compositions. The PL spectra of the GaAsSb nanowires reveal emission peaks in the 1.27–0.93 eV spectral range with the specific energies dependent upon the composition. The range shows the red shift with increasing Sb composition from 3 at.% to 26 at.%, and there is an associated peak broadening with increasing Sb content. It is noted that.

GaAs exhibits twin peaks at higher energy of ∼1.47 eV and 1.33 eV, which are identified with the ZB band-to-band transition and As defect (V_{As}) level [23] transition located ∼0.14 eV below the conduction band, respectively.

Since the CB discontinuity is very small in this heterostructure, the change in band gap with increasing Sb content is predominantly accommodated by the increasing valence-band (VB) offset [24]. An estimation of the VB offset was
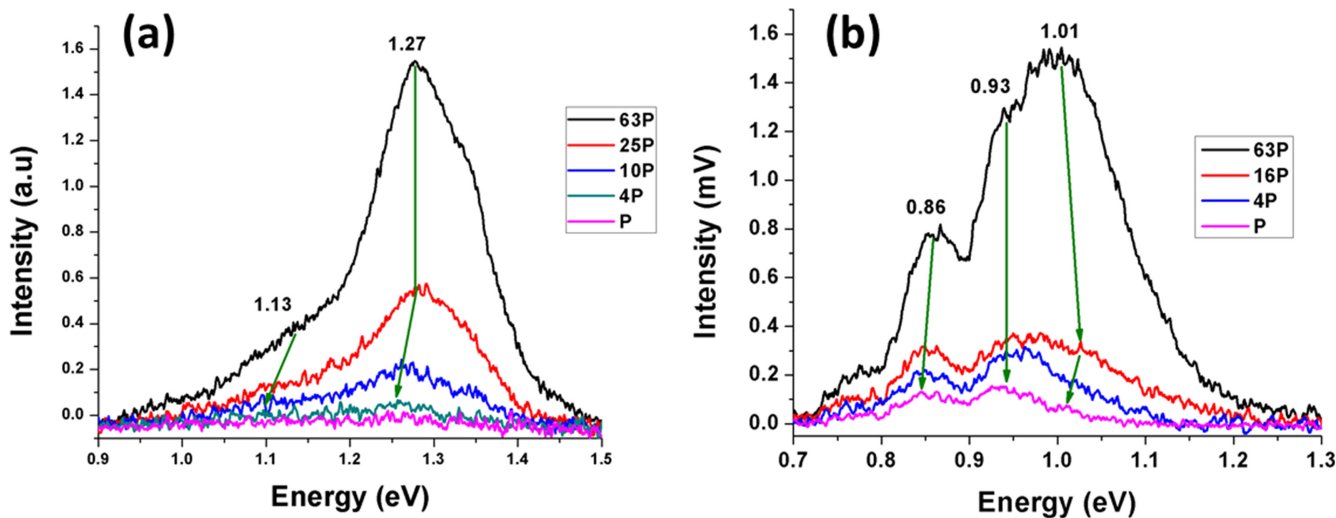
Q4
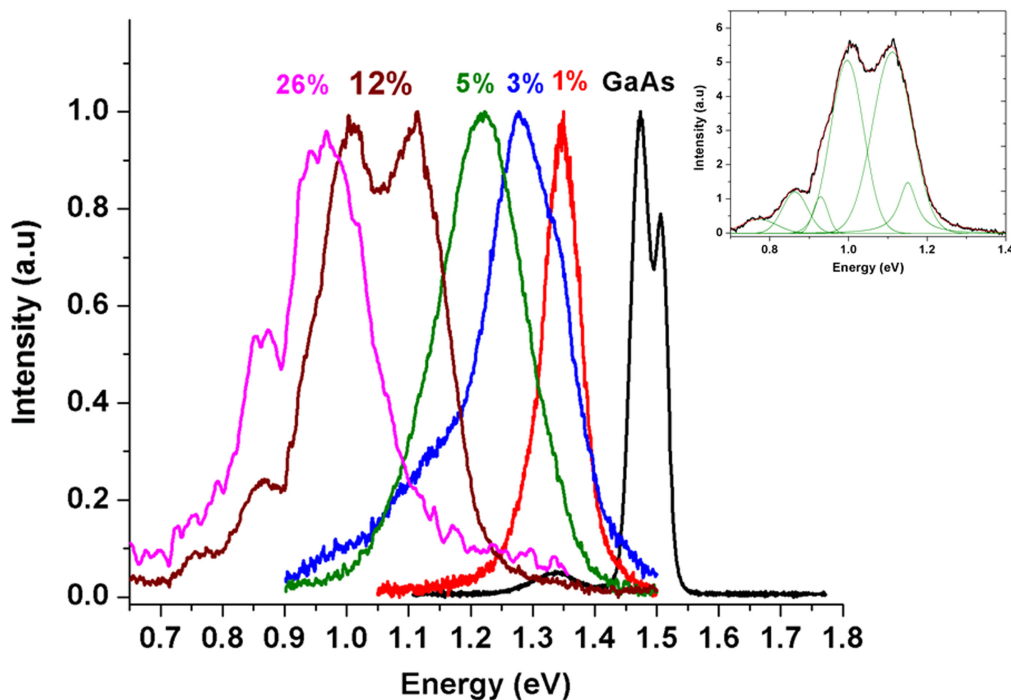
Figure 6. Photoluminescence spectra of GaAs/GaAsSb nanowires with different Sb compositions (inset: deconvolution of peaks for 12 at.% Sb composition).
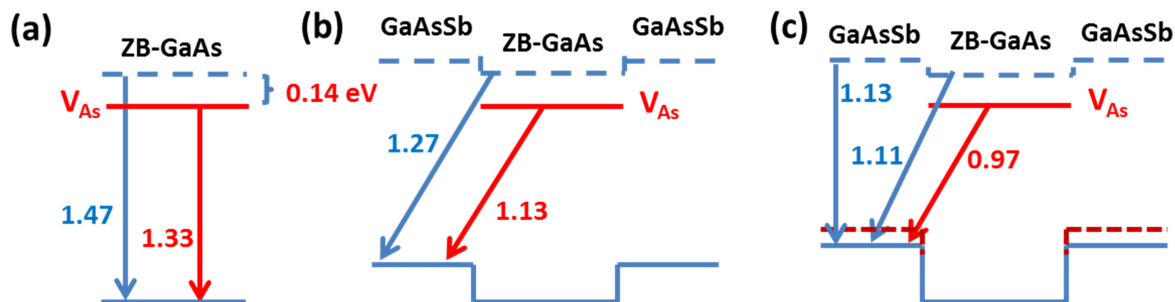
Figure 7. Proposed schematic energy band diagram of (a) ZB GaAs, (b) GaAs/GaAs$_{0.97}$Sb$_{0.03}$, and (c) GaAs/GaAs$_{0.88}$Sb$_{0.12}$ (only a few transitions are shown and the dotted line in the VB corresponds to the 2nd Sb composition).

Figure 8. Excitation power dependence PL of (a) GaAs/GaAs$_{0.97}$Sb$_{0.03}$ and (b) GaAs/GaAs$_{0.74}$Sb$_{0.26}$ nanowires.
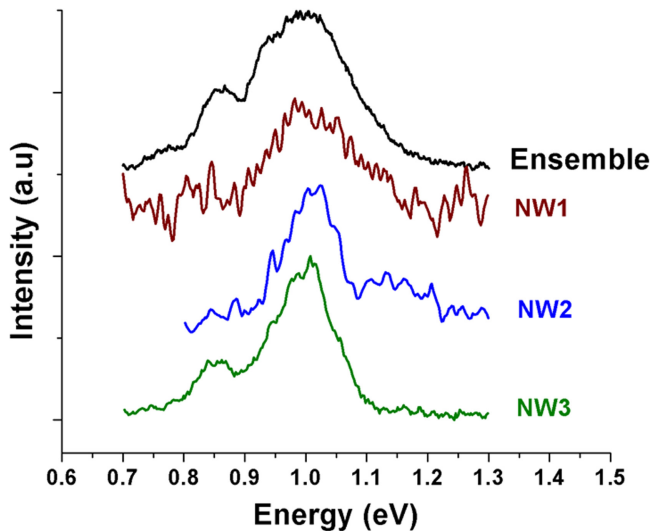
Figure 9. Comparison of the PL spectra for single and ensemble of nanowires.

made using the simulation software Optel ZB, which provides the evaluation of this offset through interpolation of the VB edges for compound semiconductors [25, 26]. The nature of the transitions was inferred from the excitation power dependence of the 4 K PL spectra discussed below. These were then used to develop the proposed band alignment depicted in figure 7.

Figure 8 displays the excitation power dependence PL for GaAs/GaAs$_{0.97}$Sb$_{0.03}$ and GaAs/GaAs$_{0.74}$Sb$_{0.26}$ nanowires. Although data on only two samples at the two extremes of Sb composition range are presented, the intensity dependence was conducted on all the samples discussed earlier over the entire composition range. For 3 at.% Sb, a Gaussian fit to the observed PL spectra results in two peaks at 1.27 eV and 1.13 eV (figure 8(a)) exhibiting a blueshift of ∼20–30 meV with increasing incident PL power by 60x (P is used to denote the lowest baseline intensity, which was 0.5 mW). Such large

blue shifts are a signature of type II heterostructures, which is caused by confinement of carriers in a narrow well width due to electric field-induced band bending [27, 28]. The electric field is created by the spatial separation of electron and hole pairs in these structures. Thus, the two transitions we observe are assigned to ZB GaAs CB to GaAsSb VB and V$_{As}$ defect level to GaAsSb VB, respectively. PL spectra of 12 at.% Sb composition are characterized by multitude of peaks occurring at 1.13 eV, 1.11 eV, 1.0 eV, 0.97 eV, and 0.86 eV (inset of figure 6). Except for the 1.13 eV transition, all the transitions are type II in nature due to the blue shift of ∼20 meV observed with the increase in incident power. The presence of two pairs of PL peaks suggests the existence of two different Sb compositions. Peaks at 1.11 eV and 0.97 eV are assigned to a CB of GaAs to VB of GaAsSb and V$_{As}$ to GaAsSb VB, respectively, of one composition and the other two, 1.0 eV and 0.86 eV, for similar transitions corresponding to a second composition in the 12 at.% Sb nanowires. The shoulder on the highest energy peak at 1.13 eV is assigned a transition inside the GaAsSb shell itself. The invariance of the peak with incident excitation power was used to determine the type I nature of this transition. For Sb composition of 26 at.%, PL peaks were observed at 1 eV, 0.93 eV, 0.86 eV, and a weak peak near 0.75 eV as shown in figure 8(b). The dominant peak at 0.93 eV does not exhibit any shift with excitation intensity (figure 8(b)) suggesting a direct band-to-band type I transition in GaAsSb, while the 1 and 0.86 eV emission peaks are identical to those observed in the 12 at.% Sb composition nanowires. Thus, both direct and indirect radiative transitions are present and are excitation-level dependent, with the direct transition dominating at lower excitation level. Finally, the small peak observed at ∼0.75 eV is most likely due to the presence of GaSb phase, which is consistent with the XRD data discussed above.

Figure 9 compares the PL spectra for a selection of nanowires with that for a single NW. Reasonable replication of the low-temperature PL of the NW ensemble is observed in
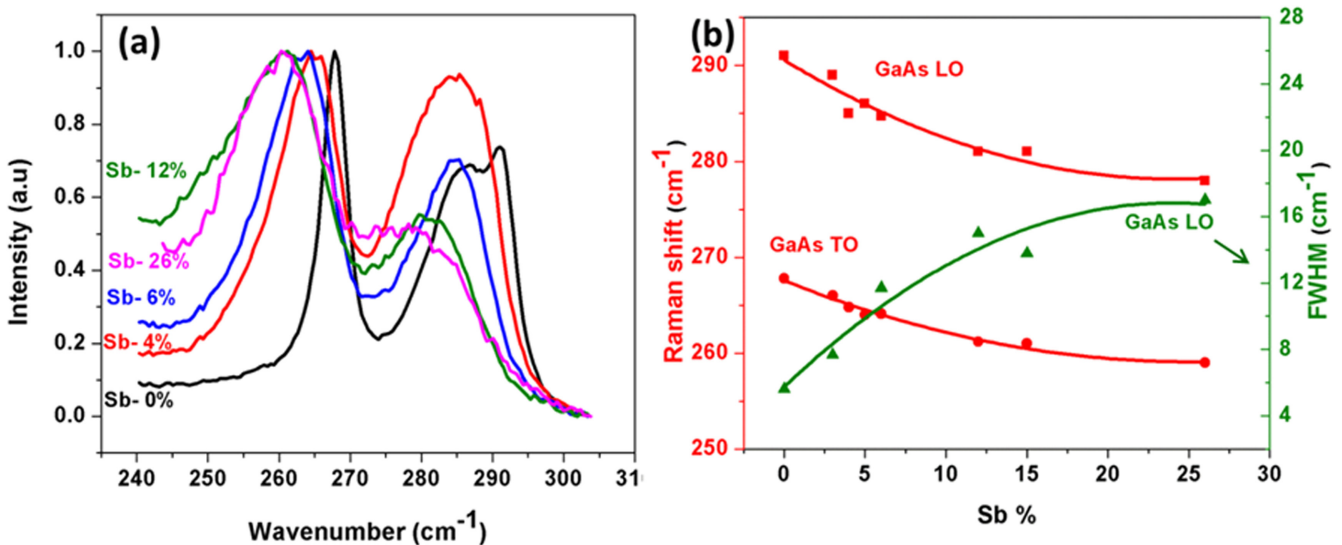
Figure 10. (a) Raman spectra of GaAs/GaAsSb core–shell nanowires and (b) Raman shift and FWHM of core–shell nanowires for different Sb compositions.
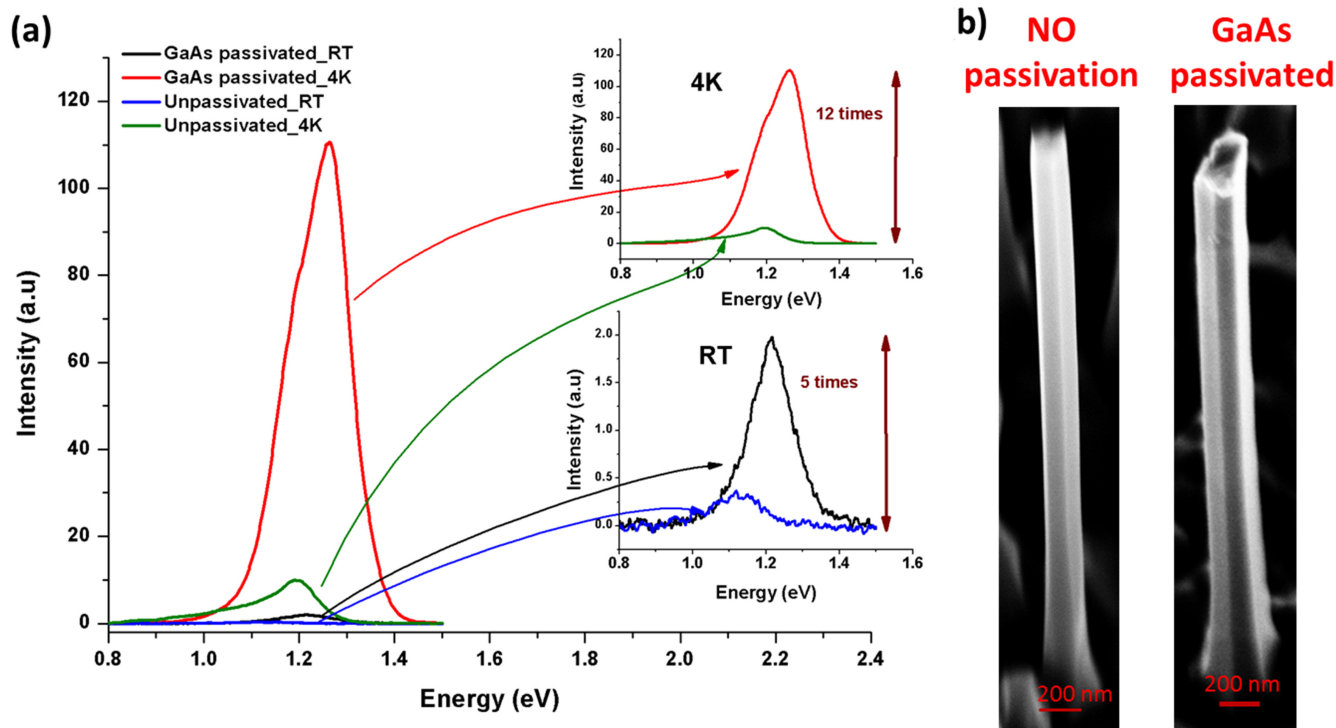
Figure 11. (a) Photoluminescence spectra of GaAs/GaAsSb/GaAs and GaAs/GaAsSb core–shell nanowires and (b) SEM image of GaAs/GaAsSb and GaAs/GaAsSb/GaAs core–shell structured nanowires.
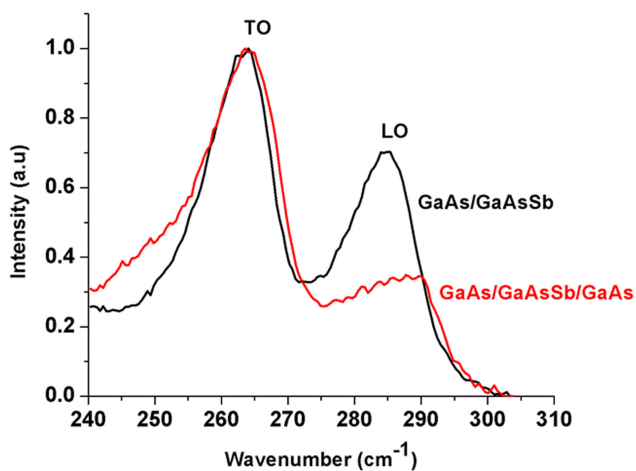
Figure 12. Comparison of the Raman spectra of GaAs/GaAsSb and GaAs/GaAsSb/GaAs nanowires.

Figure 10(a) shows the room-temperature Raman spectra of core–shell GaAs/GaAsSb nanowires with increasing Sb composition. The Raman spectra of reference GaAs nanowires display LO and TO modes at $291\,cm^{-1}$ and $267.8\,cm^{-1}$, respectively, which corresponds to the ZB structure. A shoulder on the LO mode is observed only in the reference sample at $287\,cm^{-1}$ and is attributed to a surface optical mode (SO) [31, 32], which has been commonly observed in thin nanowires. This is not observed in any of the GaAsSb nanowires most likely due to the larger diameter of the core–shell nanowires. A red shift in both the TO and LO modes is observed, which is accompanied by an increase in the FWHM with increasing Sb content, as shown in figure 10(b). The onset of significant asymmetric broadening in Raman peaks and suppression of the LO mode at 12 at.% suggests degrading quality of the nanowires due to the increased strain and compositional inhomogeneity, which is consistent with the XRD and PL observations.

Lastly, a significant improvement in PL intensity has been demonstrated in a double-shell NW configuration, in which an additional GaAs shell is grown around the GaAs/GaAs$_{0.94}$Sb$_{0.06}$ core–shell nanowires. Similar results were also reported for GaP/GaNP/GaNP core/shell/shell nanowires [33]. The diameter of the double shell is also found to be larger, ~200 nm, as expected (figure 11(b)). The PL intensity of the dominant peak (~1.2 eV) is enhanced 12-fold at 4 K and 5-fold at room temperature with respect to the corresponding GaAs/GaAsSb core/shell configuration (figure 11(a)). Room temperature emission is not often observed at this Sb content for the single-shell configuration but is consistently observed in the double-shell NW

the single NW, which attests to the homogeneous composition of these nanowire ensembles. It is commonly reported [29] that the line width of the PL peak in core–shell nanowires is larger due to the electron leakage to the shell. In particular, in the GaAs/GaAsSb system, it is expected to be more pronounced due to the weak electron confinement in the GaAs core. In addition, inhomogeneous strain in the shell, which is enhanced for larger mismatch and higher shell thickness (as is the case in our samples) with increasing Sb composition, also contributes to the increased linewidth. Stacking faults and surface defects are also contributors to the PL broadening [30].

configuration. The increased intensity is attributed to the annihilation of the surface defects on the GaAsSb shell. Figure 12 shows a comparison of the Raman spectra of single- and double-shell configured nanowires. The GaAs LO mode is significantly suppressed in the double-shell configuration and is attributed [34] to the LO mode being forbidden from certain surface facets as opposed to no such restrictions imposed on the TO phonon modes. The presence of the LO mode in the single-shell configuration is most likely associated with defects modulating the selection rules to enable the LO mode, normally forbidden, to be observed. Thus, the absence of the LO mode in the double-shell configuration may be viewed as evidence of reduced defects.

It should be noted that these are the preliminary results and GaAs as an outer shell is not an ideal passivating material due to the small conduction band offset between GaAsSb and GaAs and its comparatively low band gap. However, significant enhancement observed in intensity with the use of GaAs outer shell is very promising and indicates future prospects for much improvement in PL efficiency with the use of an appropriate higher band-gap material, namely GaAlAs, as an outer shell material. Also, further tailoring of the growth parameters as well as shell thickness can have a significant effect on improving the PL efficiency.

4. Conclusions

A detailed investigation was carried out on GaAs/GaAsSb core–shell nanowires grown by Ga-assisted MBE intended for next-generation photodetectors in the near-IR spectral regime. These are the first preliminary reports to the best of our knowledge on achieving low PL peak energy of 0.93 eV on these nanowires. The nanowires exhibit a ZB structure, and planar defects, namely twins and stacking faults, are observed. For 12 at.% Sb content and beyond, evidence of compositional instability is observed, resulting in the increased strain accumulation in the shell leading to rough surface morphology, multi-faceted growths, curved nanowires, and deterioration in the structural and optical quality. The type of the optical transitions observed are dependent on the Sb content; a type II transition is seen at low Sb content while a mixture of type I and type II transitions occur at 12 at. % Sb content and beyond. Fairly good replication of the low-temperature photoluminescence spectra of the nanowire ensemble compared to that of a single nanowire attest to the compositional uniformity of the nanowires. Significant enhancement in the PL intensity observed with the passivation of surface defects by implementing a double-shell configuration provides a pathway for future improvement.

Acknowledgments

References

Q7

[1] Teissier R, Sicault D, Harmand J C, Ungaro G, Le Roux G and Largeau L 2001 *J. Appl. Phys.* **89** 5473

[2] Hossain N, Hild K, Jin S R, Sweeney S J, Yu S Q, Johnson S R, Ding D and Zhang Y H 2010 *Photonics Global Conference IEEE* **1** 14

[3] Hwang J S, Tsai J T, Su I C, Lin H C, Lu Y T, Chiu P C and Chyi J I 2012 *Appl. Phys. Lett.* **100** 222104

[4] Jabeen F, Grillo V, Martelli F and Rubini S 2011 *Selected Topics in Quantum Electronics, IEEE Journal of* **17** 794

[5] Chuang L C, Chen R, Sedgwick F G, Ko W S, Ng K W, Tran T D and Chang-Hasnain C 2010 *Conference on Lasers and Electro-Optics* (Optical Society of America) paper CMFF6   Q8

[6] Qiu Y, Walther T, Liu H Y, Jin C Y, Hopkinson M and Cullis A G 2007 *Inst. Phys. Conf. Ser.* **120** 263

[7] Plissard S, Dick K A, Wallart X and Caroff P 2010 *Appl. Phys. Lett.* **96** 121901

[8] Dheeraj D L, Zhou H L, Moses A F, Hoang T B, van Helvoort A T J, Fimland B O and Weman H 2010 *Nanowires*   Q9

[9] Kauko H, Grieb T, Bjørge R, Schowalter M, Munshi A M, Weman H, Rosenauer A and van Helvoort A T J 2013 *Micron* **44** 254

[10] Kauko H, Fimland B O, Grieb T, Munshi A M, Müller K, Rosenauer A and van Helvoort A T J 2014 *J. Appl. Phys.* **116** 144303

[11] Ghalamestani S G, Munshi A M, Dheeraj D L, Fimland B O, Weman H and Dick K A 2013 *Nanotechnology* **24** 405601

[12] Todorovic J, Kauko H, Ahtapodov L, Moses A F, Olk P, Dheeraj D L, Fimland B O, Weman H and van Helvoort A T J 2013 *Semicond. Sci. Technol.* **28** 115004

[13] Iyer S, Reynolds L, Rawdanowicz T, Ojha S K, Kasanaboina P K and Bowen A 2014 *Nanoscience and Nanoengineering: Advances and Applications* ch 3(CRC Press) p 31   Q10

[14] Kasanaboina P K, Ojha S K, Sami S U, Reynolds L, Liu Y and Iyer S 2015 *Proc. of SPIE* **9373** 937307–1

[15] Kuang Y J, Sukrittanon S, Li H and Tu C W 2015 *Appl. Phys. Lett.* **107** 012101

[16] Araki Y, Yamaguchi M and Ishikawa F 2013 *Nanotechnology* **24** 065601

[17] Anyebe E A, Rajpalke M K, Veal T D, Jin C J, Wang Z M and Zhuang Q 2014 *Nano Res.* (Tsinghua University Press)   Q11

[18] El Kazzi S, Desplanque L, Wallart X, Wang Y and Ruterana P 2012 *J. Appl. Phys.* **111** 123506

[19] Jenichen B, Brandt O, Pfuller C, Dogan P, Knelangen M and Trampert A 2011 *Nanotechnology* **22** 295714

[20] Pavankumar K, Venkateswarlu K, Rameshbabu N and Muthupandi V 2012 *Key Eng. Mater.* **493** 739

[21] Stanchu H, Kladko V, Kuchuk A V, Safriuk N, Belyaev A, Wierzbicka A, Sobanska M, Klosek K and Zytkiewicz Z R 2015 *Nanoscale Res. Lett.* **10** 51

[22] Palosz B, Grzanka E, Gierlotka S and Stelmakh S 2010 *Zeitschrift für Kristallographie Crystalline Materials* **225** 588

[23] Prucnal S, Gao K, Anwand W, Helm M, Skorupa W and Zhou S 2012 *Opt. Express* **20** 26075

[24] Alberi K, Wu J, Walukiewicz W, Yu K M, Dubon O D, Watkins S P, Wang C X, Liu X, Cho Y J and Furdyna J 2007 *Phys. Rev.* B **75** 045203

[25] Vurgaftman I, Meyer J R and Ram-Mohan L R 2001 *J. Appl. Phys.* **89** 5815

[26] http://users.wpi.edu/~lrram/Publications/AllPub.html

[27] Chiu Y S, Ya M H, Su W S and Chen Y F 2002 *J. Appl. Phys.* **92** 5810

[28] Morozov S V, Kryzhkov D I, Yablonsky A N, Antonov A V, Kuritsin D I, Gaponova D M, Sadofyev Y G, Samal N, Gavrilenko V I and Krasilnik Z F 2013 *J. Appl. Phys.* **113** 163107

[29] Hussain A M P, Sarangi S N and Sahu S N 2010 arXiv preprint arXiv:1004 2319

[30] Zhang G, Tateno K, Birowosuto M D, Notomi M, Sogawa T and Gotoh H 2015 *Nanotechnology* **26** 115704

[31] Esther A L, Conesa-Boj S, Wallart X, Caroff P and Morral A F 2013 *Nanotechnology* **24** 405707

[32] Dobrovolsky A, Sukrittanon S, Kuang Y J, Tu C W, Chen W M and Buyanova I A 2014 *Appl. Phys. Lett.* **105** 193102

[33] Stehr J E, Dobrovolsky A, Sukrittanon S, Kuang Y, Tu C W, Chen W M and Buyanova I A 2015 *Nano Lett.* **15** 242

[34] Begum N, Piccin M, Jabeen F, Bais G, Rubini S, Martelli F and Bhatti A S 2008 *J. Appl. Phys.* **104** 104311

Q12

Appendix F

S K Ojha, P K Kasanaboina, C L Reynolds.Jr , Y Liu and S Iyer, "Effects of Sb variation in Ga assisted GaAs/GaAsSb/GaAs axial heterostructure nanowires" draft copy

Effects of Sb variation in Ga assisted GaAs/GaAsSb/GaAs axial heterostructure nanowires

S K Ojha[1], P K Kasanaboina[1], C L Reynolds.Jr [2], Y Liu[b] and S Iyer [1,3,*]

[1] Department of Electrical and Computer Engineering, North Carolina A and T State University, 1601,E Market St, Greensboro, NC 27411,USA

[2] Department of Materials Science and Engineering, North Carolina State University, 911 Partners Way

Engineering Building I, Raleigh, NC 27606, USA
[3] Department of Electrical and Computer Engineering/Nanoengineering, NCAT State University, 1601 E Market St, Greensboro, NC, 27411,USA

*email:iyer@ncat.edu Tel: +1 3362853710; Fax number: (+1) 336-500-0115

Abstract

In this work we report on the effect of Sb on the optical and structural properties of GaAs / GaAs$_{1-x}$Sb$_x$ /GaAs axial NWs which were grown on (111) Si substrate by Ga assisted molecular beam epitaxy (MBE). The Sb composition in the ~ 3 µm GaAsSb segment was varied up to 8.5 at. %, which was verified by energy dispersive x-ray spectroscopy (EDX). All the NWs exhibited a zinc blende (ZB) crystal structure and the high quality of the NWs was attested by the lack of any defects in the GaAsSb segment with mixed wurtzite and zinc blende phases towards the top of the NW as ascertained by high resolution transmission electron microscopy (HR-TEM) imaging. The vertical alignment of the NWs gradually changed to curved with increasing Sb concentration and has been attributed to increased strain in the NW. 4K micro-photoluminescence (PL) shows a red shift to 1.07 eV with increasing Sb to 8.5 at.% with a corresponding reduction in PL intensity with increasing Sb. The excitation power dependent PL of these NWs displayed a blue shift of ~15-20 meV, which is characteristic of a type-II

transition. With increasing Sb, the LO mode of the Raman spectra is shifted towards lower wavenumbers and also the spectra broadens. Both decreased PL intensity and broadening of PL and Raman spectra with increasing Sb suggest degradation of optical quality of the NWs.

Introduction:

The distinguishing characteristics of one dimensional feature of semiconductor nanowires (NWs) and associated large surface to volume ratio can be suitably exploited in developing band engineered nanostructures of desirable opto-electronic properties[1, 2]. Amongst the different III-V material systems GaAs $_x$ Sb $_{1-x}$ material system offers highly tunable bandgap in the 1.3 µm -1.55 µm wavelength range of interest for telecommunication applications. In the NW configuration this alloy system creates additional opportunity for applications in optical interconnects and quantum computing. Extensive work has been performed on $GaAs_xSb_{1-x}$ /GaAs NWs by different groups [3-7]. One of the interesting feature of III-Sb based NWs is the preference of these NWs being always grown in zinc blende (ZB) phase [8, 9] due to the presence of Sb, which stabilizes the ZB crystal structure as opposed to wurtzite (WZ) structure. due to material dependence critical supersaturation value[10, 11]. As GaAs can exhbit either ZB or WZ structure, the optical properties of GaAs/GaAsSb are strongly influenced by the structure of the GaAs NW as the bandgaps of WZ and ZB GaAs differ by almost 30 meV, it is to be expected that the nature of the optical transitions also exhibit strong dependency on the structural phases of the heterostructured NWs.

Though there has been innumerable body of literature on the structural investigation of the GaAsSb/GaAs heterostructured NWs using both Au-assisted as well as self-catalyzed growth, comparatively there have been fewer reports on the optical investigations. Todorovic et

al. [4] reported the effects of Sb composition variation within the GaAsSb insert of ~80nm in length, which were sandwiched between wurtzite (WZ) GaAs NWs grown using Au assisted MBE. We have also earlier reported on GaAsSb segments of few microns[6] . Though the density of NWs grown was low, the work showed great promise of using longer GaAsSb segment leading to higher active volume that can be advantageously utilized for optoelectronic device applications. Optical characteristics of effects of Sb on GaAs/GaAsSb core shell configured NWs have also been reported [12] and red shift up to 1.3 um has been demonstrated.

In this work, we report on the axial growth of GaAs/GaAsSb/GaAs with GaAsSb insert of µm length. A systematic work has been carried out using variety of characterization technique to ascertain the correlation between the effect of Sb on the morphology, red shift in the PL and nature of the PL transitions and also on the vibrational mode. The characteristics of the axial structure is compared with core-shell NWs and the characteristics are found to differ quite significantly with the vapor solid growth mechanism seems to yield better quality NWs.

Experimental details:

The NWs were grown on chemically etched p-type Si (111) substrates by the conventional solid source EPI 930 MBE system. The NW growth was performed at a growth temperature of 620˚C and the growth was initiated by first opening the Ga shutter for 15seconds followed by the opening of As_4 source with a beam equivalent pressure (BEP) of 4.8×10^{-6} Torr for the growth of GaAs NW stem. The GaAsSb insert growth was then subsequently grown by opening Sb source terminating with GaAs cap layer. The configuration of the NW structures were (500nm) GaAs/ (3.5µm-4.0µm) GaAsSb /(500nm)GaAs, The heterostructured NWs of GaAs (0 at. % Sb), GaAs/GaAsSb/GaAs (1 at. % Sb), GaAs/GaAsSb/GaAs (4.5 at. % Sb),

GaAs/GaAsSb/GaAs (8.5 at. % Sb) referred as S1, S2, S3 and S4, respectively, were grown. Scanning electron microscope (SEM) imaging was performed using a Carl Zeiss Auriga-BU FIB FESEM with an attached energy dispersive x-ray spectroscopy (EDX) system, which was used to determine the elemental composition in the NWs. EDX point analysis was used to determine the Sb concentration by performing composition analysis at several locations along the GaAsSb segment. The STEM analysis was performed on an aberration-corrected (probe) FEI Titan G2 system operated at 200 kV. Optical characteristics of the nanowires were measured by µ-photoluminescence (PL) using a 633 nm He–Ne laser as the excitation source with a 0.32 m double grating monochromator for wavelength dispersion and InGaAs detector along with a conventional lock-in amplifier system. An Olympus IR 50X lens was used to focus the laser on the nanowires. A closed-cycle optical cryostat from Montana Cryostation with the sample chamber interfaced with a fiber coupled confocal microscope was used to study the variation of PL characteristics at low temperature of 4K. Raman spectroscopy was performed at room temperature in a Horiba Jobin Yvon ARAMIS Raman microscope. The excitation source was a He-Ne laser with 633 nm as the excitation wavelength and the signal were detected with a multichannel air cooled charged couple device.

Results and Discussion

Figure 1(a) shows a SEM image of highly dense and vertical GaAsSb NWs with a density in the range of ~8×10^8/cm^2. Figure 1(b) displays the changes in surface morphology of single NWs of different Sb content 1at.%, 4.5 at.% and 8.5 at.%. With increasing Sb at.% the diameter of the NW increases from 70 nm to 180 nm consistent with the reports of Dheeraj et al. [9] where they also observed similar increase in diameter of NW with simultaneous decrease in the insert length

with rising Sb at.% incorporation. All the NWs exhibited well faceted hexagonal structure independent of Sb at. % in the segment though the vertically aligned NWs curved with increasing Sb content. Figure 2 shows the bending angle of the ZB GaAs/GaAsSb NWs as a function of Sb concentration. Sb is a well-known surfactant which leads to reduction in the surface energy of the NW side walls, thereby allowing retention of excess Sb on the surface promoting enhanced radial growth rate as well multiple faceted growth[13, 14]. The increased bending of the NWs with Sb content can be associated with the increased mismatch between the GaAs and GaAsSb interface [12] as well as thicker diameter NWs both leading to enhancement in the accumulation of the strain in the segment. Similar results were also observed in core-shell configured GaAs/GaAsSb NWs [5, 12, 14].
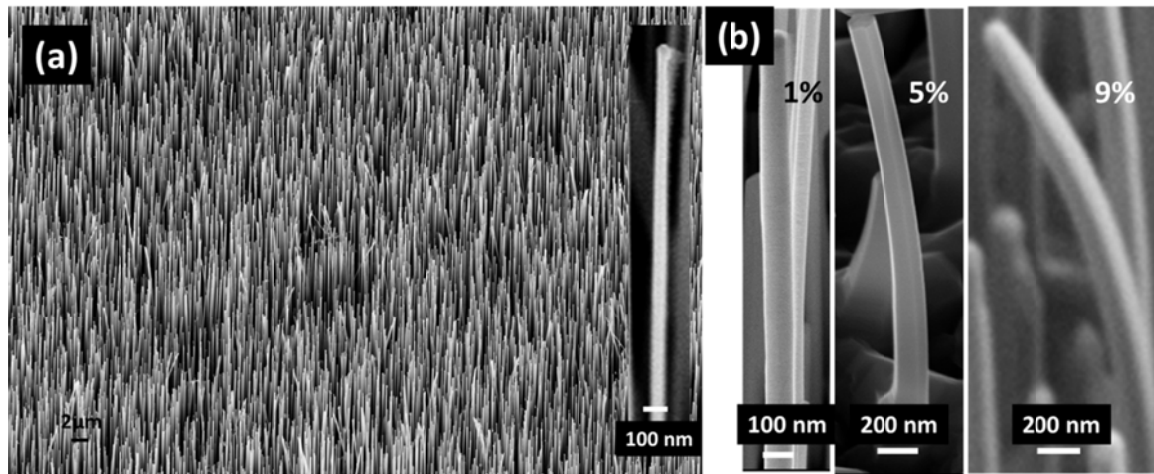
Figure 1. SEM images of a) GaAs/GaAsSb/GaAs NWs and b) is the magnified single NWs with Sb composition of 1 at. %, 4.5 at.% and 8.5 at.%.
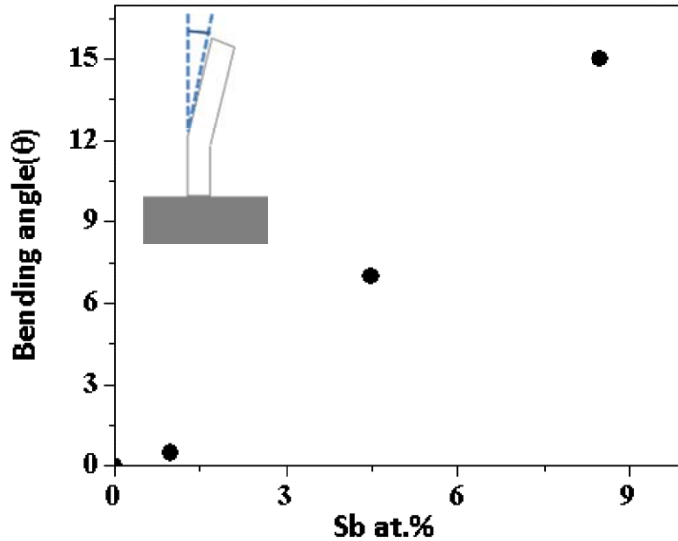
Figure 2. Bending angle of the NWs with respect to Sb content in the GaAsSb segment.

Bright field transmission electron microscope (TEM) image of segmented NW with Sb of 4.5 at.% is shown in figure 3. The increased diameter of the GaAsSb segment over the diameter of the GaAs cap is clearly evident in figure 3(a). The GaAsSb segment exhibits pure ZB structure (figure 3(d) and figure 3(e)) with no traces of planar defects, namely, stacking faults and twins, whereas, GaAs cap displays WZ structure as shown in figure 3(b). A mixture of both ZB and WZ is observed in the transition region, ~500 nm below the tip, at the GaAsSb and GaAs cap interface (figure 3(c)), which is attributed to the presence of traces of Sb in the Ga liquid droplet on the tip of the NW. Selected area diffraction (SAED) pattern (figure 3(e)) taken at the central region of the GaAsSb segment further attest to the pure ZB structure of GaAsSb and absence of any satellite spots corroborates the lack of twins. This was also verified on quite a few NWs from the same sample as shown in figure 4. Though absence of planar defects cannot be completely ruled out, nevertheless our TEM data clearly show that the defects are minimal in the majority of GaAsSb segment, in contrast to the GaAs/GaAsSb/GaAs core shell NWs which always exhibit twins[14]. In addition, the morphology of the NWs retained well faceted

hexagonal structure even at high Sb content of 8.5 at.% investigated, while the core shell NWs exhibited deterioration in the surface morphology with increasing Sb content in the shell structure. These attributes can be viewed as clear demonstration of the superiority of the vapor liquid solid growth mechanism responsible for axial growth, yielding better structural quality NWs over the core-shell NWs grown by vapor solid mechanism. Further, the larger active volume associated with long GaAsSb segments of high structural quality can be more advantageous for optoelectronic device applications as compared to previously reported shorter GaAsSb segments [3, 4] due to availability of large amount of carrier there by increasing overall mobility.
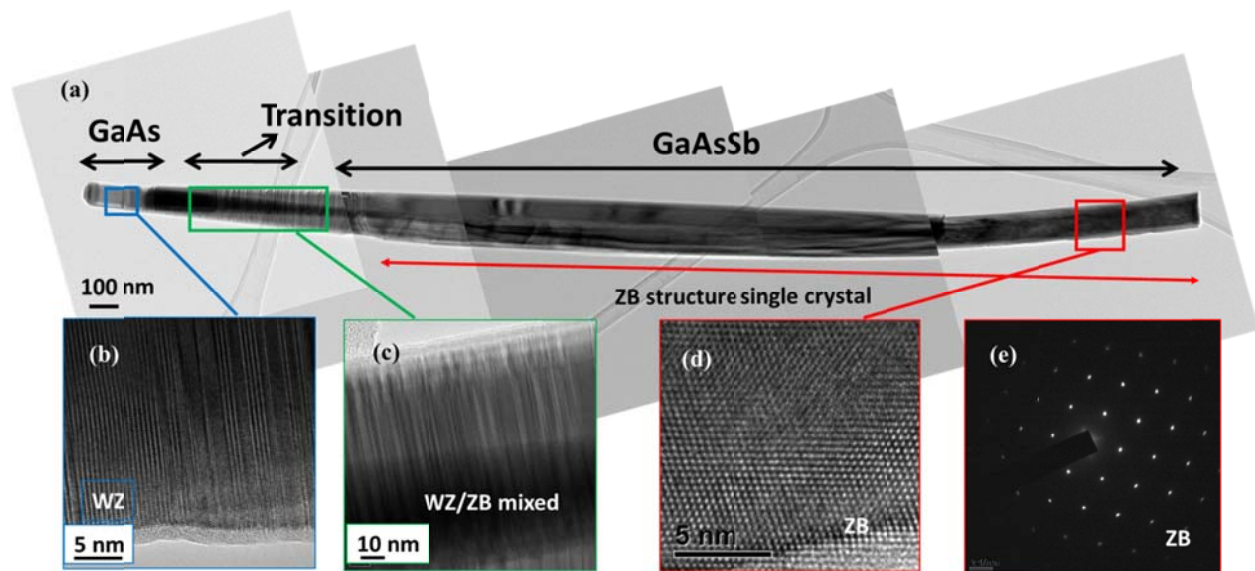
Figure 3. a) TEM image of the segmented NW showing different regions; HR-TEM images show b) WZ structure in GaAs cap region, c) mixture of WZ/ZB in the transition region and d) pure ZB structure in GaAsSb segment. e) SAED pattern of the GaAsSb segment display pure ZB structure with no planar defects.
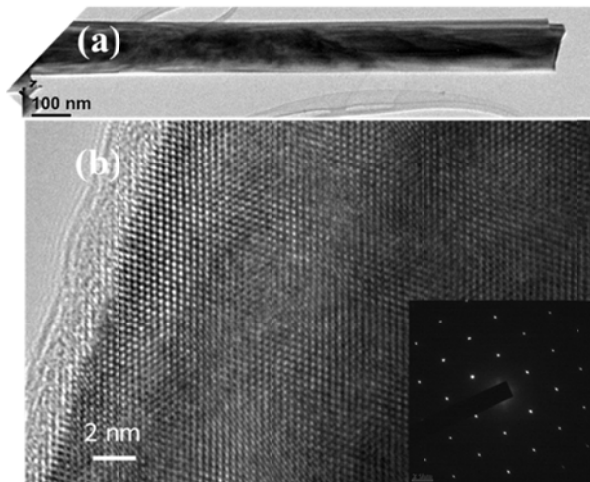
Figure 4. TEM image of a broken NW segment which predominantly shows (a) defect free GaAsSb segment with (b) high resolution STEM image exhibiting the ZB structure and corresponding SAED pattern (inset).

Figure 5 shows the 4K normalized micro-photoluminescence (µ-PL) spectra of single NW for different Sb concentration in the segment. A reference GaAs NW exhibits dominant peak around 1.47 eV and 1.33eV. These peaks are signatures of band to band transition in ZB phase and As vacancy defect level[15], respectively. The higher Sb at. %, NWs are characterized by multiple PL peaks, though all red shifted towards the lower energy, in the range of 1.26 eV to 1.07 eV.
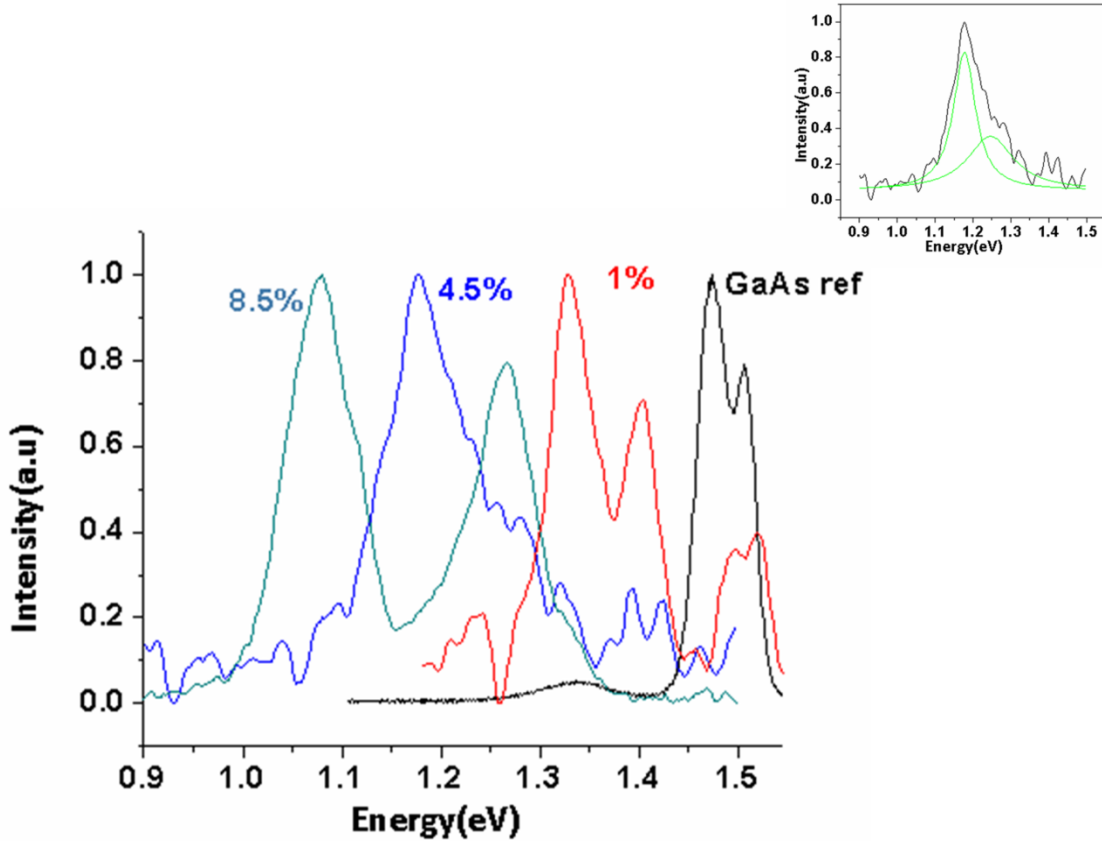
Figure 5. Low temperature (4K) normalized photoluminescence spectra of single NWs for different Sb composition in the GaAsSb segment. Inset is the Lorentzian line shape fit of the PL spectrum of 4.5 at.% Sb.

The nature of the PL transitions were ascertained from the excitation power dependence of the PL spectra on all the single NWs. Figure 6 shows the low temperature(4K) power dependence PL spectra of single NWs for Sb concentration of 4.5 at.% and 8.5 at. %, where the intensity was increased up to 10x (P= lowest intensity of 0.5mW). The prominent PL peak is observed at 1.17 eV for 4.5 at. % Sb, which doesn't exhibit any shift with increasing excitation power as shown in figure 6(a). Similar results were observed for 1 at.% Sb (figure not shown). The invariant nature of the peak is indicative of type I transition and as it is towards lower energy

it is attributed to the transition within the GaAsSb segment. For higher Sb content of 8.5 at.% , two distinct peaks were observed at 1.26 and 1.07 eV. Both the peaks show a blue shift of 20 meV and 60 meV, respectively with increasing intensity. This blueshift of the PL transitions is attributed to the electric field induced band bending [16, 17] creating a notch near the GaAs and GaAsSb interface. The electric field is supposedly resultant of the spatial separation of electron and hole pairs in the type II structures. Thus this transition is assigned to transition of carriers from confined energy levels from ZB GaAs conduction band (CB) to ZB GaAsSb valence band (VB). With increasing incident intensity, the band bending becomes more pronounced at the interface with higher carrier confinement resulting in larger blue shift.
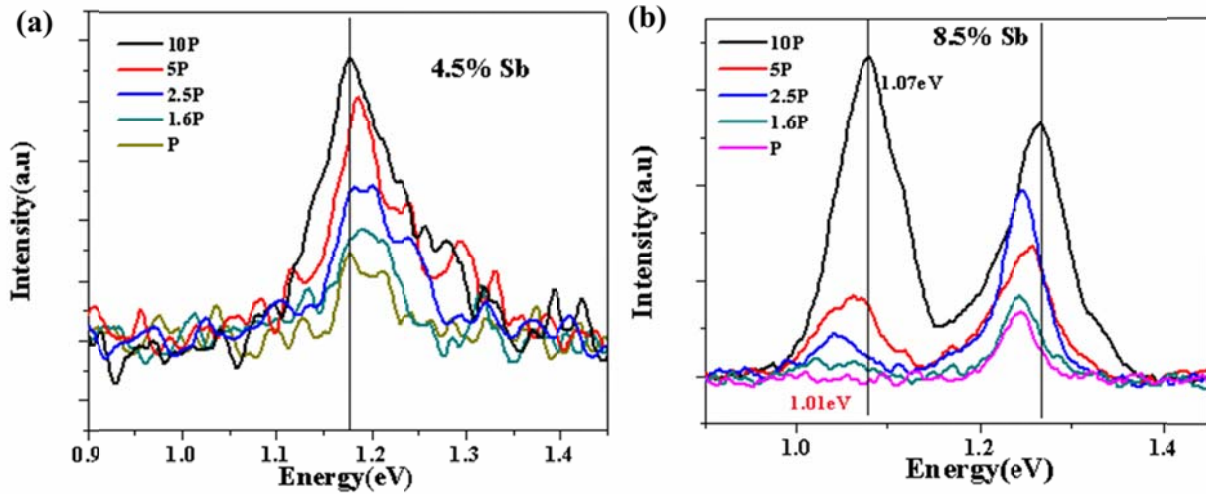
Figure 6. Excitation power dependent photoluminescence spectra of segmented single NWs with a) 4.5at.% Sb and b) 8.5 at.% Sb.

Figure 7 shows the room temperature Raman spectra of GaAs/GaAsSb/GaAs segmented NW ensemble for different Sb compositions. The Raman spectra for reference GaAs NW exhibits LO and TO modes at 291 cm^{-1} and 267.8 cm^{-1}, respectively. Both LO and TO modes are broadened and red shifted to 281 cm^{-1} and 260.7 cm^{-1}, respectively, with increasing Sb content in

the segment. The large peak broadening of both LO and TO GaAs modes are clear indicative of increased lattice distortion with Sb at. % incorporation. The red shift in Raman modes can occur due to the various mechanisms which are as follows: (i) alloying, (ii) strain, (iii) alloy disorder, (iv) laser heating, (v) phonon confinement and (vi) phonon localization at the defects. All the first four mechanisms are likely to be enhanced with increasing Sb content. Phonon confinement can be ruled out as phonon confinement has inverse dependence on the NW diameter and the diameter of the segmented NWs increase with increasing Sb content. Also the NW diameters investigated are large enough for the phonon confinement effect to be negligible. The symmetric line shape further attest to our TEM investigation that planar defects are minimal as otherwise highly asymmetric line shape would have resulted as in the case of our core-shell NWs[14], which has been shown here in the inset for comparison(figure 7). The LO/TO ratio also increases with increasing Sb content. In literature strong dependence of LO and TO mode intensities on the nanocrystallite size (R) has been reported [18] and the phonon mode contributions to dephasing rate scale is predicted to vary as $1/R^{2.5}$, which explains the increasing LO/TO ratio with larger NW diameter resulting from increased Sb at.%.
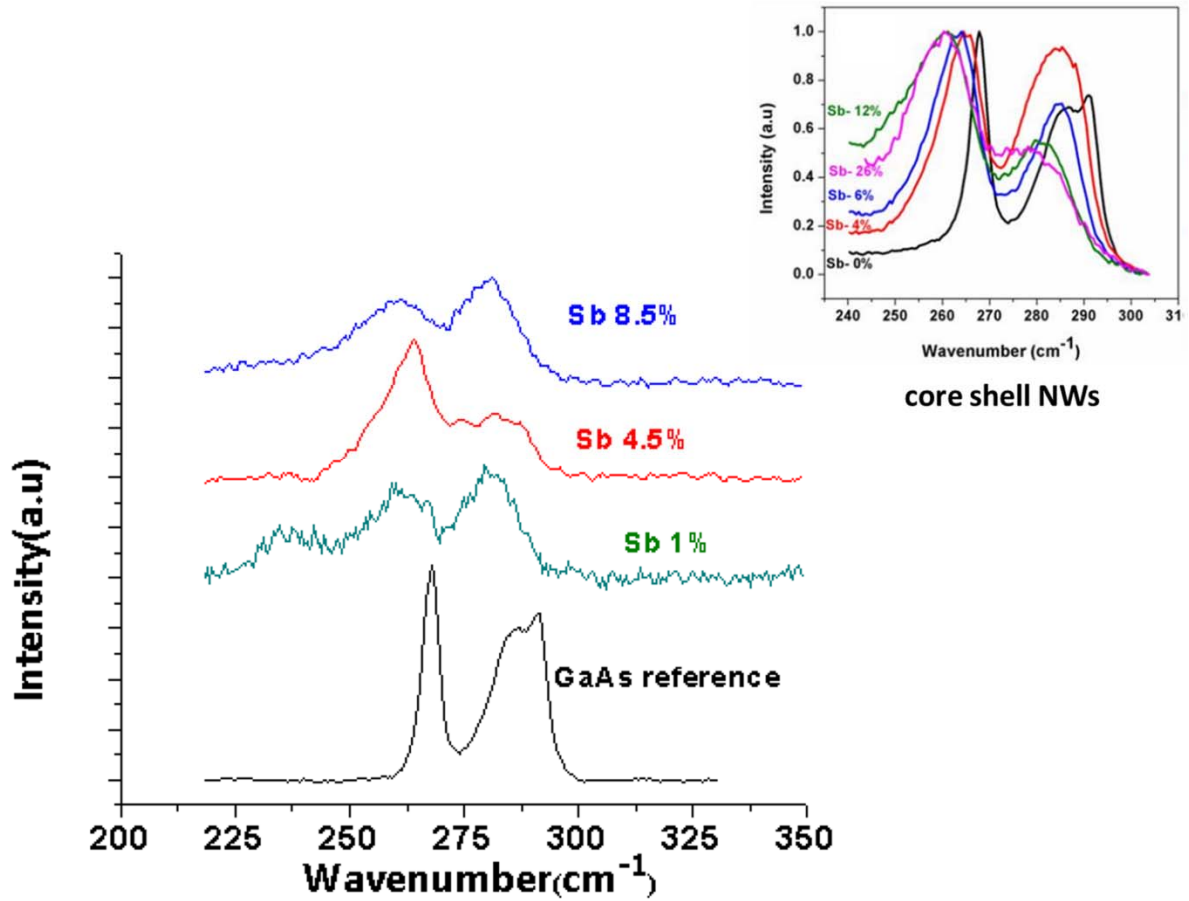
Figure 7. Raman spectra showing the movement to lower wavenumber of GaAs$_{LO}$ with the variation in the at.% of Sb in the samples with the GaAs/GaAsSb core shell NWs in the inset for comparison.

The broadening of the FWHM of the LO mode clearly shows the strain present, which is consistent with bending of NWs. Further investigation is needed for reduction of this strain and better incorporation of Sb into the NWs. These are preliminary data and further growth optimization will be initiated. Hence, a fairly good optical and structural quality of the GaAsSb NWs grown so far show great promise for applications in the 1.3 µm region and longer wavelength for optical communications.

Conclusion:

In conclusion, GaAs/GaAsSb/Sb axial NWs were grown using Ga assisted molecular beam epitaxy with a GaAsSb insert of 3.5-4.0 µm length. Sb composition was varied in the segment that resulted in producing different structural aspect of the NWs. HR TEM results showed that the GaAsSb segment had ZB structure which was of pure quality without any defects. Although a ZB/WZ combination was obtained towards the transition from GaAsSb to GaAs portion of the NW. The optical transitions were dependent on the Sb at. % which was verified by the Raman spectra. Though the Sb at. % was 8.5, low temperature PL determined the emission upto 1.07 eV in the NWs. Power dependence PL showed a blue shift of the peaks upto 60meV for 1.07 eV confirming type II transition. Significant effect of the lowering of the energy level with single high quality GaAsSb segment creates new possibilities for further band tuning of these NWs.

References:

[1]   Xiang J, Lu W, Hu Y, Wu Y, Yan H and Lieber C M 2006 *Nature* **441** 489-93

[2]   Duan X, Huang Y, Agarwal R and Lieber C M 2003 *Nature* **421** 241-5

[3]   Dheeraj D, Patriarche G, Zhou H, Harmand J, Weman H and Fimland B 2009 *J. Cryst. Growth* **311** 1847-50

[4]   Todorovic J, Kauko H, Ahtapodov L, Moses A, Olk P, Dheeraj D, Fimland B, Weman H and van

         Helvoort A 2013 *Semicond. Sci. Technol.* **28** 115004

[5]   Ghalamestani S G, Munshi A M, Dheeraj D L, Fimland B-O, Weman H and Dick K A 2013

         Nanotechnology **24** 405601

[6]   Iyer S, Reynolds L, Rawdanowicz T, Ojha S K, Kasanaboina P K and Bowen A 2014 *Nanoscience*

         and Nanoengineering: Advances and Applications 31

[7]   Plissard S, Dick K A, Wallart X and Caroff P 2010 *Appl. Phys. Lett.* **96** 121901-3

[8]   L.Dasa H W a D 2011 *Advances in III-V Semiconductor Nanowires and Nanodevices,* ed D W a R R

         L J Li: Bentham Science Publishers) pp 89-104

[9]   Dheeraj D L, Patriarche G, Zhou H, Hoang T B, Moses A F, Grønsberg S, van Helvoort A T J,

         Fimland B-O and Weman H 2008 *Nano Lett.* **8** 4459-63

[10]   Glas F, Patriarche G and Harmand J C 2010,Journal of Physics: Conference Series 209 012002

[11]   Glas F 2008 Journal of Applied Physics 104 093520

[12]   Pavan Kumar Kasanaboina, S K Ojha, Shifat Us Sami, C. Lewis Reynolds Jr., Yang Liu and Iyer a S

         2015 Semiconductor Science and Technology(Accepted on Aug 19,2015)

[11]   Zhang L, Tang H F and Kuech T F 2001 *Appl. Phys. Lett.* **79** 3059-61

[13]   Kasanaboina P K, Ojha S K, Sami S U, Reynolds L, Liu Y and Iyer S 2015 *SPIE OPTO*: International

         Society for Optics and Photonics) pp 937307--9

[14]   Kasanaboina P K, Ojha S K, Sami S M, Reynolds Jr. C L, Liu Y and Iyer S a S 2015 *Semicond. Sci.*

         Technol.(Accepted on Aug 19,2015)

[15]   Prucnal S, Gao K, Anwand W, Helm M, Skorupa W and Zhou S 2012 *Opt. express* **20** 26075-81

[16]   Chiu Y, Ya M, Su W and Chen Y 2002 *J.Appl. Phys.* **92** 5810-3

[17]   Morozov S V, Kryzhkov D I, Yablonsky A N, Antonov A V, Kuritsin D I, Gaponova D M, Sadofyev Y

         G, Samal N, Gavrilenko V I and Krasilnik Z F 2013 *J. Appl. Phys.* **113** 163107

[18]   Shiang J, Wolters R and Heath J 1997 *J.Chem. Phys.* **106** 8981-94

Appendix G

M Sai Krishna Ojha, Pavan Kumar Kasanaboina[a], C Lewis Reynolds.Jr [b], Thomas A Rawdanowicz[b], Ryan M White[b] and Shanthi Iyer [a,c,*]

 "Study of Be doping in GaAs core & core-shell nanowires using photoluminescence and Raman spectroscopy", manuscript under preparation: **.**

A **Study of Be doping in GaAs core & core-shell nanowires using photoluminescence and Raman spectroscopy.**

Sai Krishna Ojha[a], Pavan Kumar Kasanaboina[a], C Lewis Reynolds.Jr [b], Thomas A Rawdanowicz[b], Ryan M White[b] and Shanthi Iyer [a,c,*]

[a] *Department of Electrical and Computer Engineering, North Carolina A and T State University, 1601,E Market St, Greensboro, NC 27411,USA*
Author 1email:sojha@aggies.ncat.edu,Author 2 email: pavan.kmm@gmail.com
[b] *Department of Materials Science and Engineering, North Carolina State University, 911 Partners Way Engineering Building I, Raleigh, NC 27606, USA*
Author 3 email: lew_reynolds@ncsu.edu, Author 4 email: tarawdan@ncsu.edu, Author 5 email: rmwhite@ncsu.edu
[c]*Department of Electrical and Computer Engineering/Nanoengineering, NCA&T State University, 1601 E Market st Greensboro, NC, 27411,USA*

Corresponding Author 6 email:iyer@ncat.edu Tel: +1 3362853710; Fax number: (+1) 336-500-0115

Abstract:

Effective implementation of doped nanowires (NWs) in nanoscaled devices requires controlled and effective dopant incorporation. A catalyst free Ga-assisted approach for producing Be-doped GaAs NWs grown by molecular beam epitaxy is reported. A systematic and a comprehensive study is reported using a variety of characterization techniques to determine the impact of growth variants on the NW ensemble properties and thereby identify the relevant growth parameters that lead to enhanced Be incorporation. The core NWs are characterized by two photoluminescence (PL) emission peaks that are attributed to Be-related near band edge (~ 1.49 to 1.51 eV) emission and surface defects (~1.35-1.39 eV) whereas the shell NWs by the band 1.49-1.51 eV. The dominance of the former, a signature of enhanced Be incorporation, is found to occur for shell configured nanowires at a lower V/III ratio and at a higher Be cell temperature of 990°C. The enhanced GaAs $_{TO/LO}$ Raman peak ratio exhibited by these NWs further attest to the effective Be incorporation. The NWs exhibit a mixture of zinc blende (ZB) and wurtzite (WZ) structures although terminating always in a ZB structure.

Introduction:

Doping incorporation in nanowires (NWs) is much more complex in comparison to two dimensional structures and bulk semiconductors due to the additional pathways for doping as well as growth variants that influence the NW doping which are non-existent in higher dimensional structures. These are the effects of supersaturation in the seed melt, differing growth mechanisms of the core and the shell configuration, quantum confinement and crystal structure dependence on NW diameter, large defect compensation caused by the huge surface to volume ratio and to a lesser extent the III-V flux ratio as well as the actual value of flux.

Be is the commonly used p-type dopant in molecular beam epitaxy as it has a high diffusion coefficient [1] and less memory effects [2]. Additionally, high carrier lifetime [3] and carrier concentrations [4] have been demonstrated in the thin films. There have been several previous investigations on Be doping in NWs that have been reported in the literature [1,5-7] Hilse et al [5] found that Be incorporation in GaAs is limited by Be interstitials, Be_I, and the ability to achieve p-type conductivity relies on incorporating Be substitutionally on Ga lattice sites (Be_{Ga}). In a core–shell structure, the Be concentration is found to be enhanced in the shell configuration compared to the simple core-only configuration due to the reduction in the depletion layer width caused by the pinning of the Fermi level at surface defects [6].

The previous studies have been focused on single NW and the results are somewhat scattered. For effective implementation of NWs in miniaturized devices, a study of NW ensemble is more meaningful, and a good understanding of the effect of various growth variants on doping is important in order to synthesize reproducible NWs with the desired doping. In this work, a systematic and comprehensive approach is adopted to gain further insight on the effects

of growth parameters, namely Be cell temperature, V/III flux ratio, and NW core/shell configuration, on the morphological and optical characteristics of Be-doped GaAs nanowires using characterization techniques, such as scanning electron microscopy (SEM), low temperature photoluminescence (PL) and Raman spectroscopy. This has enabled us to identify the relevant growth parameters that strongly influence Be incorporation in the NWs. We also show strong evidence of Be doping in GaAs core and core shell nanowires that are responsible for higher energy PL emission, and demonstrate the combination of PL and Raman provide a powerful tool for characterizing the optoelectronic properties of core shell GaAs NWs.

Experimental Details:

Be-doped GaAs NWs were grown in an EPI 930 solid source MBE system equipped with a Ga SUMO cell, Be effusion cell and an As valved cracker as described in our previous work [8]. The Ga-assisted NW growth was performed on epiready Si (111) substrates. These substrates were chemically etched to obtain the optimum SiO_2 layer for NWs growths. Growth was initiated by opening the Ga cell's shutter for 15 seconds prior to simultaneous opening of As and Be shutters. The core GaAs NW growth was carried out at 620˚C and was grown for 10 minutes. Growth was terminated by closing the Ga and Be shutters simultaneously, while the As shutter was closed after the growth temperature reduced below 500 ˚C. However, for the shell growth, the growth was again initiated with the opening of the Ga and Be shutters along with As at the substrate temperature of 465˚C for 10 minutes. For I-V measurements on the NWs, a Poly methyl methacrylate (PMMA) layer was used to fill the gaps between the NWs. PMMA thickness was measured using an ellipsometer. Thereafter the NWs were planarized by ultra-sonicating with DI water for 2 hours in a sonication water bath. The NWs were then rapid thermal annealed under ambient atmosphere at 400˚C for 40sec duration to expose the NWs for

contact. Ti (50 nm)/Au(200 nm) and Ti (200nm) were used for the top contact on the NW and back contact on the p-type Si, respectively [9]. The electrical measurements were performed at room temperature using a Keithley 4200 characterization system using a 2 probe method. Optical characteristics of the nanowires were measured by µ-photoluminescence (PL) using a 633 nm He–Ne laser as the excitation source with a 0.32 m double grating monochromator for wavelength dispersion and InGaAs detector with a conventional lock-in amplifier system. An Olympus IR 50X lens was used to focus the laser on the nanowires. A closed-cycle optical cryostat from Montana Cryostation with the sample chamber interfaced with a fiber coupled confocal microscope was used to study the variation of PL characteristics at low temperature of 4K. A Horiba Jobin Yvon LabRam ARAMIS Raman microscope was used to determine the vibrational characteristics and hence quality of the nanowires using a He-Ne laser with 633 nm excitation wavelength at room temperature. Scanning electron microscope (SEM) imaging was performed using a Carl Zeiss Auriga-BU FIB FESEM Microscope. The STEM analysis was performed on an aberration-corrected (probe) FEI Titan G2 system.

Results and Discussion:

The Be-doped core NWs C1, C2 and C3 were grown at 620°C for three different Be cell temperatures of 800°C, 900°C and 990°C. A typical 45°- tilted view SEM image of Be doped NWs grown on (111) Si is shown in figure 1(a). The diameter of the NWs ranged from 90-130 nm. The core shell nanowires with both being doped with Be at different cell temperatures of 900°C (S1& S2) and 990°C (S3 & S4) and for two different shell V/III ratios of 70 and 35, respectively. The SEM image of the core-shell NWs (figure 1(b)) show the vertical and straight NWs with diameters in the range of 160-188 nm grown on the (111) Si substrate. The length of all the NWs were in the range of 2.5- 3.5 µm.
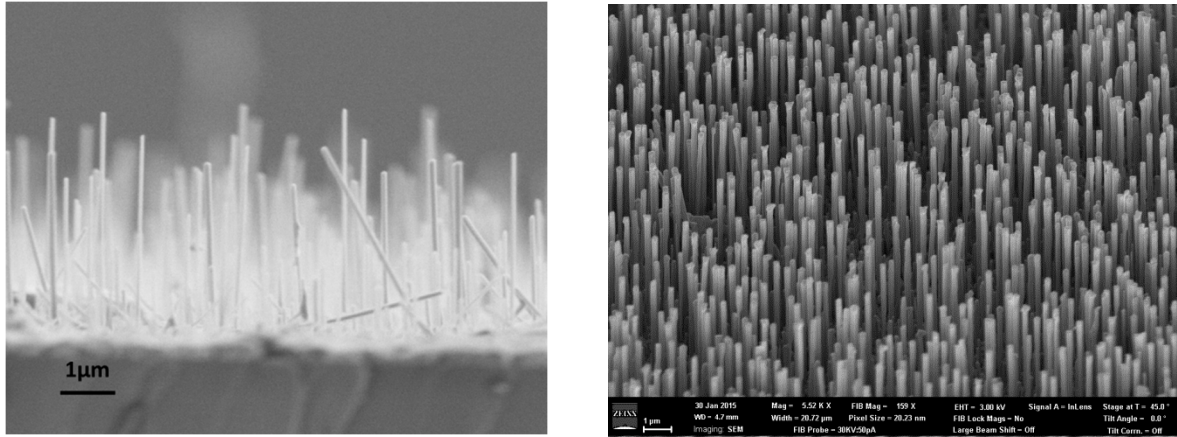
Figure.1 (a) Side view SEM images of Be doped core & (b) 45° tilted view of core-shell GaAs NWs grown by self-assisted MBE.

Figure 2 displays the bright field scanning tunneling electron microscope images of core NWs grown at a Be cell temperatures of 900 °C exhibit predominantly a ZB crystal structure with traces of twinning defects. At the very tip of these NWs they terminate in a ZB structure, as shown in figure 2(a) and 2(d). The reduced diameter region associated with a necking phenomenon occurring near the tip of sample for 900°C of Be cell temperature, exhibits a WZ structure which would be due to difference in the supersaturation. The necking of the NW is observed only in nanowires in which the cores are doped. This behavior can be attributed to termination of the Be flux while the As flux remains "on". In the absence of Be, supersaturation is increased and with the availability of As flux, the wire continues to grow albeit with a smaller diameter, which strongly favors the WZ structure.
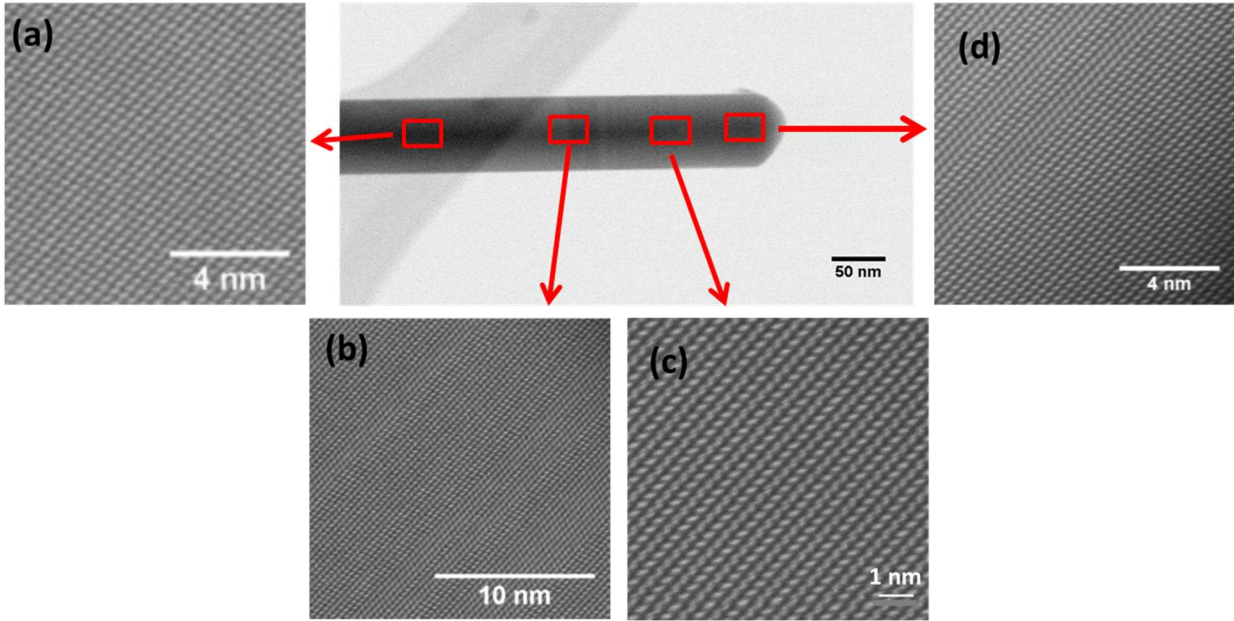
Figure.2 Bright field STEM image with selected areas annotated for region identification and correlation of subsequent images viewed from different axes (a) viewed along the [011] ZB zone axis indicating a predominantly ZB region (b) viewed along the [$2\overline{1}\overline{1}0$]||[011] (WZ||ZB) zone axes indicating a transition region from twinning ZB to polytype WZ congruent with NW diameter reduction c) viewed along the [$2\overline{1}\overline{1}0$] WZ zone axis indicating predominantly polytype wurtzite crystal structure and d) viewed along [$2\overline{1}\overline{1}0$]||[011] (WZ||ZB) zone axes at the NW tip terminating in a ZB structure.

Figure 3(a) represents the photoluminescence spectra of the core NWs at 4K grown at different Be cell temperatures. The NW C1 grown at 800˚C shows a dominant peak at 1.51 eV with long tail towards lower energy. The PL peak energy showed a large red shift to 1.49 eV with an increase in the cell temperature to 900˚C and marginal shift to 1.487 eV with a further increase in Be cell temperature to 990˚C. A broad peak in the range of 1.35 -1.39 eV was observed for the NWs grown at 900˚C. This peak we have consistently observed in NWs which were grown without any chemical etching and associated with deep impurities and defects

commonly attributed to the presence of two complexes, As_{Ga}-Si_{Ga} and Si_{As}-V_{As}. The red shift towards lower energy with increase in the cell temperature is indicative of bandgap narrowing [10-12]. The peak at 1.49 eV can be identified as (e, A) peak whereas at 1.51 eV as the (B, B) peak [10, 13].
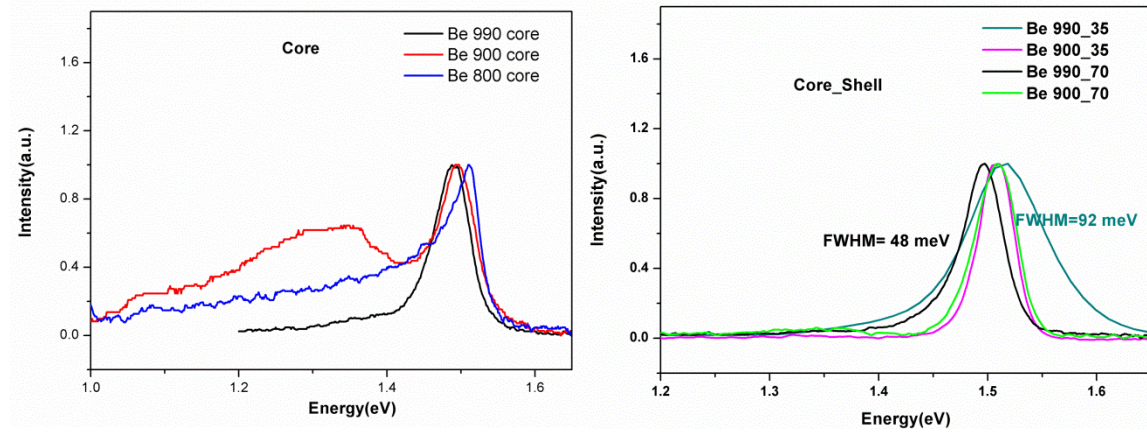

Figure 3(a) 4K photoluminescence spectra of core and (b) core-shell GaAs NWs grown with different Be cell temperatures.

Figure 3(b) displays peak of sample S4 at 1.51 eV. For S2 and S3, the peak is consistent at 1.51 eV whereas for S4, the peak shifts to 1.49 eV. For samples S2 and S4, there is not much peak shift where as there is a red shift for S1 to S3, where Be concentration is same for S2 &S4 (~ 10^{18} cm^{-3}) and S1& S3 (~ 10^{19} cm^{-3}), respectively. In comparison to the core GaAs NWs, the emission spectra of the core-shell NWs was found to only exhibit the peak at the higher energy side. There is enhancement of the PL spectra at low temperature which could be due to the passivation of the GaAs core with GaAs shell. As the V/III ratio of the shell increases from 35 to 70, there is an increase in the Be incorporation in the core shell structure which matches with the results from pao et al where the Be doping was performed on GaAs thin films [15]. Although their samples detoriated at high V/III ratio, our NWs were structurally good. There is clearly

shown in the shift in the peak to lower energy of 1.49 eV. This could be due to a significant

reduction in the bandgap with the increase in the concentration of free carriers and impurity ions.

There are well defined bound states associated with each dopant ions which broadens into

distinct impurity bands due to overlap among dopant-ion orbits. When the density of the dopants

increases still further, impurity band merges with the main band [13]. As mentioned above, there

are two distinct peak observed i.e. (e,A) peak and (B,B) peak found in these samples. In S1, both

the peaks are very close. As the acceptor concentration increases, main peak is (e, A) peak which

shifts towards lower energy as seen in S3. Here both the (e, A) and (B,B) peaks appears to be

found at high dopant level where both the impurity band and the valence band are found to be

merged which is consistent with results from Feng et al [10, 16].
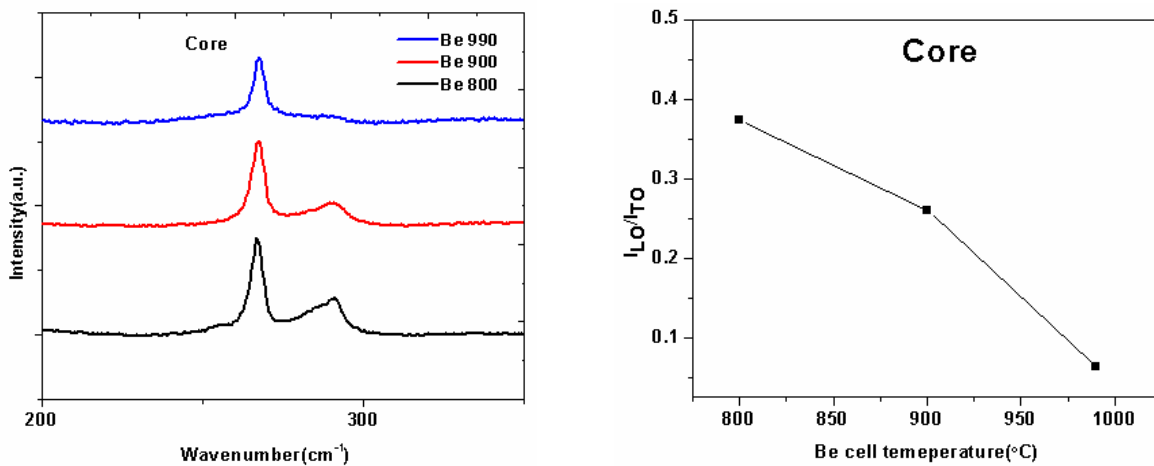
Figure.4 (a) Room temperature Raman plots of the NW core grown at different Be cell

temperatures. (b) I_{LO}/I_{TO} for the GaAs peaks as a function of Be cell temperature.

Raman spectra of the Be doped samples C1, C2 and C3 are shown in the figure 4(a). All

the spectra exhibit the peaks at 267 and 290 cm^{-1} representing the TO and LO Raman modes of

GaAs NWs, respectively [17]. The intensity of TO and LO peaks reduces with an increase in the

Be cell temperature as shown in figure 4(b). Amongst the 990°C grown NW samples (sample C3), the LO peak intensity is the least. With an increase in the Be doping level, the probability of incorporation of Be in the interstitial sites increase [5, 18]. Although the Be_i related defect peaks was not detected at 384 cm^{-1} [5] due to the instrumentation limitation, the low I_{LO}/I_{TO} was a clear indication of the high Be incorporation.

Figure 5(a) exhibits the Raman spectra of the core-shell GaAs NW samples of S1, S2, S3 and S4. The distinct peaks are at 267 cm^{-1} corresponding to the TO mode of GaAs and the second peak at 289 cm^{-1} seems to be a function of both the Be cell temperature and V/III flux ratio. A downward shift of 4 cm^{-1} is observed when the Be cell temperature is increased for a given V/III flux ratio as well as for constant Be cell temperature with V/III flux ratio varying from 35 to 70. The shift indicates a clear incorporation of Be in the NWs. Figure 5(b) displays the intensity ratio of the LO/TO. There is a decrease in the I_{LO}/I_{TO} for V/III of 70 whereas for 35, the LO intensity is higher at higher Be cell temperature.
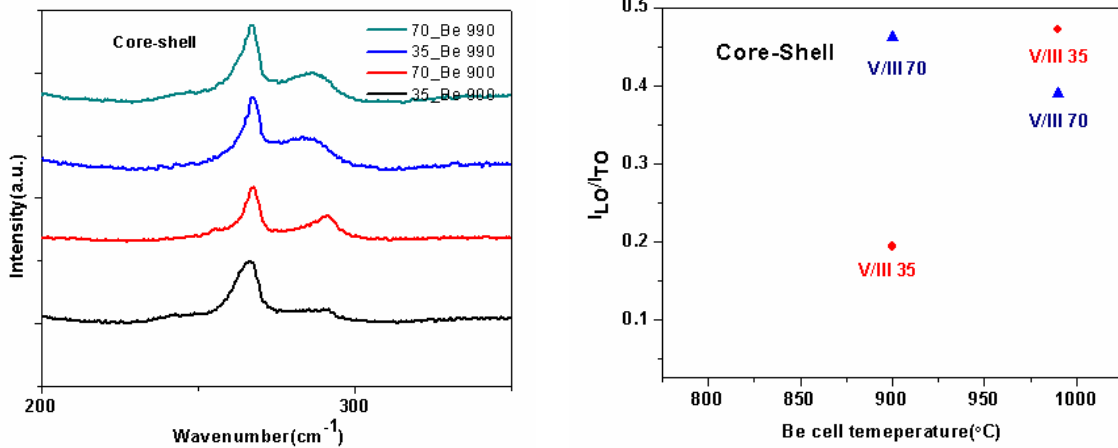

Figure.5(a) Room temperature Raman plots of the NW core-shell grown at different Be cell temperatures and V/III ratio for shell (b) I_{LO}/I_{TO} for the GaAs peaks as a function of Be cell temperature for shell configured NWs.

On the basis of the data presented above, the vibrational and optical characteristics of these MBE grown Be-doped GaAs NWs exhibit a strong dependence on the Be cell temperature. For the core configuration, the LO intensity eventually decreases as the Be cell temperature increases. The carrier concentration determined from the Hall measurement on Be doped GaAs thin films grown on a GaAs substrate at a Be cell temperature of 990˚C was 8.2×10^{19} cm^{-3}.

As discussed before, Be being a small atom would tend to fit into different available substitutional & interstitial sites in the GaAs crystal [18]. As Be doping results in predominantly p-type carriers in GaAs, most of the Be concentrate in the Ga-substitutional site. There are also possibilities of finding Beryllium clusters (Be$_{Ga}$-Be$_I$) and other cluster depending on the formation energy [18]. Beryllium on the Ga site acts like a shallow acceptor with the measured ionization energy of 28 meV [19] which is slightly more as compared to the 20 meV (1.51-1.49 eV) from sample C1 to C3 in the PL spectra. In the shell configuration, there is a clear increase in the Be doping at high V/III ratio. The doping profile for Be also depends on the diffusion mechanism during the NW growth [6, 20]. It has been shown that the Be atoms incorporate mostly through the side walls of NWs and based on the NW radius the depletion layer is generated which increases rapidly for low doping concentration. With a larger V/III ratio, the NW radius is higher generating a thinner depletion layer and better doping.

The presence of the peak at 1.49 eV at 4K photoluminescence along with a reduction of the I_{LO}/I_{TO} indicates the better Be doping. So V/III ratio of 70 was found to be optimum for better Be incorporation. These observations provide insight on the As/Ga ratio dependence of the shell configuration on our PL and Raman data.
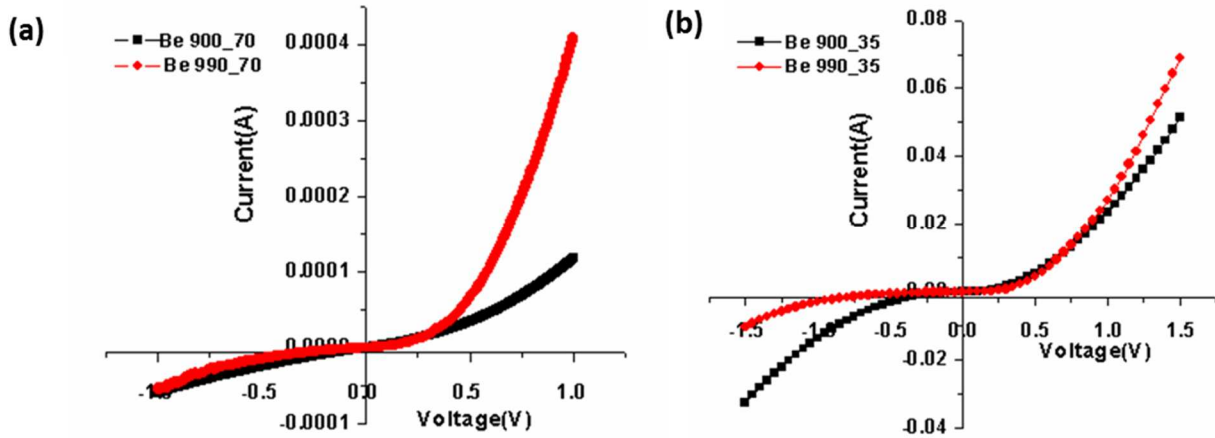
Figure.6 I-V curve for the ensemble of NWs at Be cell temperature of 900°C (represented by black squares) and 990°C (represented by red circles) with shell ratio of (a) 70 (b) 35.

Figure 6(a) and (b) shows the I-V curves of an ensemble of Be doped GaAs NWs with Be cell temperature of 900°C and 990°C and shell ratios of 70 and 35 respectively. For better comparison the electric current was measured at ± 1.5 V in both the samples. It was observed that the NWs with Be cell temperature at 990°C showed a much symmetric I-V curve with more linearity and higher current for a given voltage as compared to the ones grown at Be cell temperature of 900°C for the shell with V/III of 35 (figure 6 (a)).The latter can be attributed to the high interfacial barrier caused by the pinning of the Fermi level in the NW at the surface states. For the shell of 70, the I-V curve is non-symmetric. There was variation of the measured current from one point of the sample to other. The asymmetric behavior of the I-V characteristic is indicative of the different contact resistances present at the Si- NW and NW –metal contact, the latter being larger than the former. At higher Be cell temperature the higher doping on the semiconductor may likely causes unpinning of the Fermi level and forms an interface layer between the NW and the metal contact[21] lowering the barrier. This in turn enables enhanced tunneling of the charge carriers leading to more linear and symmetric I-V behavior, consistent with the observation of Dheeraj et al.[7]. These are clear evidences of higher Be incorporation.

Conclusion:

A detailed investigation on the effects of NW configuration, V/III flux ratio, and cell temperature on Be incorporation in MBE grown Be-doped GaAs NWs have been presented. Presence of PL emission in the 1.49 eV to 1.51 eV energy range are signatures of enhanced Be incorporation. Be incorporation is found to be preferentially incorporated through side facets. Be cell temperature and V/III ratio of the shell strongly influence dopant incorporation.

Acknowledgements

Reference:

[1] M. Tejwani, H. Kanber, B. Paine, J. Whelan, Growth and diffusion of abrupt beryllium-doped profiles in gallium arsenide by organometallic vapor phase epitaxy, Applied physics letters, 53 (1988) 2411-2413.
[2] J. Nagle, R.J. Malik, D. Gershoni, A comparison of atomic carbon versus beryllium acceptor doping in GaAs grown by molecular beam epitaxy, Journal of Crystal Growth, 111 (1991) 264-268.
[3] W. Walukiewicz, J. Lagowski, L. Jastrzebski, H.C. Gatos, Minority-carrier mobility in p-type GaAs, Journal of Applied Physics, 50 (1979) 5040-5042.
[4] M. Ilegems, Beryllium doping and diffusion in molecular-beam epitaxy of GaAs and AlxGa1– xAs, Journal of Applied Physics, 48 (1977) 1278-1287.
[5] M. Hilse, M. Ramsteiner, S. Breuer, L. Geelhaar, H. Riechert, Incorporation of the dopants Si and Be into GaAs nanowires, Applied Physics Letters, 96 (2010) 193104.
[6] A. Casadei, P. Krogstrup, M. Heiss, J.A. Rohr, C. Colombo, T. Ruelle, S. Upadhyay, C.B. Sørensen, J. Nygard, A. Fontcuberta i Morral, Doping incorporation paths in catalyst-free Be-doped GaAs nanowires, Applied Physics Letters, 102 (2013) 013117-013117-013114.
[7] D.L. Dheeraj, A.M. Munshi, O.M. Christoffersen, D.C. Kim, G. Signorello, H. Riel, A.T.J. van Helvoort, H. Weman, B.O. Fimland, Comparison of Be-doped GaAs nanowires grown by Au- and Ga-assisted molecular beam epitaxy, Journal of Crystal Growth.
[8] I. Shanthi, R. Lew, R. Thomas, O. SaiKrishna, K. PavanKumar, B. Adam, A Study of Ga-Assisted Growth of GaAs/GaAsSb Axial Nanowires by Molecular Beam Epitaxy, in: Nanoscience and Nanoengineering, CRC Press, 2014, pp. 31-50.

[9] M.P. Patkar, T.P. Chin, J.M. Woodall, M.S. Lundstrom, M.R. Melloch, Very low resistance nonalloyed ohmic contacts using low-temperature molecular beam epitaxy of GaAs, Applied Physics Letters, 66 (1995) 1412-1414.

[10] M. Feng, C.A. Fang, H. Chen, Bandgap shrinkage of degenerate p-type GaAs by photoluminescence spectroscopy, Materials chemistry and physics, 42 (1995) 143-147.

[11] M.S. Lundstrom, M.E. Klausmeier-Brown, M.R. Melloch, R.K. Ahrenkiel, B.M. Keyes, Device-related material properties of heavily doped gallium arsenide, Solid-State Electronics, 33 (1990) 693-704.

[12] D. Olego, M. Cardona, Photoluminescence in heavily doped GaAs. I. Temperature and hole-concentration dependence, Physical Review B, 22 (1980) 886.

[13] G. Borghs, K. Bhattacharyya, K. Deneffe, P. Van Mieghem, R. Mertens, Band-gap narrowing in highly doped n- and p-type GaAs studied by photoluminescence spectroscopy, Journal of Applied Physics, 66 (1989) 4381-4386.

[14] S. Prucnal, K. Gao, W. Anwand, M. Helm, W. Skorupa, S. Zhou, Temperature stable 1.3 μm emission from GaAs, Optics express, 20 (2012) 26075-26081.

[15] Y. Pao, J. Franklin, J. Harris, Influence of As 4/Ga flux ratio on Be incorporation in heavily doped GaAs grown by molecular beam epitaxy, Journal of Crystal Growth, 95 (1989) 301-304.

[16] E.I.C. A. N. Titkov, E. M. Komova, and N. G. Ermakova, Lowtemperature luminescence of degenerate p-type crystals of direct-gap semiconductors, Sov. Phys. Semicond, 15 (1981) 198-202.

[17] I. Zardo, S. Conesa-Boj, F. Peiro, J. Morante, J. Arbiol, E. Uccelli, G. Abstreiter, A.F. i Morral, Raman spectroscopy of wurtzite and zinc-blende GaAs nanowires: Polarization dependence, selection rules, and strain effects, Physical Review B, 80 (2009) 245324.

[18] H.-P. Komsa, E. Arola, J. Pakarinen, C.S. Peng, T.T. Rantala, Beryllium doping of GaAs and GaAsN studied from first principles, Physical Review B, 79 (2009) 115208.

[19] S.B. Zhang, J.E. Northrup, Chemical potential dependence of defect formation energies in GaAs: Application to Ga self-diffusion, Physical Review Letters, 67 (1991) 2339-2342.

[20] S. Yu, T. Tan, U. Gosele, Diffusion mechanism of zinc and beryllium in gallium arsenide, Journal of applied physics, 69 (1991) 3547-3565.

[21] M.J. Howes, D.V. Morgan, Gallium arsenide: materials, devices, and circuits, Chichester, England and New York, Wiley-Interscience, 1985, 592 p. No individual items are abstracted in this volume., 1 (1985).

Appendix H

Pavan Kumar Kasanaboina, Estiak Ahmad, Jia Li, Lewis Reynolds, Yang Liu and Shanthi Iyer, "Self-catalyzed growth of dilute nitride GaAs/GaAsSbN/GaAs core-shell nanowires by molecular beam epitaxy, Appl. Phys. Lett. 107, 103111 -5(2015).

.

Self-catalyzed growth of dilute nitride GaAs/GaAsSbN/GaAs core-shell nanowires by molecular beam epitaxy

Pavan Kumar Kasanaboina, Estiak Ahmad, Jia Li, C. Lewis Reynolds Jr., Yang Liu, and Shanthi Iyer

---

Articles you may be interested in

Te-doping of self-catalyzed GaAs nanowires
Appl. Phys. Lett. **107**, 012101 (2015); 10.1063/1.4926494

Growth and characterization of dilute nitride GaNxP1−x nanowires and GaNxP1−x/GaNyP1−y core/shell nanowires on Si (111) by gas source molecular beam epitaxy
Appl. Phys. Lett. **105**, 072107 (2014); 10.1063/1.4893745

Hexagonal and pentagonal shapes of self-catalyzed one-dimensional GaAs nanostructures: Shape dependence of the phase evolutions
Appl. Phys. Lett. **100**, 133112 (2012); 10.1063/1.3698468
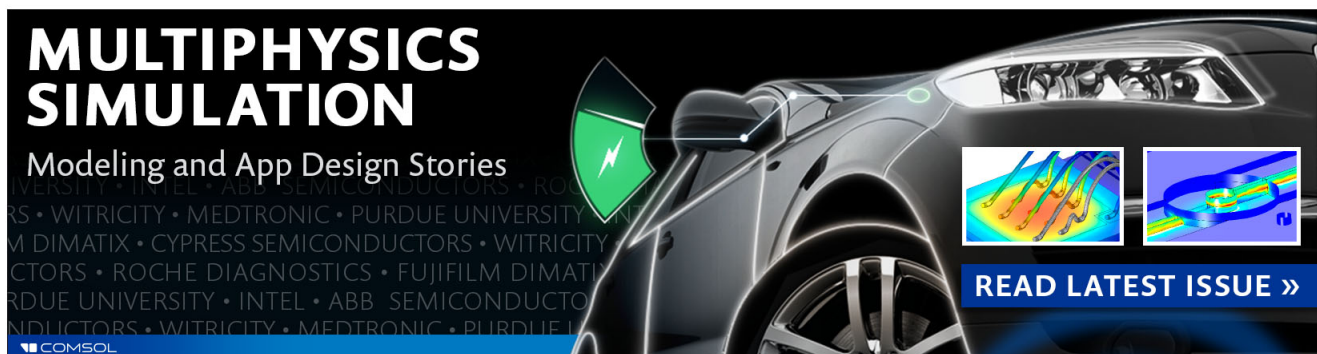
Growth and photoluminescence of self-catalyzed GaP/GaNP core/shell nanowires on Si(111) by gas source molecular beam epitaxy
Appl. Phys. Lett. **100**, 053108 (2012); 10.1063/1.3681172

Vapor-liquid-solid and vapor-solid growth of self-catalyzed GaAs nanowires
AIP Advances **1**, 042142 (2011); 10.1063/1.3664133

Self-catalyzed growth of dilute nitride GaAs/GaAsSbN/GaAs core-shell nanowires by molecular beam epitaxy

Pavan Kumar Kasanaboina,[1] Estiak Ahmad,[2] Jia Li,[1,2] C. Lewis Reynolds, Jr.,[3] Yang Liu,[3] and Shanthi Iyer[1,2]

[1]*Department of Electrical and Computer Engineering, North Carolina A&T State University, Greensboro, North Carolina 27411, USA*
[2]*Nanoengineering, Joint School of Nanoscience and Nanoengineering, NCA&T State University, Greensboro, North Carolina 27401, USA*
[3]*Department of Materials Science and Engineering, North Carolina State University, Raleigh, North Carolina 27695, USA*

Bandgap tuning up to 1.3 μm in GaAsSb based nanowires by incorporation of dilute amount of N is reported. Highly vertical GaAs/GaAsSbN/GaAs core-shell configured nanowires were grown for different N contents on Si (111) substrates using plasma assisted molecular beam epitaxy. X-ray diffraction analysis revealed close lattice matching of GaAsSbN with GaAs. Micro-photoluminescence (μ-PL) revealed red shift as well as broadening of the spectra attesting to N incorporation in the nanowires. Replication of the 4K PL spectra for several different single nanowires compared to the corresponding nanowire array suggests good compositional homogeneity amongst the nanowires. A large red shift of the Raman spectrum and associated symmetric line shape in these nanowires have been attributed to phonon localization at point defects. Transmission electron microscopy reveals the dominance of stacking faults and twins in these nanowires. The lower strain present in these dilute nitride nanowires, as opposed to GaAsSb nanowires having the same PL emission wavelength, and the observation of room temperature PL demonstrate the advantage of the dilute nitride system offers in the nanowire configuration, providing a pathway for realizing nanoscale optoelectronic devices in the telecommunication wavelength region. © 2015 AIP Publishing LLC. [http://dx.doi.org/10.1063/1.4930887]

Dilute nitride semiconductor III-V material systems have the distinguishing feature of simultaneous reduction in band gap and lattice parameter with the addition of small amounts of N to the III-V lattice. Further, this system enables independent tuning of conduction and valence band offsets by adjusting concentrations of N and other group V elements, respectively. Extensive work has been reported on nanostructured dilute nitride thin films in the telecom wavelength region of 1.3–1.55 μm.[1–9] However, there has been little work on such dilute III-V-N systems in a nanowire configuration. The potential advantages offered by one dimensional nanowire architectures are better stress control, improved defect tolerance, enhanced light trapping, greater flexibility in materials selection and device design. These can be strategically utilized for efficient band gap tuning and creating a niche in a variety of nanoscale applications, for example, single photon emitters and detectors for quantum networking and nanophotonic integrated circuits.[5]

The dilute III-V nitride systems based nanowires that have been reported to date are GaAs/GaAsN and GaP/GaPN core-shell nanowires which are focused towards bandgap tuning at higher energy 1–2 eV.[10–13] The competing dilute nitride material systems that have been investigated in nanostructured thin films for the telecom wavelength range are InGaAsN, GaAsSbN, and InGaAsSbN.[2,4,6,8,9,14] In a nanowire configuration, the alloys consisting of two group III elements pose a compositional homogeneity challenge due to their differing diffusion coefficients.[15] Hence, GaAsSbN is the preferred material system since it avoids having two

group III species. Here, we report the investigation on the growth of dilute nitride GaAs/GaAsSbN/GaAs core-shell nanowires by Ga assisted molecular beam epitaxy (MBE) in which a band gap shift corresponding to a wavelength of 1.3 μm is presented. The effect of N incorporation on the structural and optical properties of the nanowires is investigated in detail.

The growth of dilute nitride GaAs/GaAsSbN/GaAs core-shell nanowires was carried out on chemically cleaned (piranha/HF) p-type Si (111) substrates by plasma assisted MBE. GaAs core nanowires were grown at 620 °C with Ga as a catalyst and As flux with a beam equivalent pressure (BEP) of 4.8×10^{-6} Torr. The shell growth was initiated at 540 °C by opening the Sb and N shutters. A constant Sb BEP of 1.4×10^{-6} Torr was used for the three different samples under investigation while the N beam equivalent pressures were set at 0 Torr, 8.5×10^{-8} Torr (1.7% flux), and 1.8×10^{-7} Torr (3.7% flux), which are referred to as reference, LN and HN samples, respectively. Both Sb and N shutters were closed for the growth of final GaAs shell at 540 °C. It is to be noted that the scanning transmission electron microscope (STEM) energy-dispersive X-ray spectroscopy (EDS) analysis performed on these nanowires could not provide accurate composition of N due to the close proximity of the N-K line and Sb-M line energies. Detailed growth procedure and characterization tools used are provided in our previous work.[16,17]

Figure 1(a) shows the 45° tilted scanning electron microscope (SEM) image of highly vertical GaAs/GaAsSbN/GaAs
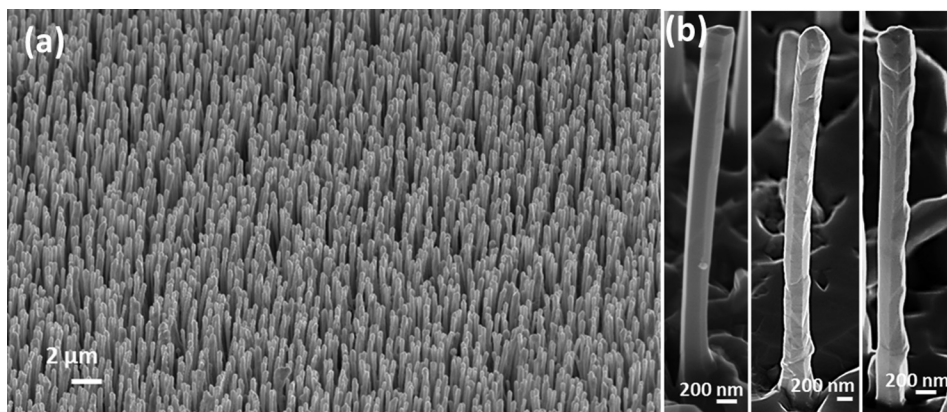
FIG. 1. (a) SEM image of 45° tilted GaAs/GaAsSbN/GaAs nanowires and (b) variation in the nanowire morphology for reference, LN, and HN samples.

nanowires. The nanowires are typically ∼4 μm long with a core diameter of ∼80 nm. The GaAsSbN and outer GaAs shells were ∼70 nm and 20 nm thick, respectively.

The reference GaAsSb nanowires exhibit smooth and well defined hexagonal facets in contrast to the corrugated side facets observed in the dilute nitride nanowires (Figure 1(b)). Also the radial growth rate increased from 0.78 Å/s for GaAsSb core-shell nanowires to 1.4 Å/s for GaAsSbN core-shell nanostructures. This increased growth rate can be explained by a Sb-N exchange mechanism, in which N readily occupies the group V lattice site due to a Sb kick-out mechanism; essentially the smaller size of N relieves the strain.[6] This results in a reduction in the diffusion length of N adatoms on the nanowire surface,[3,6] thereby promoting nucleation sites on the surface[18] that results in rough surface morphology. Further, as N diffuses inwards Sb coverage on the growth front is expected to increase due to the N kicking out Sb to the surface, which is likely to alter the surface energy. This mechanism then leads to the observed enhancement in growth rate in dilute nitride nanowires. The HN nanowires exhibit more regularly spaced sawtooth-faceted sidewalls (Fig. 1(b)). Similar nanowire morphology albeit with more closely spaced sawtooths has been observed in InAs/InAsSb core-shell nanowires[19] and has been attributed to rotation of the crystallite by 60° around the growth axis with formation of twins through the cross section of the nanowire.

Figure 2(a) displays high-angle annular dark-field (HAADF) STEM image of a typical GaAs/GaAsSbN/GaAs core-shell nanowire. EDS compositional mapping of the nanowire confirms the shell structure (Fig. 2(b)). The high resolution TEM (HR-TEM) image (Fig. 2(c)) and selected-area electron diffraction (SAED) pattern (Fig. 2(d)) confirm the zinc-blende (ZB) structure of the nanowire, which is consistent with the preferred structure observed in GaAsSb nanowires. The presence of twins and stacking faults (Fig. 2(c)) further attest to our earlier conjecture on the saw-tooth faceted nanowire morphology displayed by these nanowires.

Figure 3 shows the X-ray diffraction patterns of GaAs/GaAsSbN/GaAs nanowires with varying N content. The presence of only GaAs(111), Si(111) and their higher order Bragg peaks attest to highly vertical ⟨111⟩ oriented nanowires. GaAsSb nanowires exhibit a broad GaAsSb peak towards lower Bragg angles away from the GaAs peak, in contrast to GaAsSbN nanowires, which show only peaks

corresponding to (111) GaAs (Fig. 3(b)). The shift of Bragg angle from lower to higher values is clear evidence of the strain compensation by N leading to an X-ray signature that is closely lattice matched to the GaAs peak. Further, the decreased FWHM with increasing N content (Fig. 3(c)) corroborates the strain relieving effect in GaAsSb lattice due to the additional N. The FWHM of GaAs (111) peak in HN sample is close to that of GaAs, which reveals lattice matching of GaAsSbN to GaAs with good crystalline quality.

Figure 4(a) displays the normalized 4K microphotoluminescence (PL) spectra of as grown nanowires as a function of N content. The dilute nitride nanowires exhibit a red shift with respect to the GaAsSb nanowire PL peak energy, and the shift increases with increasing N content as
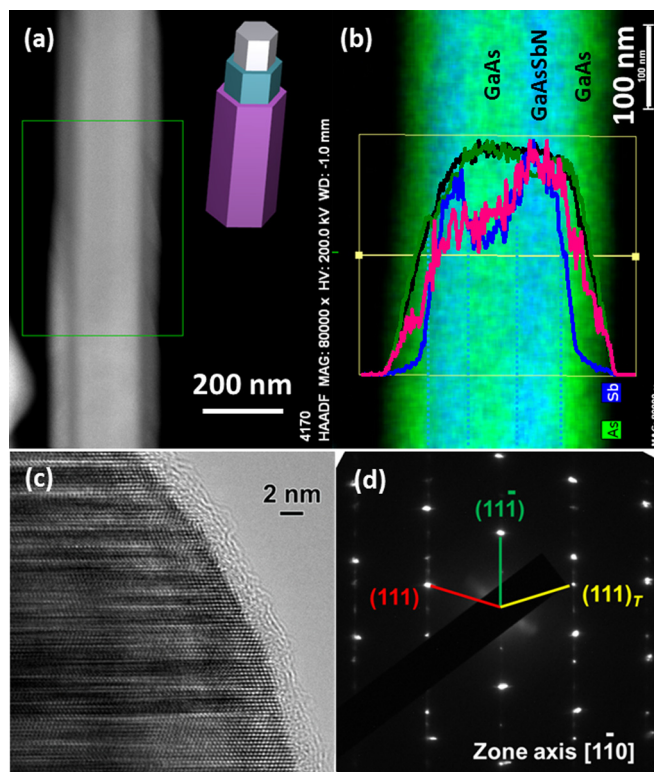

FIG. 2. (a) and (b) HAADF-STEM image with EDS compositional mapping of HN nanowire. Inset shows schematic of core-shell nanowire structure, (c) HR-TEM image displays both twins and stacking faults, and (d) SAED pattern shows ZB structure exhibiting twins, viewed from zone axis of [1$\bar{1}$0].
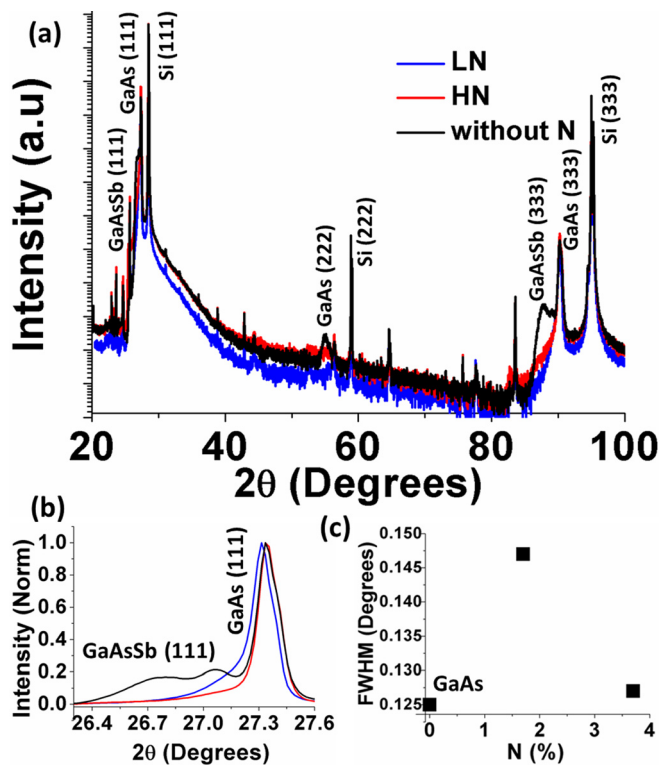
FIG. 3. (a) X-ray diffraction patterns of GaAs/GaAsSbN/GaAs nanowires for different N content, (b) GaAsSb nanowires show a broad GaAsSb peak towards lower Bragg angle away from the GaAs peak in contrast to the GaAs peak in GaAsSbN nanowires, and (c) variation of FWHM of GaAs (111) peak with N content.

FIG. 5. Room temperature Raman spectra of GaAs/GaAsSbN/GaAs nanowires with increasing N content.

expected. This is characteristic of dilute nitrides attributed to lowering of the conduction band manifesting in the reduction of the band gap.[1] Since we do not have a quantitative relationship between N flux and N incorporation in the nanowire, it is difficult to assess quantitatively the PL shift due to N only. Nevertheless, our data clearly show an increasing red shift with increasing N flux. The PL intensity decreases with increasing N content, as is evident from the noisy spectra observed for HN nanowires, which is consistent with observations on the dilute nitride thin films.[20,21] The suppression of intensity in the thin films is commonly attributed to N related defects and non-radiative centers created by the addition of N to the GaAsSb lattice.[9,21] The lower energy peak at ~0.87 eV in the PL spectra of both LN and HN samples is attributed to N-induced defect level,[8] and the relative

intensity of this peak increases with increasing N content. These unannealed, HN, nanowires exhibit room temperature PL emission at 1.3 μm with a quantum efficiency estimated to be ~20% (inset of Fig. 4(a)).

As shown in Fig. 4(b), good compositional homogeneity amongst the nanowires was ascertained by the replication of 4K PL spectra of the nanowire array by its single nanowire counterpart with similar FWHM of 150 meV.

Figure 5 is a comparison of the room temperature Raman spectra of GaAs/GaAsSbN/GaAs nanowires with the reference GaAsSb nanowires. The Raman spectrum of reference GaAs/GaAsSb/GaAs nanowires is highly asymmetric and displays LO and TO modes at 290.3 cm^{-1} and 265.6 cm^{-1}, respectively, which correspond to the ZB structure. A symmetric line shape and large redshifts in both LO and TO modes to 278.7 cm^{-1} and 257.2 cm^{-1}, respectively, are observed in the dilute nitride nanowires. There are various mechanisms that can induce red shifts in the Raman spectra. These are (i) alloying, (ii) strain, (iii) alloy disorder, (iv) laser heating, (v) phonon confinement, and (vi) phonon localization at the defects. First, as both LN and HN display LO at 278.7 cm^{-1} contrary to our earlier PL and XRD results which exhibit a monotonic dependence on N, alloying is not a likely contributor for the observed Raman shift. Second, strain in the nanowires is sufficiently small, as evidenced by the XRD spectra, that a strain contribution to the red shift can be ruled out. Third, a more symmetric line shape and absence of any disorder activated phonon
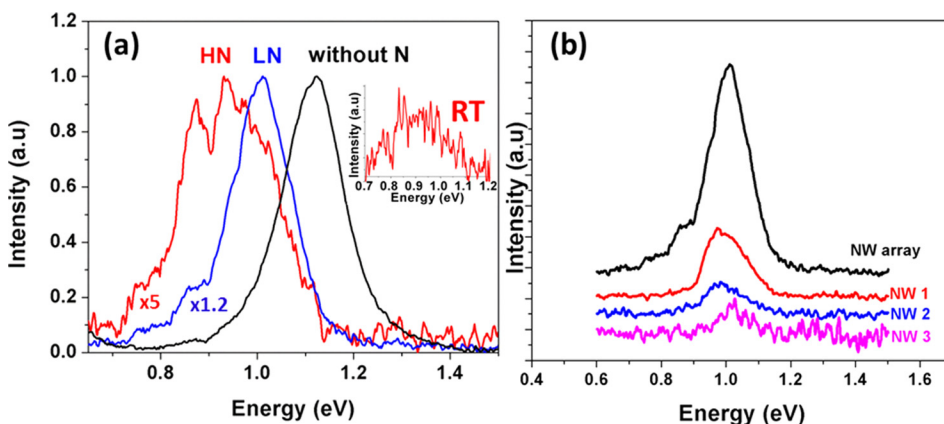

FIG. 4. Photoluminescence spectra of (a) GaAs/GaAsSbN/GaAs nanowires for different N contents and (b) comparison of nanowire array with single nanowires.
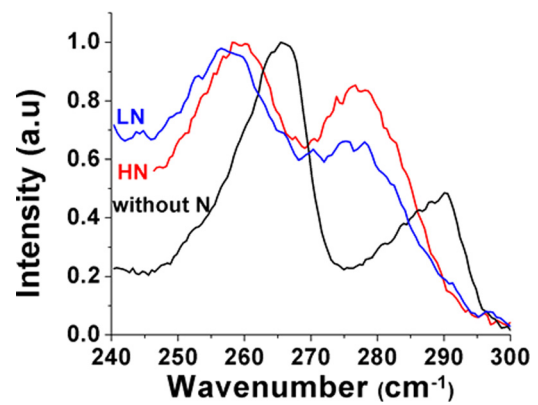
modes at lower phonon frequency make the contribution from compositional disorder to be unlikely. Fourth, it has been reported that heating effects can cause significant red shift in nanowires.[22] Hence laser intensity variation of the Raman signal was carried out. The phonon modes in both the GaAsSb and GaAsSbN nanowires exhibited the same red shift of $\sim$4 cm^{-1} on increasing the laser intensity by 100 fold, which rules out this contribution as well. Fifth, phonon confinement can cause a red shift and broadening of the Raman spectra; however, when compared to the shift reported in other nanowires,[22] such large shifts are associated with significantly thinner nanowires. Also as the phonon confinement has inverse dependence on the diameter, the nitride nanowires being larger in diameter than the reference non-nitride nanowires, the phonon confinement is expected to be weaker in our GaAsSbN nanowires than in the GaAsSb ones. Finally, in ZnO nanowires, a red shift of the order of 5 cm^{-1} has been reported previously[22] and has been attributed to phonon localization at the defects. The TEM investigation reveals the presence of planar defects, namely, stacking faults and twins in dilute nitride nanowires as discussed earlier. It has been theoretically reported[23] that planar defects induce high asymmetry in the Raman line shape but do not give rise to a significant red shift. In contrast, point defects induce a spectral shift, but no asymmetry. Introduction of N in III-V alloys is well known[1,11] to induce N-related clusters in thin films due to the large disparity in the size of the N and other group V atoms. As these nanowires were not intentionally annealed, point defects are likely to be present thus contributing to the observed red shift. We have also carried out rapid thermal annealing (RTA) of the nanowires at 700 °C for 30 s to test this hypothesis. Indeed, the Raman signal approached closer to that of the GaAsSb nanowires and was accompanied with the transformation from a symmetric to asymmetric line shape, which is characteristic of the dominance of planar defects over point defects. Hence, the perturbation of the phonon propagation due to the point defects appears to be the major contributor to the observed large red shift in the Raman spectra of our dilute nitride nanowires.

As noted above, these dilute nitride nanowires were not intentionally annealed. Room temperature PL from as-grown dilute nitride thin films has not been reported, and it has been firmly established that annealing is a necessary prerequisite.[1,8,9,21] The dilute nitride nanowires exhibit planar defects, namely, stacking faults and twins, in addition to the point defects as evidenced by TEM and Raman analysis, respectively, while in thin films N-related clusters and compositional disorder dominate.[1,8,21] Also the carriers are confined laterally in nanowires as opposed to being free in the two-dimensional plane. Further, during the PL measurement, evidence of laser heating is observed with the nanowire becoming smaller in length. Thus possibility of laser induced annihilation of the defects also has to be taken into consideration. We believe that all the above contribute to a reduction in the density of non-radiative recombination centers in the nanowire configuration, enabling observation of room temperature PL.

It may be argued that GaAsSb nanowires also undergo similar laser heating. However, the dilute nitride material system is well known to be dominated by N-related centers,

alloy potential fluctuations and hence the effect of annealing is likely more pronounced in dilute nitride nanowires. Another advantage of dilute nitride composition is the reduction in strain, leading to straight nanowires, instead of the curved nanowires that are observed in GaAsSb[16] of similar length and PL peak wavelength.

In conclusion, 1.3 μm PL emission in dilute nitride GaAs/GaAsSbN/GaAs core-shell nanowires is reported. The 4K PL spectrum of a single nanowire corresponds well to the spectrum of the array, indicating good homogeneity. Close lattice matching of the X-ray peak to GaAs and the red shift of the PL are clear indications of N incorporation in the nanowires. Large red shift in Raman optical phonon modes has been found to be caused by the phonon localization at the defects. The decreased strain in the nanowires leading to the growth of straight vertical nanowires can be advantageous for devices. The observation of room temperature PL in these nanowires is encouraging, and *ex situ* annealing is expected to further improve the quality. These are preliminary report and there is still much room for improvement. Thus dilute nitride nanowires hold great promise towards realization of devices operating in the telecommunication wavelength range.

[1]J. C. Harmand, L. Li, R. Mouillet, G. Ungaro, V. Sallet, L. Travers, G. Patriarche, L. Largeau, R. Kudrawiec, G. Sek *et al.*, in *Dilute Nitride Semiconductors*, edited by M. Henini (Elsevier, 2005), Chap. 15, p. 471.

[2]V. Gambin, W. Ha, M. Wistey, H. Yuen, S. R. Bank, S. M. Kim, and J. S. Harris, Jr., IEEE J. Sel. Top. Quantum Electron. **8**, 795 (2002).

[3]J. C. Harmand, L. H. Li, G. Patriarche, and L. Travers, Appl. Phys. Lett. **84**, 3981 (2004).

[4]J. S. Harris, R. Kudrawiec, H. B. Yuen, S. R. Bank, H. P. Bae, M. A. Wistey, D. Jackrel, E. R. Pickett, T. Sarmiento, L. L. Goddard, V. Lordi, and T. Gugov, Phys. Status Solidi B **244**(8), 2707 (2007).

[5]R. Carron, D. Fekete, P. Gallo, B. Dwir, A. Rudra, M. Felici, B. Bartova, M. Cantoni, and E. Kapon, Appl. Phys. Lett. **99**, 101107 (2011).

[6]D. Wu, Z. Niu, S. Zhang, S. H. Ni, Z. He, Z. Sun, Q. Han, and R. Wu, J. Cryst. Growth **290**, 494 (2006).

[7]H. B. Yuen, S. R. Bank, H. Bae, M. A. Wistey, and J. S. Harris, J. Appl. Phys. **99**, 093504 (2006).

[8]S. Bharatan, S. Iyer, K. Nunna, W. J. Collis, K. Matney, J. Reppert, A. M. Rao, and R. C. P. Kent, J. Appl. Phys. **102**, 023503 (2007).

[9]K. Nunna, S. Iyer, L. Wu, J. Li, and S. Bharatan, J. Appl. Phys. **102**, 053106 (2007).

[10]I. A. Buyanova, W. M. Chen, G. Pozina, J. P. Bergman, B. Monemar, H. P. Xin, and C. W. Tu, Appl. Phys. Lett. **75**, 501 (1999).

[11]Y. Araki, M. Yamaguchi, and F. Ishikawa, Nanotechnology **24**, 065601 (2013).

[12]S. L. Chen, S. Filippov, F. Ishikawa, W. M. Chen, and I. A. Buyanova, Appl. Phys. Lett. **105**, 253106 (2014).

[13]S. Sukrittanon, Y. J. Kuang, A. Dobrovolsky, W. M. Kang, J. S. Jang, B. J. Kim, W. M. Chen, I. A. Buyanova, and C. W. Tu, Appl. Phys. Lett. **105**, 072107 (2014).

[14]H. B. Yuen, S. R. Bank, M. A. Wistey, J. S. Harris, and A. Moto, J. Appl. Phys. **96**, 6375 (2004).

[15]F. Martelli, *Advances in III-V Semiconductor Nanowires and Nanodevices* (Bentham Science Publishers, 2011), Chap. 6, p. 105, ISBN 9781608050529.

[16]P. K. Kasanaboina, S. K. Ojha, S. U. Sami, L. Reynolds, Y. Liu, and S. Iyer, Proc. SPIE **9373**, 937307 (2015).

[17]S. Iyer, L. Reynolds, T. Rawdanowicz, S. K. Ojha, P. K. Kasanaboina, and A. Bowen, *Nanoscience and Nanoengineering: Advances and Applications* (CRC Press, 2014), Chap. 3, p. 31, ISBN 9781482231199.

[18]D. Kandel and E. Kaxiras, Solid State Phys. **54**, 219–262 (2000).

[19]T. Xu, K. A. Dick, S. Plissard, T. H. Nguyen, Y. Makoudi, M. Berthe, J. P. Nys, X. Wallart, B. Grandidier, and P. Caroff, Nanotechnology **23**, 095702 (2012).

[20]L. Wu, S. Iyer, K. Nunna, J. Li, S. Bharatan, W. Collis, and K. Matney, J. Cryst. Growth **279**, 293 (2005).

[21]J. Li, S. Iyer, S. Bharatan, L. Wu, K. Nunna, and W. Collis, J. Appl. Phys. **98**, 013703 (2005).

[22]I. Calizo, K. A. Alim, V. A. Fonoberov, S. Krishnakumar, M. Shamsa, A. A. Balandin, and R. Kurtz, Proc. SPIE **6481**, 64810N (2007).

[23]L. A. Falkovsky, Phys. Rev. B **64**, 024301 (2001).

Appendix I

Shanthi Iyer, Pavan Kumar Kasanaboina and Jia Li, Invention disclosure NC A&T Ref # EN0095 0915 " Band Gap Tuning up to 1.3 µm in GaAsSbN Nanowires grown by Ga assisted Molecular Beam Epitaxy".

September 8, 2015
VIA E-MAIL

Dr. Shanthi Iyer
Mr. Pavan Kasanaboina
Dr. Jia Li
North Carolina Agricultural and Technology State University
Joint School of Nanoscience and Nanoengineering
2907 E. Gate City Blvd, Greensboro, NC
Greensboro NC 27401

Iyer@ncat.edu
pkkasana@aggies.ncat.edu
JiaLi@ncat.edu

RE: **Innovation Disclosure "1.3 μm Emission from Dilute Nitride GaAs/GaAsSbN/GaAs Core-Shell Nanowires grown by Epitaxy"**
NC A&T Reference Number: EN0095 0915

Dear Dr. Iyer, Mr. Kasanaboina and Dr. Li,

Thank you for your submission on September 8, 2015 of the above-referenced Innovation Disclosure. The Office of Technology Transfer will undertake an investigation of the potential commercial applications and patentability of your innovation. The Office will determine the next steps in pursuing intellectual property protection of your disclosure. If deemed appropriate, we will aggressively pursue patent protection for your innovation.

Until you are notified of our decision, please do not provide confidential, proprietary information to third parties outside the university. Specifically, please do not make public your innovation via submission or presentation of a paper or poster or discuss your innovation at a conference or electronically, as in a blog.

If you are contacted about your innovation, particularly by a potential licensee, please notify me before releasing any relevant information about it.

Please note that publically disclosing aspects of your innovation before filing a patent application may adversely affect our ability to obtain patent rights both within and outside the U.S. At present, we understand that you have disclosed some potentially related aspects of your invention in an abstract that was publicly available on November 7, 2014: Md Shifat Us Sami, Jia Li, Sai Krishna Ojha, Pavan Kumar Kasanaboina and Shanthi Iyer, "A low temperature micro-photoluminescence study of self-assisted MBE grown core and core/shell configured GaAsSb(N)/GaAs Nanowires for nanoscale photodetectors." MRS/ASM/AVS 11/7/2014. As you are aware, this disclosure likely acts as a bar to filing for patent protection in any foreign country, thus if our understanding is incorrect or you believe that you may have disclosed other details of your invention, please notify me as soon as possible.

Thank you for your ingenuity and diligence. Please do not hesitate to contact me (336-285-3188) if you have any questions or concerns.

Best Regards,

Laura Collins
Director of IP Development/Patent Agent

cc: Louis Judge, Director, Outreach and Technology Transfer
    Dr. Barry L. Burks, Vice Chancellor for Research & Economic Development

Division of Research and
Economic Development

Fort IRC Building
4th Floor - Room 416

1601 East Market Street
Greensboro, NC 27411

Office (336) 334-7995
Fax (336) 256-2240

Appendix I

Shanthi Iyer, Pavan Kumar Kasanaboina and Jia Li, Invention disclosure NC A&T Ref # EN0095 0915 " Band Gap Tuning up to 1.3 µm in GaAsSbN Nanowires grown by Ga assisted Molecular Beam Epitaxy".

September 8, 2015
VIA E-MAIL

Dr. Shanthi Iyer   Iyer@ncat.edu
Mr. Pavan Kasanaboina   pkkasana@aggies.ncat.edu
Dr. Jia Li   JiaLi@ncat.edu
North Carolina Agricultural and Technology State University
Joint School of Nanoscience and Nanoengineering
2907 E. Gate City Blvd, Greensboro, NC
Greensboro NC 27401

RE: Innovation Disclosure "1.3 μm Emission from Dilute Nitride GaAs/GaAsSbN/GaAs Core-Shell
        Nanowires grown by Epitaxy"
        NC A&T Reference Number: EN0095 0915

Dear Dr. Iyer, Mr. Kasanaboina and Dr. Li,

Thank you for your submission on September 8, 2015 of the above-referenced Innovation Disclosure. The Office of Technology Transfer will undertake an investigation of the potential commercial applications and patentability of your innovation. The Office will determine the next steps in pursuing intellectual property protection of your disclosure. If deemed appropriate, we will aggressively pursue patent protection for your innovation.

Until you are notified of our decision, please do not provide confidential, proprietary information to third parties outside the university. Specifically, please do not make public your innovation via submission or presentation of a paper or poster or discuss your innovation at a conference or electronically, as in a blog.

If you are contacted about your innovation, particularly by a potential licensee, please notify me before releasing any relevant information about it.

Please note that publically disclosing aspects of your innovation before filing a patent application may adversely affect our ability to obtain patent rights both within and outside the U.S. At present, we understand that you have disclosed some potentially related aspects of your invention in an abstract that was publicly available on November 7, 2014: Md Shifat Us Sami, Jia Li, Sai Krishna Ojha, Pavan Kumar Kasanaboina and Shanthi Iyer, "A low temperature micro-photoluminescence study of self-assisted MBE grown core and core/shell configured GaAsSb(N)/GaAs Nanowires for nanoscale photodetectors." MRS/ASM/AVS 11/7/2014. As you are aware, this disclosure likely acts as a bar to filing for patent protection in any foreign country, thus if our understanding is incorrect or you believe that you may have disclosed other details of your invention, please notify me as soon as possible.

Thank you for your ingenuity and diligence. Please do not hesitate to contact me (336-285-3188) if you have any questions or concerns.

Best Regards,

Laura Collins
Director of IP Development/Patent Agent

cc: Louis Judge, Director, Outreach and Technology Transfer
    Dr. Barry L. Burks, Vice Chancellor for Research & Economic Development